UNIVERSITY OF CALIFORNIA

Santa Barbara

ANTARCTIC RAISED BEACHES: INSIGHT ON GEOCHRONOLOGY, RELATIVE SEA LEVEL, AND COASTAL PROCESSES

A dissertation submitted in partial satisfaction of the

requirements for the degree of

DOCTOR OF PHILOSOPHY

in Geological Sciences

BY

LAUREN MILLER SIMKINS

Committee in charge:

Professor Alexander Simms, Chair

Professor Regina DeWitt

Professor Syee Weldeab

Professor Edward Keller

September 2014

The dissertation of Lauren Miller Simkins is approved.

_____

Regina DeWitt

_____

Syee Weldeab

_____

Edward Keller

_____

Alexander Simms, Committee Chair

August 2014

ACKNOWLEDGMENTS

Firstly, I would like to thank the National Science Foundation (grant OPP-0838781) awarded to Dr. Alexander Simms and Dr. Regina DeWitt for providing financial support for the projects completed for my dissertation. Without the funding, sample collection and dating measurements of Antarctic beach deposits would not have been possible.

I would like to thank my adviser, Dr. Alexander Simms, for encouraging and inspiring me throughout my graduate school career. I must also thank him for the countless hours spent revising manuscripts. From the first drafts completely covered in red ink to the finished products, it is only through his meticulous review of my writing that I have a better understanding of how to convey research to a wide-range of audiences. I must thank Dr. Regina Dewitt who was my mentor in the laboratory where I conducted the geochronology for my dissertation. I remember the first month or so I was in the lab thinking I would never understand optically stimulated luminescence, but through her patient guidance and encouragement I was able to learn a wealth of information necessary for the completion of this project.

I would like to thank Daniel Livsey for numerous fruitful discussions and assistance in the field. I thank Hanna Alexander, Laura Reynolds, Elisabeth Steel, and Carlye Peterson, Christopher Pynn for support, encouragement, and always being available to discuss questions and issues regarding my research.

I would like to thank Chris Denker of Raytheon Polar Services for assistance in the field and Edison Chouest for logistical support during the NBP10-02 cruise. I thank UNAVCO supported by the National Science Foundation and National Aeronautics and Space Administration under NSF Cooperative Agreement No. EAR-0735156 for lending a Trimble differential GPS for field surveying. I thank Robert Turner at the University of Oklahoma and Brett Bonotto and Hanna Alexander at the University of California Santa Barbara for assistance in crushing samples, Joe Pettit at UNAVCO for GPS training, and Eduardo Yukihara at the Radiation Dosimetry Laboratory at Oklahoma State University for the use of dating equipment. I thank Sophie Briggs and Gareth Seward at the University of California Santa Barbara for providing valuable help with petrographic analysis of thin sections and running elemental analyses on samples, respectively. Thanks to Deborah Khider for assistance in running Monte-Carlo simulations.

Finally, I would like to thank my parents, Stephen and Teresa Miller, and sister Hannah Miller for support and encouragement throughout not only graduate school, but over a lifetime to guide me to where I am today. I would like to thank my husband, Walt Simkins, for supporting me emotionally and listening to me talk about Antarctic beaches and optically stimulated luminescence for countless hours. It is only through the support and guidance of my mentors, family, and friends mention here that I was able to complete my dissertation research and develop as a person and a geologist.

VITA OF LAUREN MILLER SIMKINS

June 2014

EDUCATION

Bachelors of Science in Geology and Spanish, Oklahoma State University, December 2009
Doctor of Philosophy in Geologic Sciences, University of California Santa Barbara, July 2014 (expected)

PROFESSIONAL EMPLOYMENT

2008-2010: Research Assistant, Boone Pickens School of Geology, Oklahoma State University
2010: Research Assistant, Department of Physics, Oklahoma State University
2010-2014: Research Assistant, Department of Geological Sciences, University of California
2012: Summer Mentor, Internships in Nanosystems Science, Engineering and Technology, University of California Santa Barbara
2013: Summer Mentor, Jack Kent Cooke Bridges and Condor Tech Programs, Internships in Nanosystems Science, Engineering and Technology, University of California Santa Barbara
2013-2014: Teaching Assistant, Department of Geological Sciences, University of California Santa Barbara
2014: Teaching Assistant, Department of Environmental Studies, University of California Santa Barbara

PUBLICATIONS

Simms, A., Aryal, N., Miller, L., and Yokoyama, Y., 2010, The Incised Valley of Baffin Bay, Texas: A Tale of Two Climates: Sedimentology 57, 642-669.

Simms, A., Ivins, E., DeWitt, R., Kouremenos, P. and Simkins, L., 2012, Timing of the Little Ice Age in the Antarctic Peninsula from optically stimulated luminescence of cobble surfaces within raised beaches: Quaternary Science Reviews 47, 41-55.

Simkins, L., Simms, A., Cruse, A., Troiani, T., Atekwana, E., Puckette, J., and Yokoyama, Y., 2012, Correlation of early and mid-Holocene events using magnetic susceptibility in estuarine cores from the Gulf of Mexico: Palaeogeography, Palaeoclimatology, and Palaeoecology 346-347, 95-107.

Simkins, L., DeWitt, R., and Simms, A., 2013. Methods to reduce sample carrier contamination for luminescence measurements: Ancient TL 31 (1), 19-27.

Simkins, L., Simms, A., and DeWitt, R., 2013, Relative sea-level history of Marguerite Bay derived from optically stimulated luminescence-dated raised beaches: Quaternary Science Reviews 77, 141-155.

Simkins, L., and Simms, A., *in review*, Assessing the link between coastal morphology, wave energy, and sea ice throughout the Holocene from Antarctic raised beaches.

AWARDS

University of California Santa Barbara-National Science Foundation Bridge to Doctorate Fellowship, 2010-2012
Coast Geological Society Scholarship, Ventura, California, 2013
Philip and Aida Siff Educational Foundation Graduate Fellowship, University of California Santa Barbara, 2013-2014
Research Excellence, Department of Geological Sciences, University of California Santa Barbara, 2014

FIELDS OF STUDY

Major field: Antarctic beaches

Study of relative sea-level history of Marguerite Bay, Antarctic Peninsula with Dr. Alexander Simms and Dr. Regina Dewitt
Study of improvements for luminescence dating of cobble surfaces with Dr. Regina Dewitt and Dr. Alexander Simms
Study of coastal morphology, wave energy, and sea ice throughout the Holocene from Antarctic raised beaches with Dr. Alexander Simms and Dr. Regina Dewitt

ABSTRACT

ANTARCTIC RAISED BEACHES: INSIGHT ON GEOCHRONOLOGY, RELATIVE SEA LEVEL, AND COASTAL PROCESS

BY

LAUREN MILLER SIMKINS

Beaches are preserved above sea level along ice-free portions of the Antarctic coastline due to post-glacial rebound associated with glacial isostatic adjustment since the Last Glacial Maximum. The ages and elevations of these beaches provide relative sea-level constraints for glacial isostatic adjustment models and ice-sheet histories. Due to harsh field conditions and difficulty dating Antarctic materials, a lack of geochronological constraints on raised beaches limits our understanding of relative sea level around Antarctica. The focus of the studies discussed here is on Antarctic raised beaches with goals to improve the methods of dating cobble surfaces from raised beaches using optically stimulated luminescence and use the dated beaches to reconstruct relative sea level and better understand Antarctic coastal processes throughout the Holocene. Through a series of cleaning methods applied to sample carriers used for optically stimulated luminescence measurements of sediment, the contamination of dose-dependent, variable signals from sample carriers previously assumed to have neutral signals is eliminated through a series of cleaning methods (Chapter 2). An analysis of optically stimulated luminescence characteristics of quartz from cobble surfaces

with sample petrology and cathodoluminescence provides insight on the suitability of Antarctic materials for optically stimulated luminescence dating (Chapter 3). The limited amount of quartz (<10%) found in the majority of the samples often occurs as intergrowths in feldspars characterized by irregular, anhedral crystal form. A lack of discernible relationship between optically stimulated luminescence and cathodoluminescence properties and petrology suggest that cathodoluminescence behavior and petrology are not responsible for the poor luminescence characteristics observed from quartz extracted from cobble surfaces. A relative sea-level history of Marguerite Bay, Antarctic Peninsula derived from optically stimulated luminescence-dated beach cobble surfaces further constrains post-glacial rebound since the Last Glacial Maximum (Chapter 4). New ages suggest the Holocene marine limit for Marguerite Bay is 21.7 masl with an age of ~ 5.5-7.3 ka. Our favored hypothesis for the ages of the beaches from 21.7-40.8 masl at Calmette Bay is that the beaches formed prior to the Last Glacial Maximum. The temporal distribution of circum-Antarctic raised beaches throughout the Holocene is utilized to determine the relationship between wave-energy, sea ice, and coastal evolution (Chapter 5). The distribution of raised beaches throughout the Holocene around Antarctica show synchronous periods of beach formation in the Antarctic Peninsula and the Ross Sea centered at 2.0, 3.5, and 5.3 ky BP while East Antarctic (outside of the Ross Sea) beach formation is out-of-phase with the rest of the Antarctica at 3.2, 4.2, 5.8, and 6.5 ky BP. The distribution of beaches in the South Shetland Islands is dominated by enhanced beach formation between 0.2 and 0.7 ky BP most likely due to rapid post-glacial rebound associated with the Little Ice Age with minor peaks in beach formation from 1.3-2.2, 5.1-5.6, and 6.0-6.5 ky BP. Beach formation results from higher wave exposure during periods of reduced sea ice observed from comparison with Holocene sea-ice proxies. The

anti-phasing of beach formation in the Antarctic Peninsula and Ross Sea compared to East Antarctica is markedly similar to the phasing of modern and Holocene climate forcing around Antarctica. The findings of these studies focused on Antarctic raised beaches have implications for understanding sea-level, glacial isostatic adjustment, ice-sheet histories, and coastal processes since the Last Glacial Maximum.

TABLE OF CONTENTS

LIST OF FIGURES

CHAPTER 1

INTRODUCTION

The relationship between continental ice fluctuations and sea-level change is important for understanding spatial variations in sea levels and vital for modeling glacial isostatic adjustment (GIA) and ice-sheet histories. Since the Last Glacial Maximum (LGM), a eustatic sea-level rise of ~120 m is observed from relative sea-level (RSL) studies in the far-field (Fairbanks et al., 1989; Yokoyama et al., 2000; Peltier, 2002; Hanebuth et al., 2009). However, a large component of spatial variability in sea level arises from the dynamic solid-Earth response to mass redistribution due to GIA resulting from the solid-Earth response to loading and unloading of continental ice (Lambeck et al., 2002; Milne et al. 2002; Peltier, 2002). During periods of ice growth, the lithosphere subsides as mantle material is displaced under the weight of the ice load. As the ice load is reduced during deglaciation, the Earth's surface adjusts to the mass redistribution causing rebound in the near-field close to the centers of ice loading.

Around Antarctica, the rate of post-glacial rebound often outpaced eustatic sea-level rise following the LGM resulting in RSL fall. The elevations and ages of emergent coastal features provide the basis for Antarctic RSL reconstructions. GIA models for Antarctica are commonly constrained by these RSL histories (Nakada et al., 2000; Ivins and James, 2005;

Whitehouse et al., 2012; Gomez et al., 2013; Briggs et al., 2013; Okuno et al., 2013). Misfits between modeled and observed relative sea levels most likely result from a lack of robust constraints on Holocene RSL around Antarctica (Whitehouse et al., 2012; Okuno et al., 2013). Due to harsh field conditions, a scarcity of ice-free coastal environments, and problems associated with dating Antarctic materials, relatively few RSL data are available for constraining Antarctic GIA model predictions when compared to the data-rich high-latitudes of the northern hemisphere.

Antarctic RSL observations are derived from the ages and elevations of raised beaches and isolations basins preserved above sea level by post-glacial rebound. Isolation basins are previously marine basins that record the onset of lacustrine or marine sedimentation, reflecting a drop or rise in sea level relative to the basin-sill elevation, respectively (Zwartz et al., 1998, Bentley et al., 2005). Raised beaches form as local sea level falls due to post-glacial rebound and beaches become isolated from marine processes (Nichols, 1968; Fretwell et al., 2010; Simms et al., 2012). Isolation basins typically provide a single RSL index point whereas raised beaches provide a series of constraints on RSL. Additionally, raised beaches are capable of recording changes in rates of RSL and identifying marine limits important for constraining GIA models.

The focus of the studies discussed here is on Antarctic raised beaches with goals to improve the methods of dating raised beaches and use the dated beaches to reconstruct RSL and better understand Antarctic coastal processes throughout the Holocene. Chapter 1 consists of an overarching introduction to the topics discussed in the following chapters. Chapters 2 and 3 are centered on improving the relatively novel application of optically stimulated luminescence (OSL) to date Antarctic raised beaches. During the early stages of

dating Antarctic beach deposits, sample OSL measurements were contaminated by signals arising from sample carriers previously assumed to have neutral signals. Chapter 2 focuses on reducing the contaminant signals from sample carriers. Further improvements to the methods used to date cobble surfaces are discussed in Chapter 3 in which sample characteristics (e.g. petrology, cathodoluminescence) and OSL characteristics are compared and assumptions used in dose rate calculations are assessed. Chapters 4 and 5 discuss geologic studies from Antarctic raised beaches providing insight on the RSL history of Marguerite Bay and determining the link between coastal morphology, wave energy, and sea ice throughout the Holocene from Antarctic raised beaches, respectively. Final remarks are provided in Chapter 6 where the findings of these studies focused on Antarctic raised beaches are summarized and placed in a larger-scale context of understanding sea-level, glacial isostatic adjustment, ice-sheet histories, and coastal processes since the LGM.

CHAPTER 2

METHODS TO REDUCE SAMPLE CARRIER CONTAMINATION FOR LUMINESCENCE MEASUREMENTS

2.1. INTRODUCTION

Luminescence measurements of sedimentary quartz contaminated by unwanted signal contributions can lead to the miscalculation of equivalent doses used for optically stimulated luminescence (OSL) ages. Recent studies have identified luminescence signals from sample carriers (Schmidt et al., 2011) and silicone oil (Vandenberghe et al., 2008) used for OSL measurements. Unlike sensitivity changes and background measurements, variable signal contamination produced by sample carriers is not accounted for in the single aliquot regenerative (SAR; Murray and Wintle, 2000) dose measurement procedure thus sample carriers pose as a source of error for sediment measurements.

Typical sample carriers used for OSL dating include stainless steel and aluminum discs and cups. Schmidt et al. (2011) observed significant dose-dependent thermal luminescence (TL) signals from clean, empty stainless steel and aluminum discs with strong

A version of this chapter is published as a paper in Ancient TL under the citation: Simkins, Lauren, DeWitt, Regina, and Simms, Alexander, 2013. Methods to reduce sample carrier contamination for luminescence measurements: Ancient TL, volume 31, pages 19-26.

TL peaks at 110 °C in ultraviolet (UV; 340 nm) and UV-blue (420 nm) detection windows. Two other peaks were observed between 150 and 300 °C in the UV range and a broad peak was observed between 150 and 300 °C in the UV-blue window with a high-temperature peak at 380 °C. Additionally, Vandenberghe (pers. comm., 2012) identified ultra-fast decaying, thermally unstable, dose-dependent signals from stainless steel discs with a strong TL peak at 110°C with a UV (340 nm) detection window. Luminescence signals from empty sample carriers most likely arise from chemical reactions between silicone oil and sample carriers upon heating and irradiation that result in luminophores derived from defects in silica-, aluminum-, and iron-oxides (Schmidt et al., 2011). Since sample carriers are generally recycled from measurement to measurement, the luminescent film may build up with increased usage due to its impervious nature to cleaning.

Small sources of error have a relatively large influence on sediments with low OSL sensitivities. The goal of this study is to explore sample carriers as a possible source of contamination and devise an effective cleaning procedure in order to minimize equivalent dose distribution scatter. After determining the magnitude of contaminant signals from sample carriers, empty stainless steel cups were tested under measurement conditions typically used for sedimentary quartz. Multiple cleaning methods were conducted on stainless steel cups to eliminate contaminant signals. Modified cleaning procedures were developed for stainless steel cups based on the cleaning methods that produced the lowest and least variable contaminant signals. I investigate the effectiveness of our newly modified cleaning techniques by measuring equivalent doses of two Antarctic cobble surfaces with low OSL sensitivities using sample carriers cleaned prior to and after the adoption of our modified cleaning procedures.

2.2. METHODS

Measurements for this study were conducted at the Radiation Dosimetry Laboratory at Oklahoma State University using a Risø TL/OSL-DA-15 Reader manufactured by Risø National Laboratory including a built-in 90Sr/90Y beta source with an internal dose rate of 100 mGy s-1, and using OSL stimulation with blue LEDs (470 nm, 31 mW cm-2), infrared stimulation (IRSL) with an IR LED array (~875 nm, 110 mW cm-2), and detection in the UV band (Hoya U340, 7.5 mm, 340 nm peak; Bøtter-Jensen & Murray, 1999). A heating rate of 5°C s-1 in a N2-atmosphere was used for measurement stimulation above room temperature.

2.3. LUMINSCENCE SIGNAL FROM SAMPLE CARRIERS

2.3.1. MEASUREMENT SEQUENCE

Stainless steel cups as sample carriers manufactured by Risø DTU have a diameter of 9.8 mm and thickness of 0.5 mm. Raw material for the cups is PK11NB stainless steel (Mat.No. 1.4550, DIN X6CrNiNb18-10, AISI 347) from Metal Ravne (www.metalravne.com; H. Christiansen, pers. comm.). The cups have been recycled for several years and cleaned between measurements with our standard cleaning method (termed "Ethanol" in Appendix I) comprised of two 30-minute ultrasonic baths with de-ionized (DI) water and dish soap followed by individual cleaning with ethanol. Visually inspection of each cup insures all grains were removed during cleaning. All measurements on empty cups conducted in this study were not sprayed with silicone oil.

Nine cups were initially tested to determine whether empty stainless steel cups have contaminant signals by measuring OSL stimulation at room temperature and 125°C for 100 s.

Each data channel during OSL stimulation represents the signal emitted in 0.4 s. Further measurements were conducted on the same cups to observe the characteristics of contaminant signals under measurement conditions used for sedimentary quartz. After irradiation of 100 Gy, signals from empty cups were measured using OSL stimulation at room temperature and 125°C for 40 s. TL curves were recorded for the cups during pre-heat stimulation to 200°C followed by OSL stimulation (125°C, 40 s). IRSL stimulation is commonly used in SAR measurement sequences to bleach contaminant feldspars (Wallinga et al., 2002; Duller, 2003; Wintle and Murray, 2006) thus test were conducted to establish: (1) whether the cups have signal when exposed to IRSL stimulation (60°C, 100 s); and (2) how the signal changes when IRSL stimulation (60°C, 100 s) is used prior to OSL stimulation (125°C, 40s).

Measurements on the same nine cups were conducted with quartz (90-212 μm) extracted from an Antarctic beach cobble surface (sample CB10-059; Simkins et al., 2013a). Quartz grains (n=100-200) were adhered to the cups using silicone oil and the entire cup area was covered with a monolayer of quartz. To test whether contaminant OSL signals arise during sediment measurements, empty cups were irradiated with 100 Gy then covered the cups with bleached quartz. The quartz was pre-heated at 200°C for 60 s followed by IRSL stimulation at 60°C for 100 s and OSL stimulation at 125°C for 200 s. OSL signals of the irradiated cups with bleached sediment cover were measured at 125°C for 40 s following pre-heat (200°C, 10 s) and IRSL (60°C, 100 s) stimulations. Lastly, the cups and quartz were irradiated simultaneously with 100 Gy and OSL signals were measured following the same sequence as with bleached quartz.

2.3.2. RESUTLS

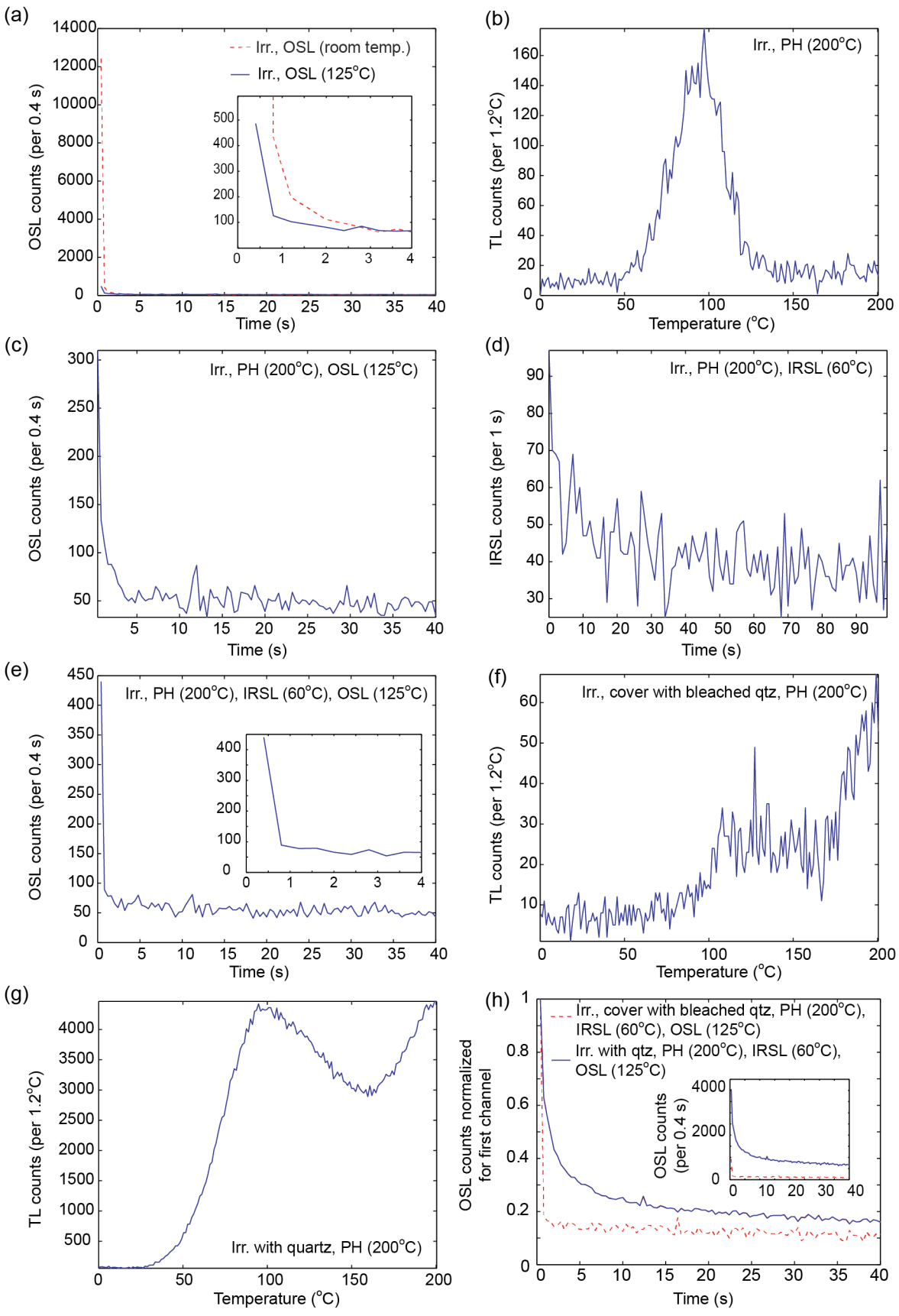
(a)
Irr., OSL (room temp.)
Irr., OSL (125°C)
OSL counts (per 0.4 s)
Time (s)
(b)
Irr., PH (200°C)
TL counts (per 1.2°C)
Temperature (°C)
(c)
Irr., PH (200°C), OSL (125°C)
OSL counts (per 0.4 s)
Time (s)
(d)
Irr., PH (200°C), IRSL (60°C)
IRSL counts (per 1 s)
Time (s)
(e)
Irr., PH (200°C), IRSL (60°C), OSL (125°C)
OSL counts (per 0.4 s)
Time (s)
(f)
Irr., cover with bleached qtz, PH (200°C)
TL counts (per 1.2°C)
Temperature (°C)
(g)
Irr. with quartz, PH (200°C)
TL counts (per 1.2°C)
Temperature (°C)
(h)
Irr., cover with bleached qtz, PH (200°C), IRSL (60°C), OSL (125°C)
Irr. with qtz, PH (200°C), IRSL (60°C), OSL (125°C)
OSL counts normalized for first channel
OSL counts (per 0.4 s)
Time (s)

Figure 1. Measurement of OSL signals from one representative empty cup out of nine measured cups. Irradiation of 100 Gy, pre-heat of 200°C for 10 s, and IRSL stimulation at 60°C for 100 s were used in all cases where mentioned. (a) Room temperature for 40 s (red dashed line) and 125°C for 40 s (blue line) following irradiation (irr.). (b) TL curve recorded during pre-heat (PH) stimulation following irradiation. (c) OSL curve measured at 125°C for 40 s following irradiation and pre-heat stimulation. (d) IRSL stimulation after irradiation and pre-heat stimulation. (e) OSL stimulation (125°C, 40 s) following irradiation and pre-heat and IRSL stimulation. Inset shows decay during the first 4 s of stimulation with the same y-axis. (f) TL curve from pre-heat stimulation (up to 200°C) using irradiated cups with bleached quartz covering the cup surface. (g) TL curve recorded during pre-heat to 200°C following cup and quartz irradiation. (h) Resulting OSL curves normalized for the signal in the first channel for bleached (red dashed line) and irradiated (blue line) quartz following irradiation, pre-heat and IRSL with an inset of the raw decay curves with the same y-axis as the normalized decay curves.

Stainless steel cups do not produce OSL signals in the absence of prior irradiation when measured at 125°C or room temperature (not shown) following cleaning with the standard cleaning method (Appendix I). Luminescence signals of samples carriers are shown for one representative stainless steel cup out of the nine measured empty cups. After irradiation of 100 Gy, the decay curves have fast components with background signals established by the first second of stimulation at both room temperature and 125°C (Figure 1a). OSL stimulation at room temperature produces higher signals than signals measured at 125°C. TL curves recorded during pre-heating (up to 200°C) show a prominent peak centered at 100°C (Figure 1b). OSL signals from empty cups are reduced to below 500 counts for all nine cups when pre-heating (200°C for 10 s) is used (Figure 1c). Empty cups show no signals above background when stimulated with IRSL with the exception of two of the nine cups with signals 20-30 counts above background (Figure 1d). OSL signals increase following IRSL stimulation (Figure 1c versus 1e). Contaminant signals from empty cups are not eliminated when pre-heat (200°C, 10 s) and IRSL (60°C, 100 s) stimulations are utilized prior to OSL stimulation (Figure 1e).

A TL curve recorded during pre-heating is shown for irradiated cups with bleached quartz covering the surface of the cups (Figure 1f) as well as for irradiated cups with

irradiated quartz (Figure 1g). The OSL curves for irradiated cups with bleached quartz (Figure 1h) shows fast decay as observed for all empty cup measurements. OSL decay curves resulting from irradiated cups with irradiated quartz (Figure 1h) show a slower component not observed from empty cups or cups covered with bleached quartz.

2.4. SAMPLE CARRIER SENSITIVITY TEST

2.4.1. MEASUREMENT SEQUENCE

Additional measurements on one empty cup were conducted to assess whether empty cups experience sensitivity changes during measurement sequences. The measurement sequence included nine repeated cycles of irradiation of 30 Gy followed by pre-heat (200°C, 10 s), IRSL (60°C, 100 s), and OSL (125°C, 40 s) stimulations.

2.4.2. RESULTS

OSL signals measured for the repeated cycles show less than 2 % deviation from the average OSL signal from the first channel of the nine cycles (Figure 2). The measurements suggest signals from stainless steel cups do not change sensitivity with repeated measurement cycles.

2.5. CLEANING PROCEDURES

2.5.1. MEASUREMENT SEQUENCE

Several cleaning techniques were applied to empty cups in addition to the standard cleaning method (Appendix I). Following two ultrasonic baths with dish soap and DI water, cleaning was performed with acetone, methanol, sand paper, and hydrofluoric acid (HF). In

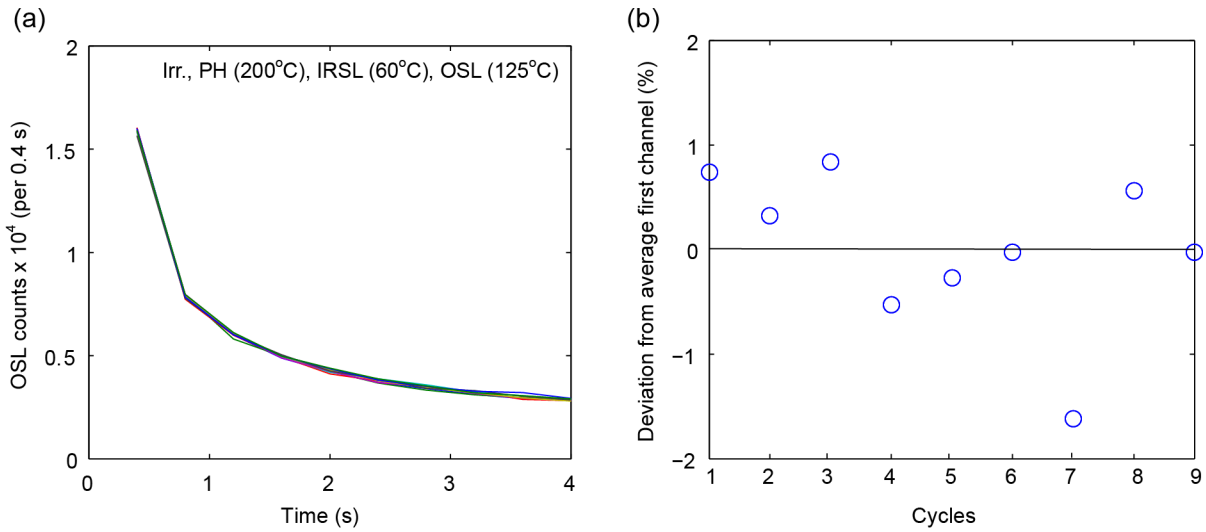

Figure 2. (a) Decay curves for one empty stainless steel cup during the first four seconds of OSL stimulation (125°C, 40 s) for nine measurement cycles including irradiation (30 Gy), pre-heat (200°C, 10 s), and IRSL (60°C, 100 s) prior to OSL stimulation. (b) Deviation in percent from average signal in first channel for the nine measurement cycles. The line at 0 along the y-axis represents the average signal.

addition, Alconox (Powdered Precision Cleaner, www.alconox.com), a detergent for ultrasonic removal of silicone oils, and Rust Stain Remover (manufactured by Whink), containing approximately 3% HF, were tested as substitutes for dish soap in the ultrasonic baths. An approximate mixing ratio of 10 g of Alconox per 1 liter of DI water was used. The ultrasonic baths with Rust Stain Remover contained 1 part Rust Stain Remover to 3 parts DI water. Each cleaning method was conducted on five randomly selected empty cups that have been previously used for sediment measurements. New (i.e. unused) cups were also tested for luminescence signals including five new cups with no cleaning treatment and five new cups cleaned with Alconox.

The higher the signal the better the resolution for testing the effectiveness of cleaning methods. For this reason, measurements of individual cleaning techniques and modified cleaning procedures were conducted with OSL stimulation at room temperature (see Figure 1a). In order to determine the dose-dependency of the cups using various cleaning

procedures, OSL signals were measured for 100 s at room temperature after irradiation of 0, 1, 10, 50, and 100 Gy. The reported signals are the sum of the first two seconds of stimulation. The slow component was removed by subtraction of the background signal (last 10 s). The cleaning methods that produced the lowest, least variable signals from the cups were combined to create modified cleaning procedures. Modified cleaning procedures were applied to the cups and tested by measuring OSL signals at room temperature for 100 s after irradiation of 100 Gy.

2.5.2. RESULTS

Irrespective of the cleaning method, OSL signals were not observed for stainless steel cups that were not irradiated prior to OSL stimulation (not shown). Results from irradiated cups cleaned with various treatments are summarized in Figure 3. Dose response curves (Appendix II) for cups cleaned with each individual cleaning technique show, with a few exceptions, a linear trend in signal growth with increased irradiation dose. Even after 1 Gy, empty cups cleaned with ethanol, acetone, and sand paper produced luminescence signals above background (> 100 counts). After irradiation of 100 Gy, cups have OSL signals up to 53000 counts. Cleaning with ethanol (standard cleaning method), acetone, and sand paper produced the highest, most variable signals suggesting these methods are least effective in removing the luminescence signal of the cups. The use of methanol, HF (48%), Alconox, and Rust Stain Remover (3 % HF) produced the lowest and least variable OSL signals.

A combination of the most effective methods was adopted to create two modified cleaning procedures for stainless steel cups (Table 1). Method (1) consists of ultrasonic

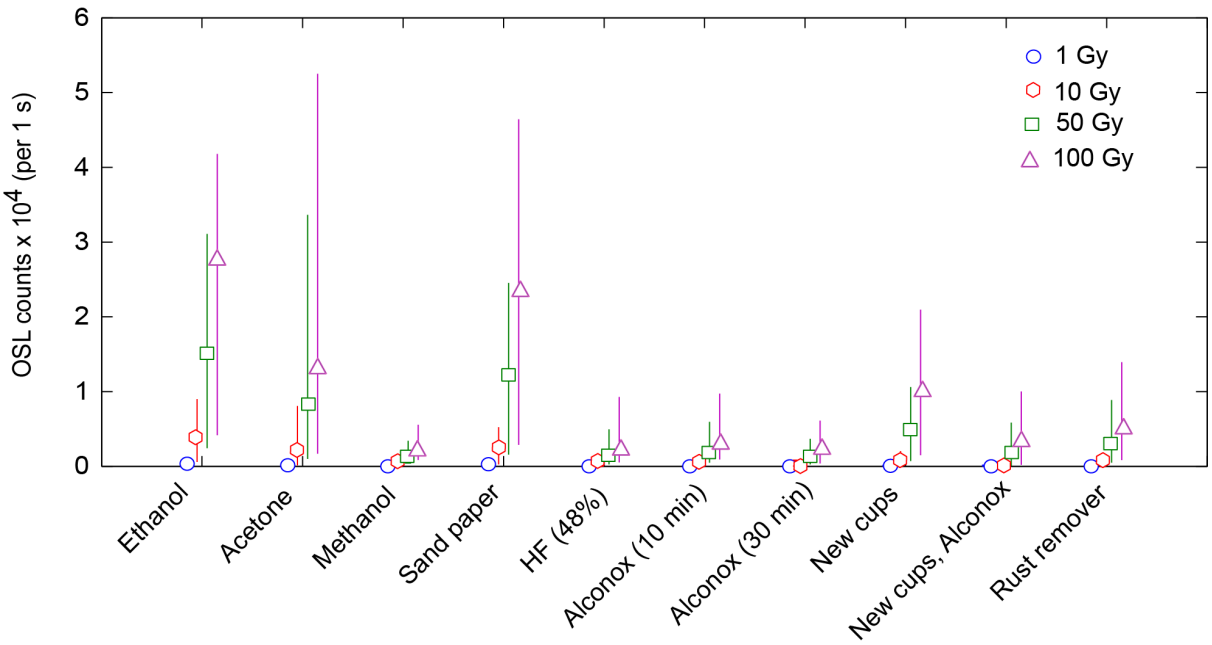

Figure 3.OSL signals measured at room temperature for 100 s from five empty stainless steel cups cleaned with various methods (see Appendix I for details) listed along the x-axis. The signals include the integral from the first two channels. The error bars represent the range of signals from the five empty cups cleaned with the same method and irradiated with the same dose while the points represent the averages. OSL measurements were conducted after irradiation doses of 1, 10, 50, and 100 Gy.

baths with Alconox, etching with 48% HF for 5 minutes, and individual scrubbing with methanol. Method (2) is similar to method (1) with the exception of using Rust Stain Remover instead of 48% HF. A total of 240 and 130 cups were cleaned with cleaning methods (1) and (2), respectively. The cleaning methods were tested on cups using irradiation of 100 Gy followed by OSL at 125°C for 100 s. The majority of cups (61%) cleaned with method (1) have OSL signals between 100-500 counts with only 2 % of the cups with signals < 100 counts. The majority of cups (89%) cleaned using method (2) have signals less than < 500 counts with a larger percentage (41%) of cups with signals below 100 counts.

2.6. IMPACT OF CONTAMINATION ON EQUIVALENT DOSES

2.6.1. MEASUREMENT SEQUENCE

OSL measurements from two quartz isolates (90-212 μm; 100-200 grains) extracted from buried Antarctic cobble surfaces were measured using stainless steel cups cleaned with our standard cleaning method (Appendix I). See Simms et al. (2011) for details on sediment sample preparation. Equivalent doses were determined following the SAR measurement protocol (Murray and Wintle, 2000) using the same laboratory facilities and stimulation and detection windows mentioned in the methods section. Measurement sequences included pre-heat (200°C, 10 s), cut-heat (180°C, 10 s), and IRSL (60°C, ≤ 100 s) stimulations, OSL stimulation at 125°C for 100 s followed by high-temperature OSL stimulation (240°C, 10 s; Murray and Wintle, 2003). The first two channels of the OSL signal curve were used as the signal for equivalent dose calculations. The slow component of the OSL curve was removed by subtraction of the background signal (last 10 s). Passing aliquots are determined by having recycling ratios < 20 %, recuperation tests with values < 10 %, and dose recovery ratios < 25

Table 1. Modified sample carrier cleaning methods

Cleaning method (1) - Alconox, HF, and methanol	
Step 1:	Rinse with DI water
Step 2:	30-minute ultrasonic bath with Alconox at 70°C
Step 3:	Rinse with DI water
Step 4:	Etch with 48% HF for 5 minutes
Step 5:	Rinse with DI water
Step 6:	30-minute ultrasonic bath with Alconox at 70°C
Step 7:	Rinse with DI water
Step 8:	Scrub each cup with methanol using a cotton swab
Cleaning method (2) - Alconox, Rust Stain Remover, and methanol	
Step 1:	Rinse with DI water
Step 2:	1-hour ultrasonic bath with Alconox at room temperature
Step 3:	Rinse with DI water
Step 4:	1-hour ultrasonic bath with Rust Stain Remover at room temperature
Step 5:	Rinse with DI water
Step 6:	1-hour ultrasonic bath with Alconox at room temperature
Step 7:	Rinse with DI water
Step 8:	Scrub each cup with methanol using a cotton swab

%. The dose recovery test differs from the dose recovery test suggested by Wintle and Murray (2006) which refers to the recovery of a dose that was administered to unheated bleached aliquots. Statistical modeling following the common age model (Galbraith et al., 1999) yielding a weighted log paleodose was used to determine the most representative equivalent dose from dose distributions. The effectiveness of our modified cleaning methods is tested by re-measuring equivalent doses of the same sediment samples using cups without contaminant signals. The measurement sequence for re-measured samples was identical to the sequence used for equivalent doses from measurements using contaminant-signal cups.

2.6.2. RESULTS

Large intra-sample scatter is evidenced in radial plots of equivalent dose distributions derived from quartz extracted from buried Antarctic cobble surfaces using cups cleaned with the standard cleaning method (Figure 4a). The scatter is quantified as overdispersion calculated by dividing the standard deviation of all passing aliquots by the simple average of equivalent doses shown as "OD" in the top left of the radial plots. Dose distributions of re-measured samples (Figure 4b) using cups cleaned with modified cleaning method (2) with Rust Stain Remover show the majority of aliquots plotting within the equivalent dose estimate from the age model. The re-measured equivalent doses show less scatter than equivalent doses derived from measurements with cups with contaminant signals. Equivalent doses for the two samples after the adoption of our modified cleaning procedure are higher than for measurements using cups with contaminant signals (Table 2). OSL signals measured

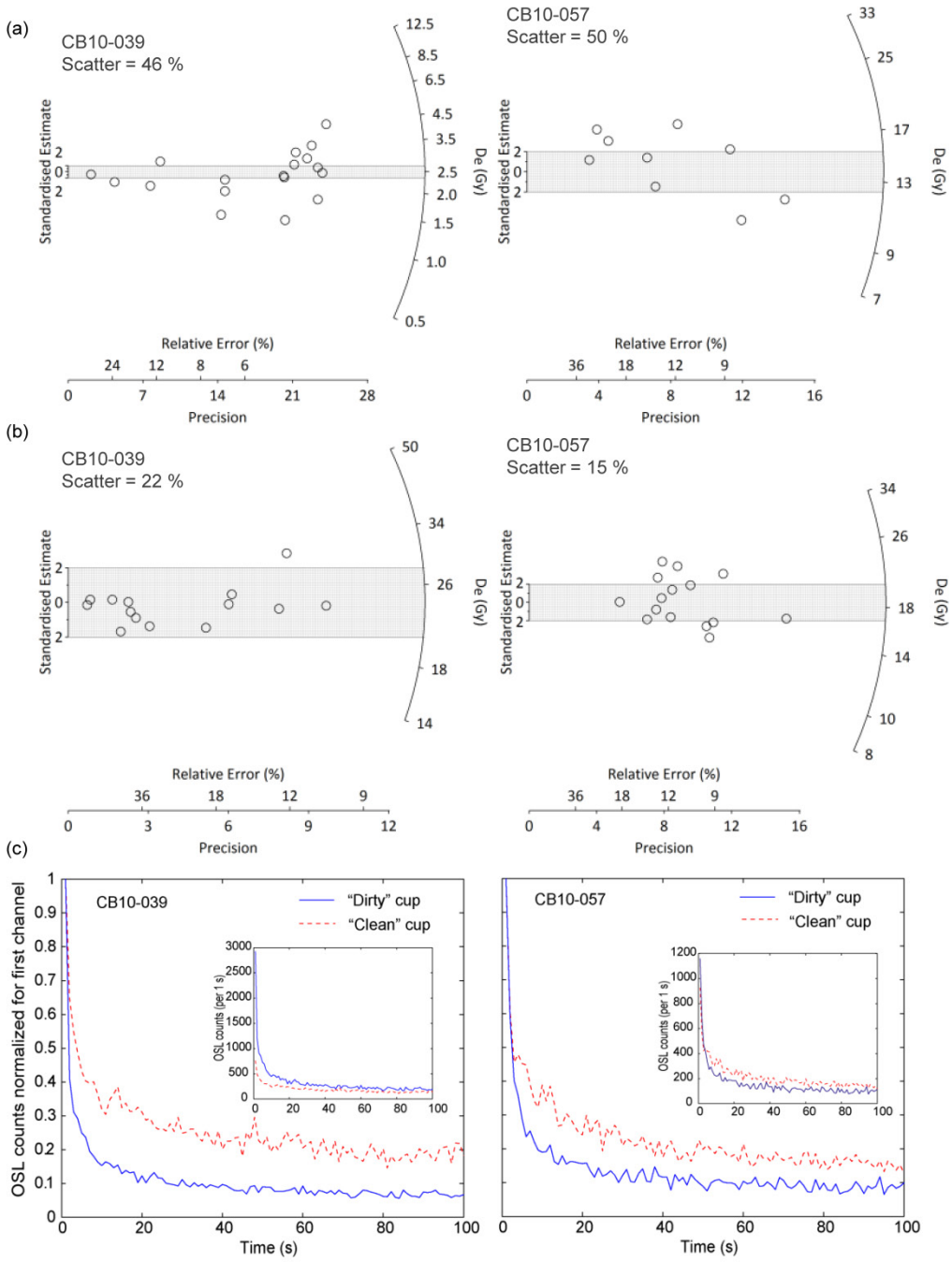

Figure 4. (a) Radial plots showing equivalent doses distributions from two quartz samples (CB10-039 and -057) from Antarctica cobble surfaces derived from measurements made using stainless steel cups cleaned with the standard cleaning method. (b) Re-measured equivalent doses distributions from the same samples using neutral-signal cups cleaned with modified cleaning method (2). (c) OSL decay curves normalized for the signal in the first channel for samples CB10-039 and CB10-057 after irradiation of 30 and 50 Gy, respectively, using cups with contaminant signals (blue line) and neutral signals (red dashed line). The inset shows the raw OSL decay curves with signal in counts per second.

after irradiation of 30 and 50 Gy for CB10-039 and CB10-057, respectively, show faster decay curves when quartz is measured on cups with contaminant signals (Figure 4c).

2.7. DISCUSSION

2.7.1. LUMINESCENCE SIGNALS FROM SAMPLE CARRIERS

Both new and previously used empty stainless steel cups produce dose-dependent signals when measured at 125°C as well as at room temperature. Figure 1 summarizes the characteristics of contaminant signals from stainless steel cups. Contaminant signals from empty cups are not eliminated by the thermal pre-treatment (pre-heat for 10s at 200°C) or the prior exposure to IRSL stimulation (60°C, 100 s). Covering the surface of the cups with bleached quartz does not mask the contaminant signals. On the contrary, despite ensuring the quartz used was bleached, OSL signals increase with cups covered with bleached quartz using the same sequence with pre-heat and IRSL stimulations (Figure 1e and 1h). Sensitivity changes could potentially explain the higher signals; however, considering sensitivity changes are not observed for empty cups (Figure 2), the higher signals cannot be attributed to sensitivity changes during measurement sequences. The fast nature observed from empty cups and cups covered with bleached quartz is not observed under typical sediment measurement conditions with irradiated quartz most likely due to the combination of slower OSL decay from the quartz with fast decay from the cups themselves (Figure 1h). Contaminant signals from stainless steel cups used as sample carriers are: (1) impervious to standard cleaning methods, (2) not eliminated using typical measurement conditions for sedimentary quartz (e.g. thermal preheating, IRSL stimulation and elevated OSL stimulation, and (3) not masked by sediment covering the cups. These findings are in support of the work

of Schmidt et al. (2011) who suggest the presence of contaminant signals from sample carriers.

2.7.2. CLEANING METHDOS

Previously used and new cups have contaminant signals when cleaned with multiple techniques; however, signals were not observed without prior irradiation. The signals observed following various cleaning methods (Figure 3) suggests the contaminant signal from stainless steel cups is variable and dose dependent. Considering sensitivity changes were not observed for empty cups, the growth in signal magnitude with increasing irradiation dose most likely results from the dose-dependency of the contaminant signals.

Signals produced by new stainless steel cups most likely result from silicone oil used in manufacturing of the cups. Luminescence signals from previously used cups most likely arise from reactions that take place upon heating and irradiation of previously used cups resulting in luminophores derived from defects in silica-, aluminum-, and iron-oxides (Schmidt et al., 2011). The standard cleaning method does not sufficiently remove OSL signals from new and previously used cups. However, the most effective cleaning methods for stainless steel cups including methanol, Alconox, HF (48 %), and Rust Stain Remover (3 % HF).

Modified cleaning procedures (Table 1) minimize luminescence signals produced by stainless steel cups. Both cleaning procedures use HF in different concentrations. HF is well known for its ability to dissolve iron- and silica- oxides and is commonly used to remove impurities from stainless steel. Of the two cleaning methods, method (2) is more effective at reducing the signal to less than 100 counts or otherwise close to background signals (Figure

Table 2. Equivalent doses (D_e) of Antarctic cobble surfaces

Sample	Contaminated cups D_e (Gy)	Neutral cups D_e (Gy)
CB10-039	2.46 ± 0.03	24 ± 1
CB10-057	13.7 ± 0.5	24.5 ± 0.5

3). Additionally, although HF is present in Rust Stain Remover, cleaning method (2) eliminates the use of strong concentrations of HF.

We advise that following the first use of either modified cleaning procedure, cups should be tested for luminescence signals following irradiation of 100 Gy. Cups that produce signals above 100 counts should be discarded or re-cleaned and re-tested prior to use of equivalent dose measurement of dim quartz. However, for brighter quartz, contaminant signals from stainless steel cups > 100 counts may be acceptable. After cups are initially cleaned and used in sample measurements, routine tests on the cups after each cleaning treatment are recommended by selecting five clean cups at random to verify that the cups have signals less than 100 counts.

2.7.3. IMPACT OF CONTAMINATION ON EQUIVALENT DOSES

Luminescence signals from stainless steel cups contaminate OSL measurements of sedimentary quartz (Figs. 1 and 4). Considering signals from cups are dose-dependent, natural signals from sediment OSL measurements for dating purposes are not contaminated by sample carriers; however, the dose response curve results from a combination of signals from sediments and stainless steel cups were identified. The resulting higher equivalent doses of sediment samples (Table 2) using cups with no signal suggest that the dose-dependent luminescence signals from stainless steel cups previously dominated the dose

response curve without contributing to the natural signal from dated samples. When using cups with contaminant signals, sediment natural signals appear relatively small compared to regenerated dose responses thus equivalent dose estimates underestimate true OSL ages. Our modified cleaning methods allow for more robust sample measurements and equivalent dose estimates for Antarctic cobble surfaces with low OSL sensitivities.

2.8. CONCLUSIONS

Variable, dose-dependent luminescence signals are produced by new and previously used empty stainless steel cups used as sample carriers for OSL measurements. Contaminant signals are reduced but not eliminated using pre-heat (200°C, 10 s) and IRSL (60°C, 100 s) stimulations. Signals generated by the cups are not masked by sediment cover. The remaining contaminate signal from stainless steel cups introduce a source of error for OSL measurements of sedimentary quartz. Our standard cleaning method is not effective in removing the luminescence signal from stainless steel cups. Two modified cleaning methods combine the use of Alconox, HF (48% and 3%), and methanol in order to reduce unwanted signals from new and used stainless steel cups. After cleaning cups using our modified cleaning methods, much of the dose distribution scatter initially observed for Antarctic cobble surfaces is resolved. The application of these cleaning methods to stainless steel cups used as sample carriers reduces signal contamination of low OSL sensitivity quartz where typically small sources of error can produce relatively large measurement uncertainty. Our modified cleaning methods may potentially be useful for other applications of luminescence methods to produce more robust measurements void of unwanted contamination from sample carriers.

CHAPTER 3

INVESTIGATION OF OPTICALLY STIMIULATED LUMINESCENCE CHARACTERISTICS OF COBBLE SURFACES: A LOOK FORWARD

3.1. INTRODUCTION

Optically stimulated luminescence (OSL) dating provides an alternate means to obtain burial ages of late Quaternary sediments, particularly in locations where material for radiocarbon dating is limited. OSL dating is commonly applied to fine-grained deposits as traditional techniques are suitable for grains < 250 μm in diameter. Recent studies utilize OSL to date buried pebble and cobble surfaces (Simms et al., 2011; Sohbati et al., 2011; Simms et al., 2012; Simkins et al., 2013a; Kenworth et al., 2014). The application of dating cobble surfaces with OSL is a relatively novel approach, therefore, the previous challenges encountered – most notably low OSL sensitivity, poor measurement reliability, and equivalent dose scatter – when dating these cobble surfaces (Simkins et al., 2013a,b) can provide insight on potential improvements to the methodology. Additionally, assumptions necessary for dose-rate calculations could potentially cause under- or over-estimation of OSL ages.

A requirement for OSL dating is that samples must have detectable signals above background measurements; however, OSL measurements of cobble surfaces have shown low

OSL sensitivity (Sohbati et al., 2011; Simkins et al., 2013a). Sediment history is a major control of OSL sensitivity (Preusser et al., 2006; Pietsch et al., 2008; Zheng et al, 2009) where sensitivity increases with repeated natural (Pietsch et al., 2008; Fitzsimmons et al., 2009; Zheng et al., 2009; Sawakuchi et al., 2011) and laboratory-induced (McKeever et al., 1996; Moska and Murray, 2006) cycles of burial and exposure. Coastal sediments from Brazil (Sawakuchi et al., 2011) and Australia (Pietsch et al., 2008) have magnitudes higher OSL sensitivities than their respective source rocks and fluvial sediments. Luminescence sensitivity changes are most likely caused by an increase in the amount of traffic between electron traps and hole traps capable of producing luminescence (Pietsch et al., 2008). The low OSL sensitivity of Antarctic cobble surfaces could result from limited transport history. Antarctic beach sediment is typically transported solely by glacial processes that are less efficient at reworking sediment than fluvial processes. As a result of this limited transport history, Antarctic beach sediment experiences fewer exposure-burial cycles compared to sediment transported by fluvial processes.

Thermal histories (i.e. crystallization temperatures) are important for determining OSL behavior. The type and amount of crystal defects in silicate minerals is largely controlled by the temperature of crystallization (Dennen et al., 1970; Göetze et al., 2001; Preusser et al., 2009; Sawakuchi et al., 2011). Defects are responsible for trapping the free electrons that are utilized for OSL dating. Typically these defects result from the incorporation of impurities during crystallization, most notably oxygen and silicon vacancies (Preusser et al., 2009). The variable petrology and thus thermal histories of cobbles may influence OSL characteristics such as equivalent dose scatter and measurement sensitivity and reliability.

Another source of error in OSL ages of cobble surfaces stem from the assumptions made for dose-rate calculations. Water in the pore space of the beach sediment absorbs radiation and reduces the effective dose rate. Typically material is taken during field sampling to determine the water content; however, due to the coarse, open-framework nature of many Antarctic beaches, representative material could not be recovered to estimate the water content for dose rate calculations (Simms et al., 2011; Simms et al., 2012; Simkins et al., 2013a). Thus assumptions about water content must be made in order to calculate dose rates. Several factors have an influence on the water content of the material surrounding the selected cobble including: (1) pore volume, (2) snow cover, (3) density of snow, (4) density of the sample, and (5) percentage of filled pores. Some of these factors have likely not been constant throughout the burial history causing temporal changes in the radiation environment; however, reasonable values for the factors included in water content calculations were used based on modern meteorological conditions and field observations. Beta radiation is attenuated during its passage through a grain, so that the beta dose rate depends on grain size. In previous studies, the mean quartz crystal size was used to correct for beta dose rate attenuation (Mejdahl, 1979) within individual quartz crystals extracted from Antarctic beach cobbles. Crystal size was determined using two methods: (1) by manual measurement of quartz size in images of thin sections; and (2) using an image analysis program in Matlab (Trauth, 2010). Both methods, however, have large uncertainty due to sampling bias, pixel resolution, and irregular crystal shape. One of the lingering questions associated with dose-rate assumptions is how much the dose rate – and subsequently the age – of samples will change if water content parameters and crystal size vary.

Possible improvements to the methodology for dating Antarctic cobble surfaces include: (1) determining the cause for low OSL sensitivity observed from cobble surfaces from Calmette Bay, Antarctic Peninsula (Simkins et al., 2013a); (2) identifying whether specific petrologies provide more reliable OSL ages; and (3) assessing the influence of dose-rate assumptions on OSL ages. For this study, cathodoluminescence (CL) was measured for thin-sections of OSL-dated samples as well as samples with no natural signal. The traps that produce luminescence utilized for OSL dating also produce CL in the visible range. Therefore, CL analysis can provide insight on the number of crystal defects available for producing luminescence. Petrographic analysis of thin sections was conducted to identify the rock types and mineral assemblages and estimate the amount of quartz within each cobble. The findings from the petrographic and CL analyses are then compared to OSL characteristics to determine the cause of low OSL sensitivity and determine physical properties of samples that provide the most reliable OSL ages. As only part of the age stems from OSL measurements, modeling of dose-rate parameters was conducted to assess the influence of assumptions used to calculate OSL ages.

3.2. METHODS

3.2.1. OSL MEASUREMENTS

Quartz fractions (63-250 μm) were extracted from Antarctic beach cobble surfaces following the sediment preparation of Simkins et al. (2013a). OSL measurements were conducted using a Risø TL/OSL-DA-15 Reader manufactured by Risø National Laboratory with a built-in $^{90}Sr/^{90}Y$ beta source at Oklahoma State University. The internal beta source dose rate ranged from 92.3-94.5 mGy s^{-1} over the duration of this study. Optical stimulation

was carried out with blue LEDs (470 nm, 31 mW cm^{-2}) and infrared (IR) stimulation with LEDs (~875 nm, 110 mW cm^{-2}) using a UV (Hoya U340, 7.5 mm, 340 nm peak) detection window (Bøtter-Jensen & Murray, 1999) with a heating rate of 5°C s^{-1} and 1 measurement reading per second. Natural signals (counts after 1s of stimulation) were measured using OSL stimulation (125°C, 100s) following IR stimulation (60°C) varying between 20 and 100 s depending on sample feldspar contamination.

3.2.2. CATHODOLUMINESCENCE

CL analysis of thin sections of Antarctic beach cobbles was measured using an optical microscope (Nikon Labophot) with a cold cathode electron gun attachment (Marshall, 1988) at California State University Chico. The applied beam current density was 0.8-1.2 μA mm^{-2} at 7-11 keV electron energy under a vacuum of 40-50 mTorr. The CL images show qualitative emission intensity of the visible range of the electromagnetic spectra overlapping with the OSL detection range at ~300-380 nm (Preusser et al., 2009).

3.2.3. MINERALOGICAL ANALYSIS

Petrographic analysis of thin sections was conducted at the University of California Santa Barbara. Qualitative modal proportions of quartz and feldspar were used to identify the petrology of the samples based on the classification of Le Maitre (2002). Pleochroism, interference colors, cleavage/fracture, and crystal form/habit were used to identify primary, secondary, and accessory minerals. Energy dispersive spectroscopy (EDS) was conducted using a FEI Quanta 400f scanning electron microscope on samples CB2, CB3, CB6, CB33,

CB21, and CB52 to estimate elemental composition of grains used for OSL measurements assumed to be composed of quartz.

3.2.4. DOSE-RATE MODELS

In order to test the influence of variable water content conditions, dose rate variations were calculated for a range of values for the amount of water filled pores, volume of cobbles, surrounding material density, snow cover, and crystal size. Dose rates are calculated by varying one parameter at a time while the other parameters are held constant using the standard values shown in (Table 2, found in Chapter 2) and realistic values for Antarctic beach cobbles. The open-framework and poorly sorted nature of Antarctic beaches results in heterogeneous dose rates between the dated sample and surrounding material; therefore, the total dose rate was calculated by using dosimetry measurements from both the dated sample and a weighted average of 2-3 representative surrounding cobbles. Half of the beta radiation affecting the buried part of the cobble surface originated from the OSL-dated cobble itself and the other half from the surrounding material. The total dose rate D_t is calculated using:

$$\frac{DR_{\beta\ cobble}}{2} + \frac{DR_{\beta\ surr\ wet}}{2} + \frac{DR_{\gamma\ cobble}}{2} + \frac{DR_{\gamma\ surr\ wet}}{2} + DR_{cosmic} \quad (1)$$

where $DR_{\beta\ cobble}$ and $DR_{\beta\ surr\ wet}$ are the beta dose rates and $DR_{\gamma\ cobble}$ and $DR_{\gamma\ surr\ wet}$ are the gamma dose rates for the dated cobble and surrounding material, respectively. Values for the surrounding material corrected for water content are termed wet. DR_{cosmic} is the cosmic dose rate calculated from a cosmic flux model following Prescott and Stephan (1982) and Barbouti and Rastin (1983). A value of 0.567 Gy ky^{-1} is used for $DR_{\gamma\ cobble}$ and 0.2042 Gy ky^{-1} is used for DR_{cosmic}. An attenuation correction factor is applied to the $DR_{\beta\ cobble}$ as beta dose absorption is dependent on grain size (Medjahl, 1979) or rather crystal size for material

extracted from cobble surfaces. Crystal size is determined using two methods: (1) by manual measurement of quartz in thin section images; and (2) using an image analysis program in Matlab (Trauth, 2010). Both methods, however, have a large uncertainty due to sampling bias, pixel resolution, and irregular crystal shape. Consequently, a standard estimate of error equivalent to 50% of the attenuation correction factor is applied. The $DR_{\beta\ cobble}$ is calculated by:

$$aX_U Y_U + bX_{Th} Y_{Th} + cX_K Y_K \quad (2)$$

where *a*, *b*, and *c* are the attenuation correction factors following Medjahl (1979). X_U, X_{Th}, and X_K are the ratios between dose rate and concentration in parts per mil for U, Th, and K and Y_U, Y_{Th}, and Y_K are the concentrations of U, Th, and K in parts per mil. $DR_{\beta\ surr\ wet}$ and $DR_{\gamma\ surr\ wet}$ are calculated using equations 3 and 4, respectively.

$$DR_{\beta\ surr\ wet} = \frac{DR_{\beta}\ dry}{1+1.25W} \quad (3)$$

$$DR_{\gamma\ surr\ wet} = \frac{DR_{\gamma}\ dry}{1+1.14W} \quad (4)$$

where $DR_{\beta\ dry}$ and $DR_{\beta\ dry}$ are the beta and gamma dose rates for the surrounding material with values of 1.268 Gy ky^{-1} and 2.591 Gy ky^{-1}, respectively, and W is water content calculated using equation (5).

$$W = \frac{\rho_{snow}\ V_{pores}\ S\ P}{V_{cobble}\ \rho_{cobble}} \quad (5)$$

where ρ_{snow} and ρ_{cobble} are the densities of snow/ice/water (0.8 g cm^{-3}) and the dated cobble (2.6 g cm^{-3}), respectively. V_{pores} is the volume of pore space, S is the annual snow cover duration, P is the percentage of filled pores, and V_{cobble} is the percentage of cobbles equivalent to 1-P.

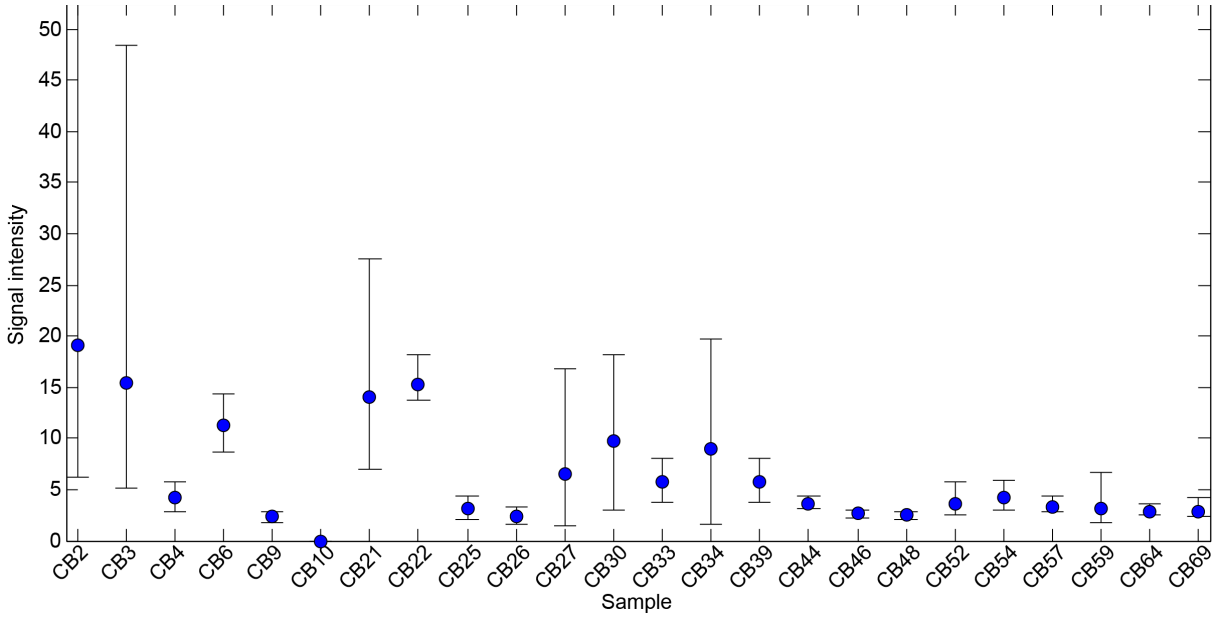

Figure 5. Natural signal intensity relative to background signals of 10 measured aliquots for each sample. The blue circles show the average of the aliquots and the vertical bars show the range of signal intensities. The natural signal is the counts measured during the first second of stimulation and the background is the average of the last 10 s of stimulation.

3.3. RESULTS

3.3.1. OSL CHARACTERISTICS

A requirement for OSL dating is that samples must have detectable signals above background measurements. Intensity of natural signals (counts after 1 s stimulation) is shown relative to background measurements (average counts from last 10 s of stimulation) from 10 aliquots for each sample (Figure 5). Measurements of natural signals from Antarctic cobble surfaces show a range of signal intensities from non-detectable signals to signals 50 times greater than background. Samples CB4, CB9, CB25, CB26, CB44, CB46, CB48, CB52, CB54, CB57, CB59, CB64, and CB69 have average natural signals less than 5 times background signals while samples CB2, CB3, CB6, CB21, CB22, CB27, CB30, CB33, CB34, and CB39 have signals greater than 5 times background signals. Sample CB10 does not have signals detectable above background.

Samples that have signals above background were dated in a previous study by Simkins et al. (2013a) where samples often showed poor measurement reliability observed from standard reliability tests (Murray and Wintle, 2000) included in the SAR measurement protocol. The percentage of passing aliquots from the total measured aliquots shows that the majority of aliquots (>50%) for each sample fail reliability tests (Table 3). Additionally, the dated samples show significant scatter in equivalent doses from a population of aliquots. Scatter in equivalent doses is shown as overdispersion calculated by dividing the standard deviation of all passing aliquots by the simple mean of the population of aliquots (Table 3).

OSL decay curves are useful for determining the behavior of signal decay during stimulation. Classification of the decay behavior is based on the percentage of the natural signal remaining after 5 s of stimulation where samples with relatively fast decay show < 50% of the natural signal remains after 5 s of stimulation and relatively slow decay is characterized by > 50% of the natural signal remaining after 5 s of stimulation (Table 3). Examples of the decay behavior are shown in Figure 6. Two samples (CB34 and CB52) have variable decay behavior with some aliquots characterized by fast decay and others with slow decay (Figure 6c).

3.3.2. CATHODOLUMINESCENCE

From the CL measurements, the samples are separated into groups based on qualitative emission colors in the visible range of quartz (Table 3). The images for samples CB4, CB6, CB10, CB39, and CB59 show predominantly dark blue emissions with light violet centers (Figure 7a-c). Samples CB2, CB3, CB25, CB26, CB33, and CB57 show dark blue with orange centers (Figure 7d). Samples CB21, CB22, and CB54 emit dark blue to

Table 3. OSL and CL characteristics

Sample	Passing aliquots[a] (%)	Overdispersion[b] (%)	Decay behavior[c]	Quartz CL characteristics
CB2	39	23	F	Dark blue with orange centers
CB3	45	74	F	Dark blue with orange centers
CB4	46	18	F	Dark with light violet centers
CB6	46	15	F	Dark blue with light violet centers
CB9	60	235	S	na
CB10	0	na	No signal	Dark blue with violet centers
CB21	40	223	F	Dark blue to violet with light violet centers
CB22	78	69	F	Dark blue to violet with light violet centers
CB25	40	75	S	Dark blue with orange centers
CB26	23	63	S	Dark blue with orange centers
CB27	44	39	S	Dark blue with violet centers
CB30	30	49	F	na
CB33	33	56	S	Dark blue with orange centers
CB34	40	73	Variable	Granular violet with blue centers[ŧ]
CB39	44	26	S	Dark with light violet centers
CB44	72	48	S	na
CB46	44	36	S	na
CB48	27	21	S	na
CB52	20	14	Variable	Granular violet with blue centers[ŧ]
CB54	0	na	F	Dark blue to violet with light violet centers
CB57	38	32	S	Dark blue with orange centers
CB59	13	na	S	Dark with light violet centers
CB64	24	64	S	na
CB69	35	21	S	na

[a] Percentage of aliquots passing standard SAR procedure tests out of all measured aliquots

[b] Overdispersion was calculated by dividing the standard deviation of all passing aliquots by the simple mean D_e

[c] Determined by percentage of natural signal after 5 s of stimulation where fast (F) < 50% and slow (S) > 50% of the signal remains

[ŧ] No quartz

violet with light violet centers (Figure 7e). Samples CB34 and CB52 do not contain quartz (discussed in Section 3.2.3); however, are characterized overall by a granular texture with dark and light violet emissions (Figure 7f).

3.3.3. MINERALOGICAL ANALYSIS

The rock types and primary, secondary, and accessory minerals of the samples are summarized in Table 4 with mineral abbreviations following Kretz (1983) and (Sivolla and Schmidt, 2007). The majority of the samples are hornblende quartz-monzodiorites with accessory apatite and monzanite and secondary alteration of hornblende (chlorite) and feldspar and hornblende (epidote). Quartz in the hornblende quartz-monzodiorites is limited (5-10%) and is often has a myrmekite texture, vermicular intergrowths in feldspar (Figure 8). Samples CB3 and CB26 are quartz monzonites with less hornblende and plagioclase than the hornblende quartz-monzodiorites and < 10% quartz. Samples CB6 and CB10 are hornblende diorites with < 5% quartz, accessory titanite, and no secondary alteration. CB39 is the most felsic sample containing mostly feldspar, some quartz (~30%), and accessory titanite with secondary alteration of hornblende (chlorite/biotite) and feldspar and hornblende (epidote). Two samples (CB34 and CB52) are syenites containing potassium feldspar, plagioclase, and epidote. Syenites have no quartz as they are under-saturated in silica. Qualitative elemental concentration spectra of the grains prepared and used for OSL measurements show a wide range of elements typically not associated with quartz (Figure 9). CB2, CB3, CB6, CB33 contain quartz dominated by silica, oxygen, and calcium peaks as well as possibly amphibole and potassium feldspars. Samples CB21, CB33, and CB52 (syenite) do not appear to contain quartz, however, are dominated by minerals high in Fe, Al, K, and Ca. The relatively high abundance of aluminum and fluorine when compared to silica suggests the material remaining after chemical preparation is contaminated with clay-like residue produced during chemical reactions with HCl and HF.

3.3.4. DOSE-RATE MODELS

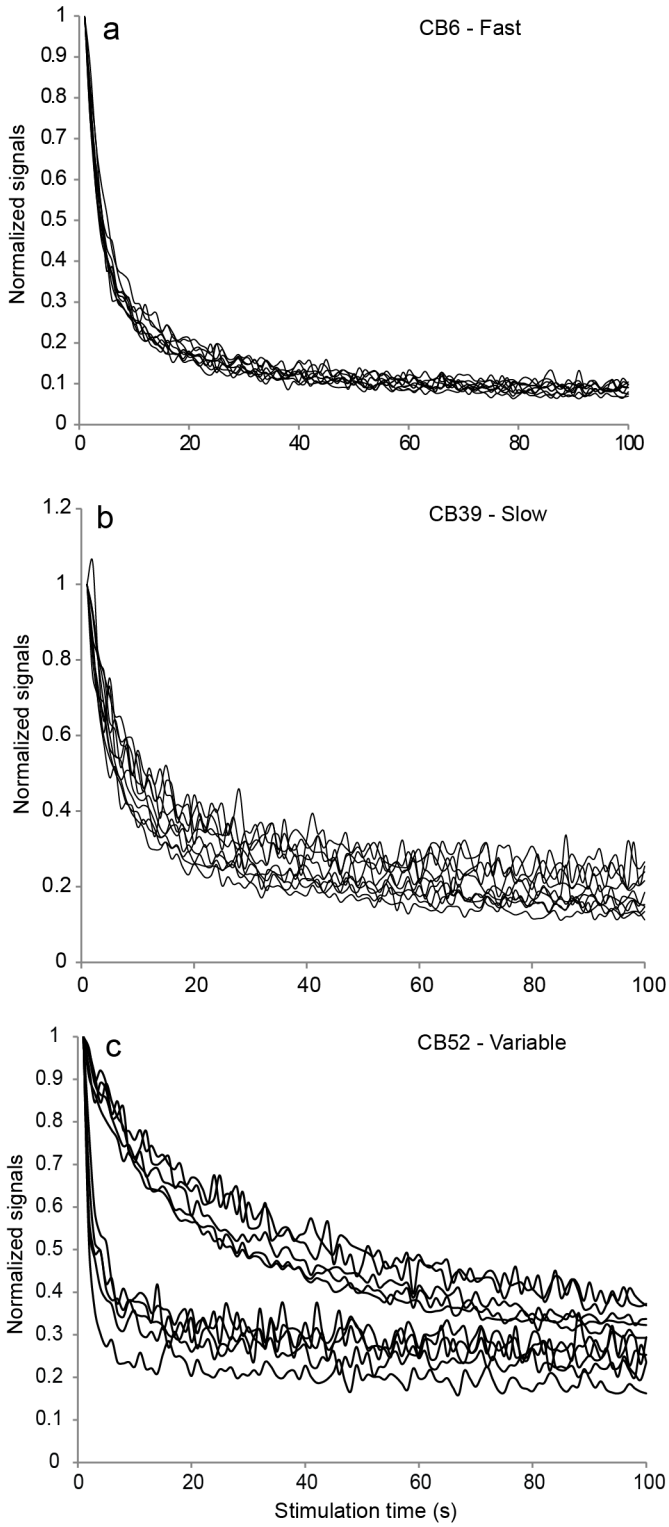

Figure 6. Examples of representative OSL decay curves of natural signals showing (a) fast, (b) slow, and (c) variable decay behavior (see text for decay classification) normalized to the first second of stimulation.

Models of the influence of water content parameters and crystal size on calculated total dose rates are shown in Figure 10. An increase in the density of surrounding material (Figure 10a) and volume of cobble packing (Figure 10b) causes an increase in the total dose rate. A linear decrease in total dose rate is observed when the amount of filled pores (Figure 10c) and snow cover (Figure 10d) are increased. An increase in crystal size results in an exponential decrease in the total dose rate (Figure 10e). Crystal size has the largest influence on dose rate calculations producing estimates from 2.5-3.4 Gy ky^{-1}. Assuming an equivalent dose (D_e) of 100 Gy and using the equation of age (t) = D_e/DR, the dose rates (DR) calculated for variable crystal size would result in a difference in ages spanning 11.3 ky whereas surrounding material density, volume of cobbles, amount of filled pores, and snow cover would result in differences in ages of 0.17, 2.3, 1.0, and 0.83 ky, respectively.

3.4. DISCUSSION

3.4.1. COMPARISON OF LUMINESCENCE PROPERTIES WITH PETROLOGY

Low OSL intensity is common among the measured samples extracted from cobble surfaces. Samples that have higher signal intensity compared to background measurements display large scatter in intensity between aliquots (Figure 5). Comparison of signal intensity with the proportion of passing aliquots, scatter in aliquot equivalent doses, and decay behavior (Table 3) does not show a clear relationship between the OSL characteristics; however, in general, samples with a slower decay behavior have a smaller percentage (average of 36%) of passing aliquots when compared with samples with faster decay (average of 41%). Additionally, slower decay behavior is observed from cobbles sampled from the lower elevation, younger beaches in the western Antarctic Peninsula (Simkins et al.,

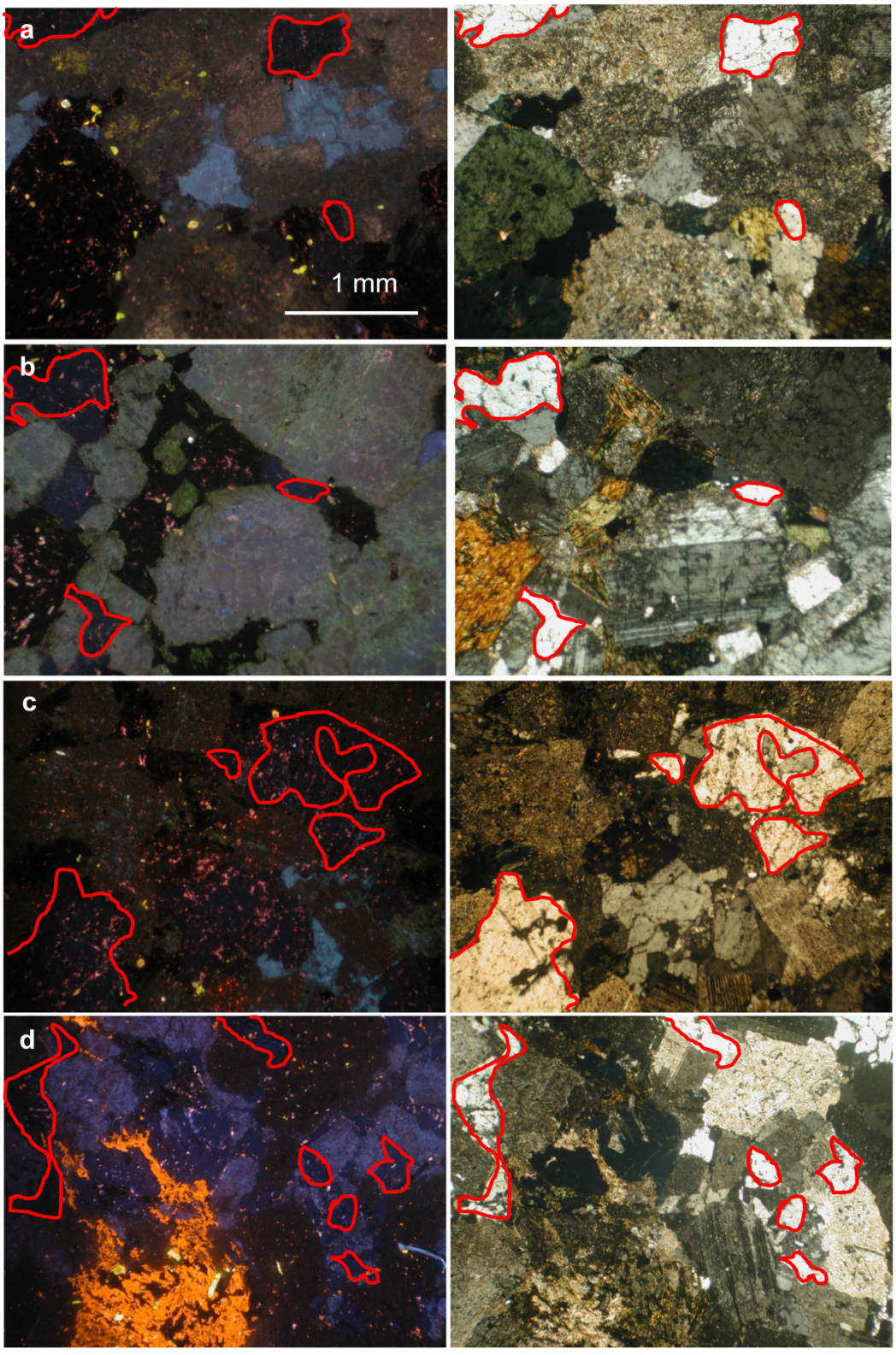
a
1 mm
b
c
d

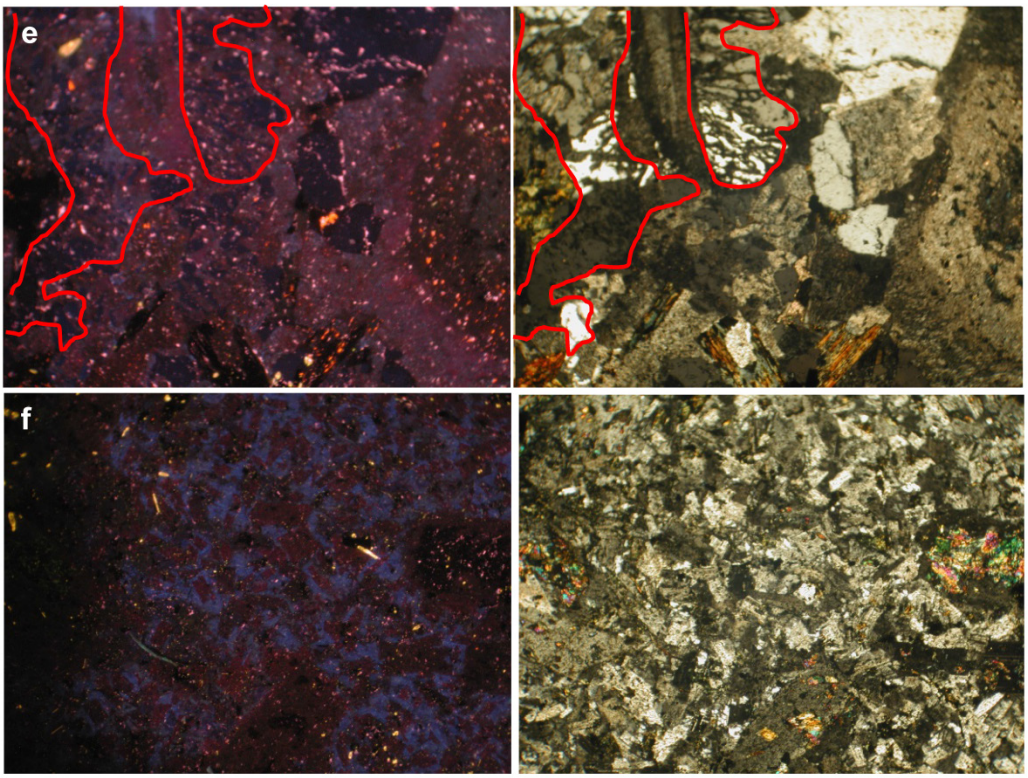

Figure 7. Examples of CL images from Antarctic cobbles with quartz outlined in red. (a-c) CB4, CB10 and CB6, respectively, show dark blue emissions from quartz with light violet centers. (d) Quartz in sample CB33 emits dark blue with orange centers. (e) CB22 containing myrmekite texture of quartz displays dark blue to violet emissions with light violet centers. (f) CB34 does not contain quartz and displays a granular CL emissions of light and dark violet. Paired images of the thin sections in cross-polarized light are provided for each sample

2013a). This could potentially be due to the younger sedimentary history of the cobbles incorporated in the lower beaches. The scatter in equivalent doses does not show distinct populations (Appendix IV) common when partially bleached and bleached grains are mixed; therefore, the large overdispersion values may result from microdosimetric effects.

The CL images of thin-sectioned portions of the Antarctic cobbles (Figure 6) show variable emission patterns from quartz with most samples emitting dark blue to violet with discrete orange and light violet centers (Figure 7). Petrographic analysis reveals that most samples contain very little quartz that often occurs as intergrowths in feldspar (Figure 8). Inclusions of K-feldspar in quartz can contribute to beta dose heterogeneity from ^{40}K decay

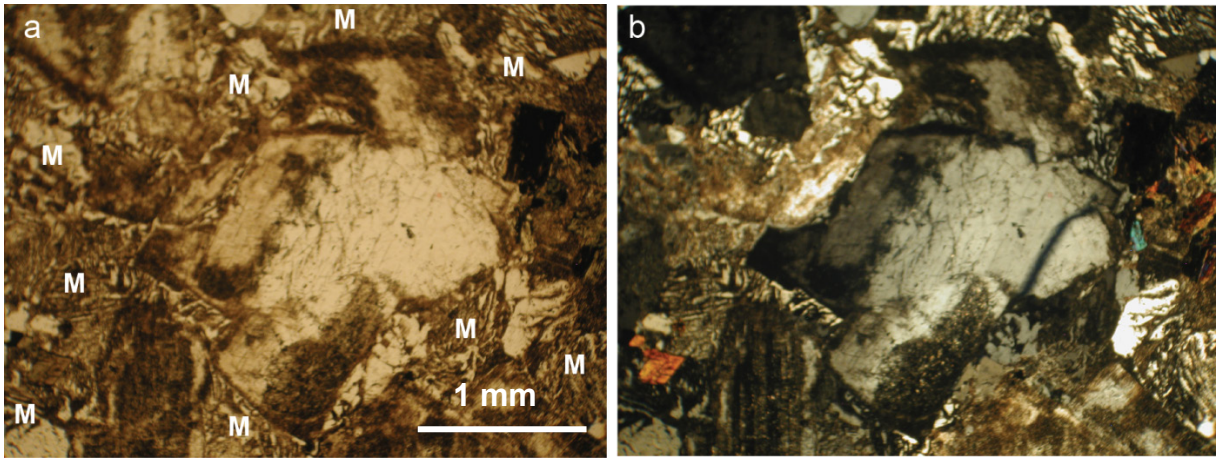

Figure 8.Myrmekite (M) texture of vermicular quartz intergrowths in feldspar from sample CB21 shown in (a) plain light and (b) cross-polarized light.

(Murray and Roberts, 1997). As quartz is associated with feldspars in many of the samples, microdosimetric effects produced by K-feldspars may have an influence on the radioactive environment of the quartz extracted from cobble surfaces potentially explaining the large scatter observed in equivalent doses. Comparison of the OSL and CL characteristics with petrology does not show a relationship, perhaps suggesting the poor OSL characteristics observed from quartz extracted from cobble surfaces are not predominantly influenced by the source rock or nature of crystal defects producing the luminescence observed in the CL images but rather the radiation environment, crystal size, or sediment transport history. This lack of relationship supports the findings of Preusser et al. (2006) who suggest young sedimentary histories of quartz are responsible for the observed poor luminescence properties – low OSL sensitivity, high overdispersion, tendency to fail measurement reliability tests – rather than resulting source rock and CL characteristics.

Two samples (CB34 and CB52) show a distinct granular texture dominated by violet CL emissions (Figure 7f) as well as variable OSL decay behavior (Figure 6). These two

Table 4. Summary of petrographic analysis

Sample	Petrology	Primary	Secondary	Accessory	Notes
CB2	Hornblende quartz-monzodiorite	Qtz, Pl, K-fsp, Fe-oxides, Hbl	Ep, Chl	Ap, Mnz	Fsp alteration; Qtz interstitial, fluid inclusions; Pl twinning, sassauntized, turbid
CB3	Quartz monzonite	Qtz, Pl, K-fsp, Fe-oxides, Hbl	Ep, Chl	Ap, Mnz	Some myrmekite; Qtz graphic
CB4	Hornblende quartz-monzodiorite	Qtz (myrmekite), Pl, K-fsp, Fe-oxides, Hbl	Ep, Chl	Ttn	Ttn coarse
CB6	Hornblende diorite	Qtz, Pl, K-fsp, Hbl	-	Ttn	-
CB10	Hornblende diorite	Qtz, Pl, K-fsp, Hbl	-	Ttn	-
CB21	Hornblende quartz-monzodiorite	Qtz (myrmekite), Pl, K-fsp, Fe-oxides, Hbl	Ep, Chl	Ap, Mnz	Pl coarse, tabular, sassuarntized; Fsp turbid
CB22	Hornblende quartz-monzodiorite	Qtz (myrmekite), Pl, K-fsp, Fe-oxides, Hbl	Ep, Chl	Ap, Mnz	Same as CB21; Pl zoned
CB25	Hornblende quartz-monzodiorite	Qtz (myrmekite), Pl, K-fsp, Fe-oxides, Hbl	Ep, Chl	-	Fsp large, altered
CB26	Quartz monzonite	Qtz, Pl, K-fsp, Fe-oxides, minor Am	Ep, Chl	-	Similar to CB25; less mafics
CB33	Hornblende quartz-monzodiorite	Qtz (myrmekite), Pl, K-fsp, Fe-oxides, Hbl	Ep, Chl	Ttn	Same as CB25
CB34	Syenite	K-fsp, Ep, Pl	-	-	Fsp fine; carlsbad twin Fsp phenocrysts; hexagonal Ne phenocrysts; elongate Ep pseudomorphs
CB39	Granite	Qtz, Pl, K-fsp, Am, Ttn	Ep, Chl/Bt	Ttn	Some Qtz, mostly Fsp; Relict Am; Ttn coarse
CB52	Syenite (foid-bearing)	K-fsp, Ep, Ne	-	-	Similar to CB34; less Ep
CB54	Hornblende quartz-monzodiorite	Qtz (myrmekite), Pl, K-fsp, Fe-oxides, Hbl	Ep, Chl	-	Altered mafics
CB57	Hornblende quartz-monzodiorite	Qtz (myrmekite), Pl, K-fsp, Fe-oxides, Hbl	Ep, Chl	-	Similar to CB21; Pl inclusion-free rims; Qtz rare; altered mafics

samples are syenities characterized as under-saturated in silica and contain no quartz. The elemental analysis shows that the material from one of the syenites (CB52) is not quartz and is dominated by Ca, Fe, Na, Br, and Si (Figure 9). Interestingly, material extracted from the syenites remained after chemical preparations intended to isolate quartz including etching

with HF and density separations. This suggests the material used for OSL measurements was not quartz but other minerals impervious to the chemical treatment with a similar density as quartz.

3.4.2. INFLUENCE OF DOSE-RATE ASSUMPTIONS ON OSL AGES

Dose-rate models of water content and crystal size show that variations in surrounding material density have the lowest influence on dose rates (Figure 10). Variations in the volume of cobble packing result in an OSL age difference of over 2 ky while a range of values used for the percentage of filled pores and snow cover produce an age difference of ~1 ky. Crystal size ranging between 0.06-10 mm has the largest effect on calculated total dose rates. The samples presented here have crystal sizes between 0.09 to 1.4 mm producing dose rates ranging from 2.96-3.41 Gy ky^{-1} corresponding to an age difference of 4.5 ky. Of the modeled parameters, crystal size has the largest influence on dose-rate estimates thus robust crystal size estimates are necessary for true burial age determination of cobble surfaces. However, estimating the size of quartz is difficult considering the variable, anhedral nature of quartz found in these samples as intergrowths in feldspars and interstitially between other minerals. Kenworthy et al. (2014) suggests overdispersion in equivalent doses results from grain-size related microdosimetric effects. Similarly, the overdispersion in equivalent doses of Antarctic beach cobbles may result from microdosimetric effects of variable crystal size.

3.4.3. RECOMMENDED PRACTICES

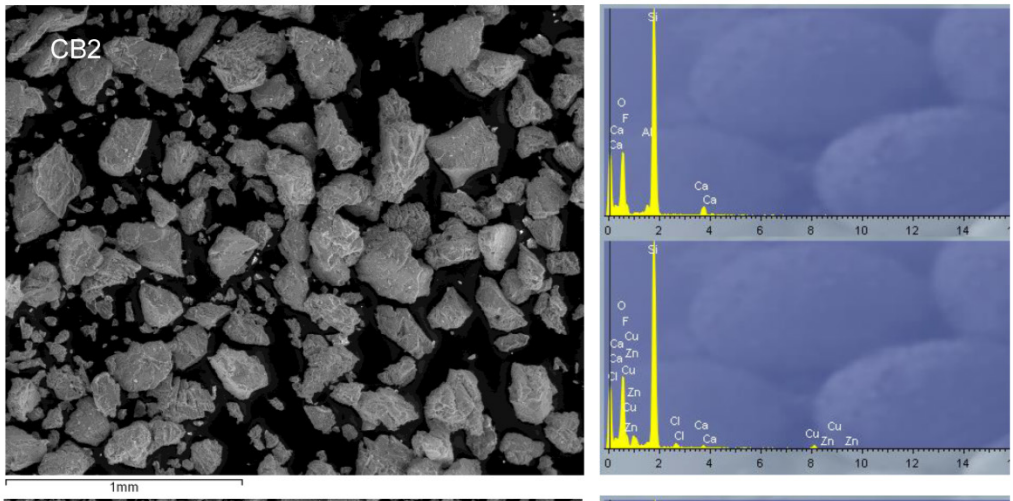
CB2
1mm

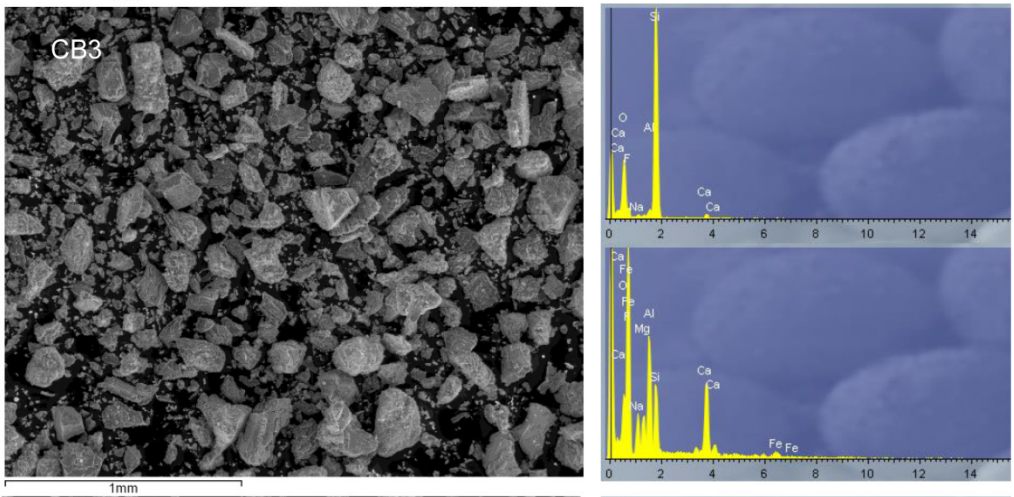
CB3
1mm

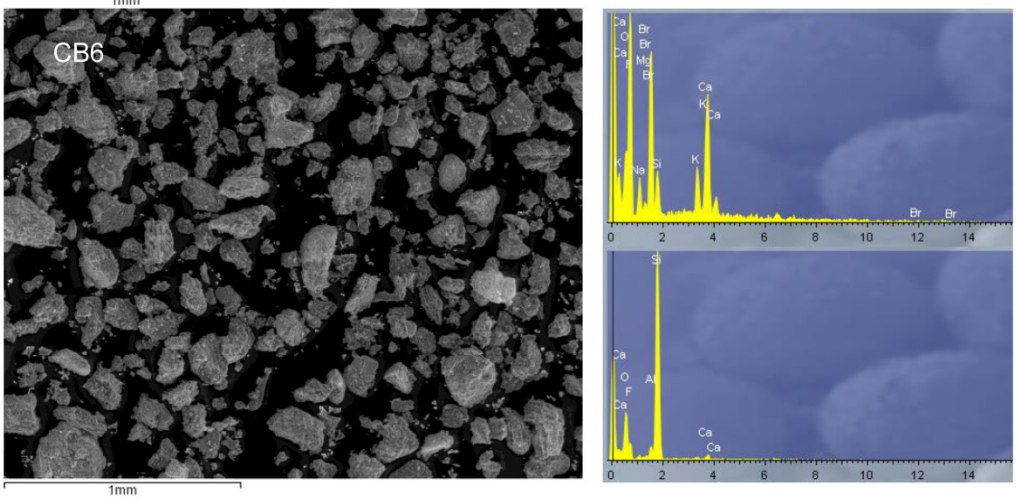
CB6
1mm

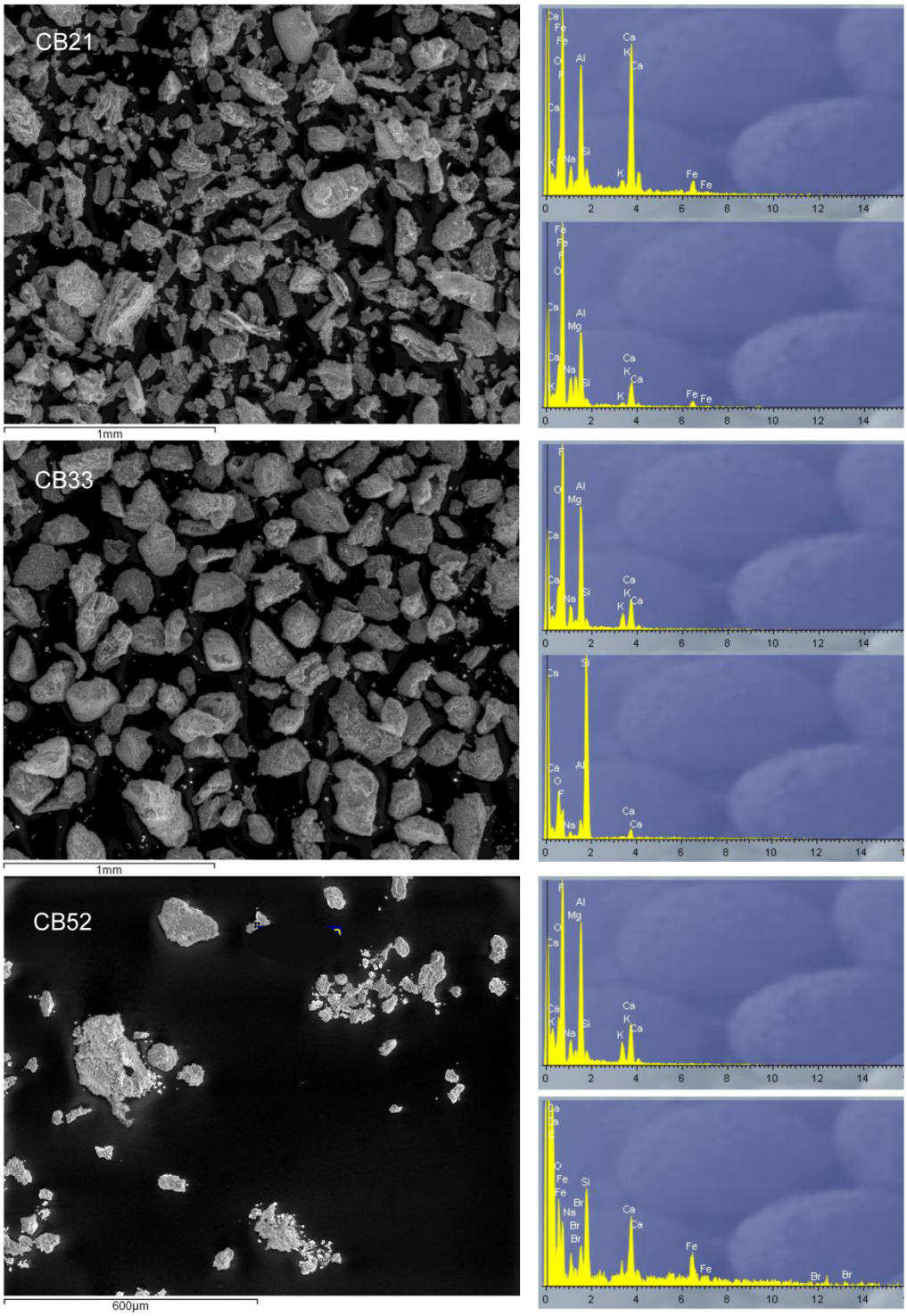

Figure 9. Energy dispersive spectra of grains used for OSL measurements extracted from cobble surfaces that have undergone chemical preparation used to isolate quartz. Images of the grains are shown on the left and example spectra are shown for 2 individual grains in each sample. The spectra show relative abundances of elements identified by emission in keV.

The nature of quartz extracted from monzonite and monzodiorite cobble surfaces is less than ideal for OSL dating considering quartz is limited to nonexistent and often occurs as anhedral intergrowths in feldspars. Despite challenges with OSL dating of cobble surfaces, OSL ages from Antarctic cobble surfaces provide are consistent with radiocarbon ages from the same sites (Simms et al., 2011; Simms et al., 2012; Simkins et al., 2013a). Thin-section analysis prior to conducting OSL measurements would be useful to determine which samples have more abundant and well-developed euhedral quartz crystals. Additionally, CL and mineralogical analysis of the material remaining after sediment chemical preparations would be useful to assess the purity of the quartz extracted from cobble surfaces used for OSL measurements. As crystal size is important to account for beta-dose attenuation, methods to estimate representative crystal sizes could be improved for further cobble surface dating by coupling petrographic and image analysis techniques to insure only the crystal size of quartz is measured. The possible residue produced by chemical reactions during sediment preparation could potential contaminate the quartz signals; therefore, re-sieving and washing the extracted material after chemical preparation would remove the fine clay-like residue. To avoid problems with dating quartz extracted from cobble surfaces, feldspars could alternatively be dated as they are typically abundant and well-formed. Instrumentation and protocol to date directly date quartz from whole cobble surfaces sans sediment and chemical preparation are currently being developed by R. DeWitt (pers. comm., 2014) which would eliminate problems with isolated quartz crystals and potential contamination by other minerals.

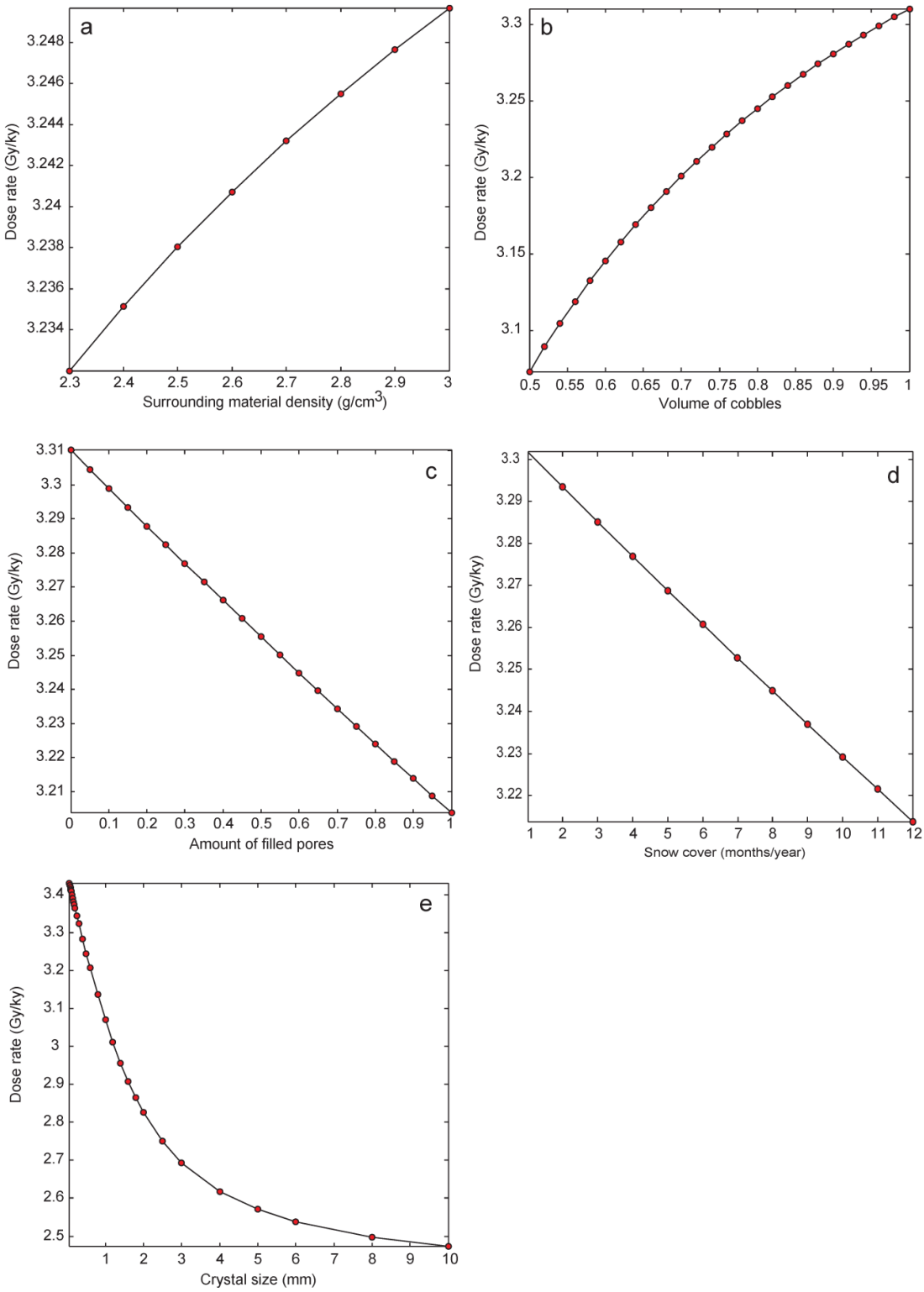

Figure 10. Dose-rate models of water content parameters (a-d) and (e) crystal size showing the trend and magnitude of changes in dose rate using a range of values for each parameter.

3.5. CONCLUSIONS

An investigation of OSL characteristics shows Antarctic cobble surfaces are characterized by low OSL signal intensity, a tendency to fail standard reliability tests, and large scatter in equivalent doses from a population of aliquots. Samples with faster decay characterized by >50% natural signal depleted after 5 s of stimulation generally have a higher percentage of passing aliquots. The limited quartz (<10%) found in the majority of the samples often occurs as intergrowths in feldspars characterized by irregular, anhedral crystal form. A lack of discernable relationship between OSL and CL properties and petrology suggest that CL behavior and petrology are not responsible for the poor luminescence characteristics observed from quartz extracted from cobble surfaces. Further measurements are necessary to assess the influence of limited sediment transport on the samples by conducting sensitivity tests of repeated laboratory-induced exposure and burial cycles. As crystal size is the most dominant factor in changing dose rates, accurate measurements of quartz size are necessary for the calculation of robust OSL ages. Additionally, the irregular, poorly-formed nature of quartz poses problems for estimating crystal size, which is necessary to obtain representative dose rates. As quartz often occurs as intergrowths in feldspars, the poor luminescence properties may result from microdosimetric effects in the radiation environment from ^{40}K decay of intergrown K-feldspars.

CHAPTER 4

RELATIVE SEA-LEVEL HISTORY OF MARGUERITE BAY, ANTARCTIC PENINSULA DERIVED FROM OPTICALLY STIMULATED LUMINESCENCE-DATED BEACH COBBLES

4.1. INTRODUCTION

The relationship between continental ice fluctuations and sea-level change is important for understanding spatial variations in global sea levels and vital for modeling ice-sheet histories. Although eustatic sea level has risen ~120 m (Fairbanks et al., 1989; Yokoyama et al., 2000; Peltier, 2002; Hanebuth et al., 2009) since the Last Glacial Maximum (LGM), 23-19 thousand years ago (ka; Huybrechts, 2002), geographic variability in relative sea level (RSL) is influenced by glacial isostatic adjustment (GIA) and results in isostatic uplift near ice sheets due to continental unloading of ice. Due to harsh field conditions, a scarcity of ice-free coastal environments, and problems associated with dating Antarctic materials, relatively few RSL observations are available for constraining Antarctic GIA model predictions.

A version of this chapter is published as a paper in Quaternary Science Reviews under the citation: Simkins, Lauren, Simms, Alexander, and DeWitt, Regina, 2013. Relative sea-level history of Marguerite Bay, Antarctic Peninsula derived from optically stimulated luminescence-dated beach cobbles: Quaternary Science Reviews, volume 77, pages 141-155.

GIA models for Antarctica are commonly constrained by RSL data (Nakada et al., 2000; Ivins and James, 2005; Whitehouse et al., 2012a; Briggs et al., 2013; Okuno et al., 2013) derived from isolation basins (Zwartz et al., 1998; Verleyen et al., 2005; Roberts et al., 2009; Watcham et al., 2011) and raised beaches (Ingólfsson, 2004; Basset et al., 2007; Hall, 2010a). Isolation basins record the onset of lacustrine or marine sedimentation, reflecting a drop or rise in sea level relative to the basin sill elevation, respectively. The marine-to-freshwater transition is typically dated above the transition to avoid error associated with radiocarbon dating of Antarctic marine materials (Zwartz et al., 1998; Bentley et al., 2005a) providing minimum ages for RSL fall. Raised beaches form as local sea level falls due to isostatic rebound and beaches become isolated from marine processes (Nichols, 1968; Fretwell et al., 2010; Simms et al., 2012). Assuming raised beaches have not been altered by post-depositional processes, raised beaches constrain the timing of isolation above the influence of wave processes.

Radiocarbon analysis of incorporated organic and calcium carbonate material (e.g., whale and penguin bones, shells, and seal fur) is commonly used to date raised beaches (Hall et al., 2004; Bentley et al., 2005a, Hall, 2010a). This method has limitations when applied to Antarctic materials, however, because of: (1) the large uncertainty in the marine reservoir correction (Pudsey and Evans, 2001; Evans et al., 2005; Hall et al., 2010b) due to the incorporation of water depleted in ^{14}C via upwelling and meltwater input; (2) the scarcity of datable material; and (3) dating reworked material incorporated in beach ridges (Bentley et al., 2005a). Reconstructing RSL from Antarctic beaches is particularly hampered by a lack of in situ material suitable for radiocarbon dating (Hall and Denton, 1999; Baroni and

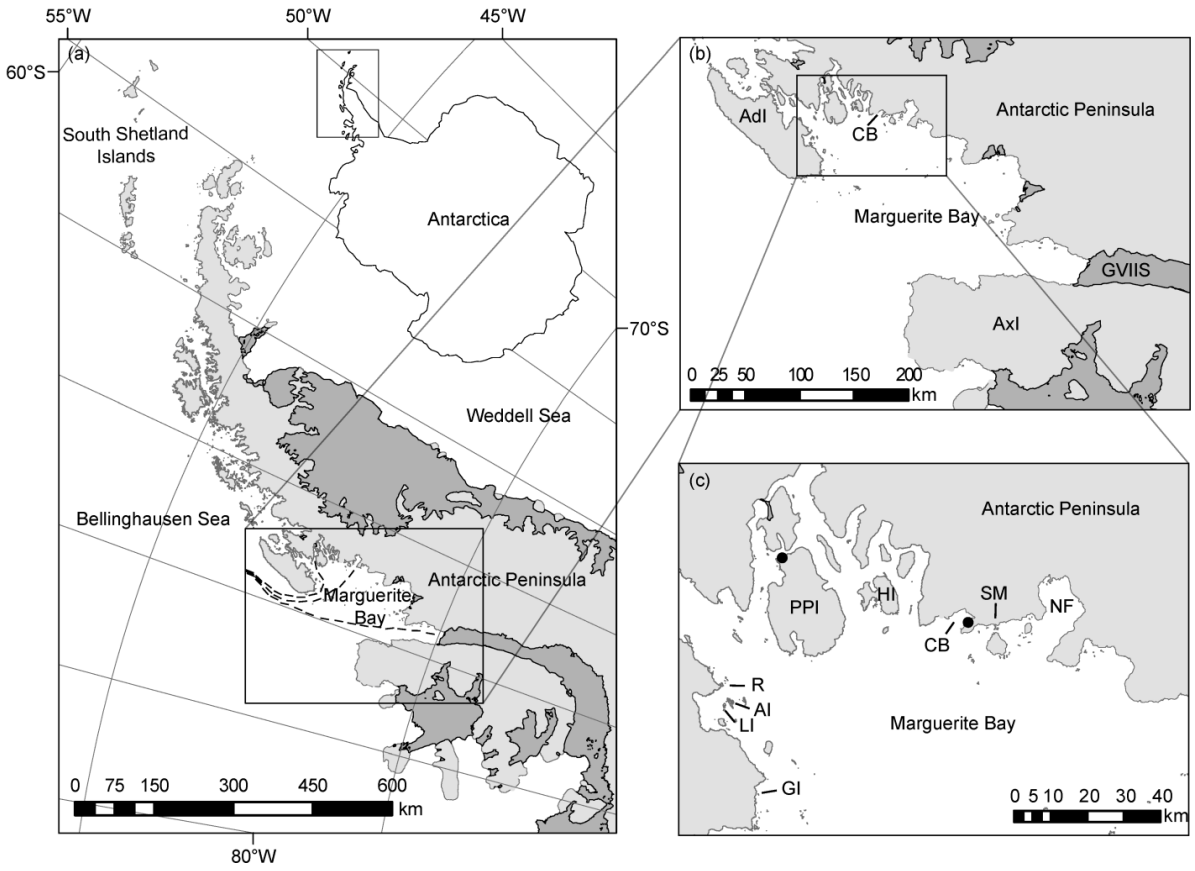

Figure 11. (a) Antarctica Peninsula with the approximate location of Marguerite Trough (dashed lines). Inset shows the location the Antarctica Peninsula in Antarctica. (b) Location of Marguerite Bay. (c) Northern portion of Marguerite Bay showing locations mentioned in text and other notable sites. AdI – Adeliade Island, AI – Anchorage Island, AxI – Alexander Island, CB – Calmette Bay, GVIIS – George VI Ice Shelf, GI – Ginni Island HI – Horseshoe Island, LI – Lagoon Island, NF – Neny Fjord, SM – San Martin, PPI – Pourquoi Pas Island, R – Rothera.

Orombelli, 1991; Hall et al., 2004; Bentley et al., 2005a; Fretwell et al., 2010; Gardner et al., 2006; Hall et al., 2010a).

Optically stimulated luminescence (OSL) dating determines the time elapsed since minerals were last exposed to sunlight, i.e. the burial age. Similar to many beaches around Antarctica, the coarse-grained nature of polar beaches results from a restricted sediment source and lack of sediment supply (St.Hilaire-Gravel et al., 2010). In an attempt to date Antarctic raised beaches, Simms et al. (2011a) conducted a pilot study in the South Shetland Islands using OSL to date buried undersides of in situ beach cobble surfaces. The OSL ages

are in good agreement with previously published radiocarbon ages from the same sites (Simms et al., 2011a; Simms et al., 2012). For this study, OSL-dated raised beach deposits are utilized to reconstruct the RSL history for Calmette Bay within Marguerite Bay situated along the western side of the Antarctic Peninsula (Figure 11). Through this study, I: (1) use a recently developed application of OSL to date cobble surfaces; (2) bracket the timing of RSL change in Marguerite Bay through a terrestrial record of RSL; and (3) identify potential problems associated with using raised beaches as a proxy for GIA.

4.2. BACKGROUND

4.2.1. GENERAL PRINCIPLES OF OSL DATING

OSL dating determines burial ages of minerals, most notably quartz and feldspars, i.e. the time elapsed since their last exposure to sunlight. Aitken (1998), Bøtter-Jensen et al. (2003), Lian and Roberts (2006), and Rhodes (2011) provide extensive discussions on OSL and its applications for dating. Upon burial, radiation from ^{238}U, ^{235}U, and ^{232}Th series, and ^{40}K decay, and of cosmic origin ionizes atoms producing free electrons within crystal lattices. Free electrons wander throughout the crystal lattice and are trapped by light-sensitive crystal defects at a high-energy state. The number of trapped electrons increases with radiation exposure and burial time. Stimulation with light evicts trapped electrons from high to low energy bands causing them to recombine with positive charges and to release energy in the form of light. This light, the so-called luminescence, is utilized for OSL dating. Burial time elapsed since the last bleaching event can be inferred from the amount of trapped charges in minerals via luminescence detected by a sensitive photomultiplier as well as the rate at which the electrons are trapped. A simplified equation for the determination of OSL

ages (t) is $t = D_e / DR$ where D_e is the equivalent natural radiation dose determined from OSL measurements and DR is the dose rate stemming from radioactive decay and cosmic rays. OSL can be used to date the burial of sediments between decades (Nielsen et al., 2006; Madsen and Murray, 2009) to 200,000 years (Rhodes, 2011) although samples as old as 500,000 years have been successfully dated (Murray and Olley, 2002; Watanuki et al., 2005). The average uncertainty for OSL ages (1-sigma) is 10 % (Murray and Olley, 2002). Young samples are limited by low luminescence signals and large uncertainties following from counting statistics. Samples at the upper age limit often have large uncertainties due to saturating dose responses and the associated fitting errors. Further contributions to the age uncertainty can stem from changes in the radiation environment over the age range, such as radioactive disequilibria or changing moisture content.

4.2.2. MARGUERITE BAY

4.2.2.1. LATE PLEISTOCENE AND HOLOCENE MARINE AND TERRESTRIAL GEOLOGICAL RECORDS

The presence of a widespread glacial unconformity as well as mega-scale glacial lineations, drumlins, and line-sourced gullies indicate that ice was grounded at the continental shelf break in many locations around Antarctica during the LGM (Anderson et al., 1992; Banfield and Anderson, 1995; Sloan et al., 1995; Bentley and Anderson, 1998; Shipp et al., 1999; Canals et al., 2002; Anderson et al., 2002; Heroy and Anderson, 2005; Domack et al., 2006; Simms et al., 2011b; Jakobsson et al., 2012). The Antarctic Peninsula Ice Sheet extended onto the outer continental shelf in Marguerite Bay (Figure 11a) along the western Antarctic Peninsula during the LGM (Kennedy and Anderson, 1989; O'Cofaigh et

al., 2002; Dowdeswell et al., 2004; Wellner et al., 2006; Anderson and Fretwell, 2008; O'Cofaigh et al., 2008; Bentley et al., 2011). A large glacial trough, Marguerite Trough, has been identified by marine-geophysical studies in Marguerite Bay (Kennedy and Anderson, 1989; Pope and Anderson, 1992; Anderson and Fretwell, 2008; Noormets et al., 2009; Bentley et al., 2011; Kilfeather et al., 2011) and was occupied by an ice stream during the LGM (O'Cofaigh et al., 2002; Dowdeswell et al., 2004; O'Cofaigh et al., 2008). Marguerite Trough has a drainage area of 10^3-10^4 km^2 with two major tributaries that extend from George VI Sound in the south and near Pourquoi Pas Island in the north to the continental shelf edge (Figure 11; Bentley et al., 2011; Kilfeather et al., 2011; Livingstone et al., 2012).

The preservation of consistently parallel mega-scale glacial lineations (O'Cofaigh et al., 2002; Dowdeswell et al., 2004; O'Cofaigh et al., 2008), lack of cross-cutting lineations (O'Cofaigh et al., 2005), and thinning rates of the ice stream in Marguerite Bay (Bentley et al., 2011) suggest that the Antarctic Peninsula Ice Sheet retreated rapidly from the continental shelf. Initial retreat from the outer shelf occurred prior to 14-13 calendar thousand years before present (cal ky BP; Pope and Anderson, 1992; Heroy and Anderson, 2005; Kilfeather et al., 2011). An ice shelf formed on the middle continental shelf around 13-12.5 cal ky BP with slow retreat and breakup followed by rapid retreat with open-marine conditions established on the inner continental shelf between 9.5-9.2 cal ky BP (Heroy and Anderson, 2007; Allen et al., 2010). The ice sheet located in George VI Sound (Figure 11b) southeast of Marguerite Bay initially collapsed at 9.6 cal ky BP (Bentley et al., 2005b) most likely due to rapid destabilization during deglaciation of the Antarctic Peninsula Ice Sheet in Marguerite Bay. Cosmogenic exposure ages derived from erratic boulders on Pourquoi Pas Island (Figure 11c) suggest > 270 m of rapid thinning of the ice stream at 9.6 ka (Bentley et

al., 2011). Coincident with rapid thinning of the Antarctic Peninsula Ice Sheet is the intrusion of relatively warm Circumpolar Deep Water on to the continental shelf in Marguerite Bay (Smith et al., 2007; Allen et al., 2010; Kilfeather et al., 2011). Despite observations from marine-geophysical and terrestrial studies, the deglaciation of Marguerite Bay has yet to be constrained by well-dated sea-level observations; however, previous studies suggest: (1) retreat of the Antarctic Peninsula Ice Sheet in Marguerite Bay was rapid; and (2) final deglaciation of the inner continental shelf occurred around 9.6 ka.

4.2.2.2. RELATIVE SEA-LEVEL RECORDS

Raised beaches and isolation basins have been used to reconstruct past sea levels at several locations in Antarctica (Sugden and John, 1973; Clapperton and Sugden, 1982; Baroni and Orombelli, 1991; Wassell and Håkansson, 1992; Hayashi and Yoshida, 1994; Hjort et al, 1997; Miura et al., 1998; Zwartz et al., 1998; Hall and Denton, 1999; Del Valle et al., 2002; Emslie and McDaniel, 2002; Baroni and Hall, 2004; Hall et al., 2004; Bentley et al., 2005a; Gardner et al., 2006; Roberts et al., 2009; Fretwell et al., 2010; Hall et al., 2010a; Roberts et al., 2011; Simms et al., 2012; Hodgson et al., 2013). Existing RSL observations for the Antarctic Peninsula are limited to the South Shetland Islands, Beak Island, James Ross Island, and Marguerite Bay. Previous work has reported ages for Holocene sea-level indices for Marguerite Bay below 20 meters above sea level (masl; Wassell and Håkansson, 1992; Emslie and McDaniel, 2002; Bentley et al., 2005a; Roberts et al., 2009); however, sea-level indices above 20 masl remain undated.

A preliminary RSL curve for Marguerite Bay (Bentley et al., 2005a) suggests exponential RSL fall since 9.0 ^{14}C thousand years before present (^{14}C ky BP) with estimated

rates of RSL fall ranging from 9.5 mm yr^{-1} shortly after the establishment of initial open-bay conditions in inner Marguerite Bay to 1 mm yr^{-1} at present. However, RSL prior to 6.5 ^{14}C ky BP is extrapolated to the highest, albeit undated, beach ridges in Calmette Bay and Pourquoi Pas Island (see Figure 11c for locations) at 41 masl. Also within Marguerite Bay, records from Narrows Lake on Pourquoi Pas Island suggest 19.4 m of RSL fall since 6.4 ^{14}C ky BP (Bentley et al., 2005b) while on Horseshoe Island Wassell and Håkansson (1992) suggest an age of 1.3 ^{14}C ky BP for the isolation of a basin at 3.4 masl. RSL data from elevated lake deltas on Alexander Island located in southern Marguerite Bay suggests 14.4 m of RSL fall since 4.6 cal ky BP (Roberts et al., 2009). Whitehouse et al. (2012a) published a GIA-predicted RSL curve tuned to RSL data for Marguerite Bay suggesting initial RSL fall near 8.0 cal ky BP with a marine limit at ~ 20 masl and a near-linear trend in RSL fall to present-day levels. The modeled RSL curves for Marguerite Bay are unable to synchronously fit both the dated RSL observations and the undated marine limits observed throughout the area. Although previous studies provide fragments of the RSL history for Marguerite Bay, a continuous Holocene record of RSL history constrained by dated sea-level indices in this region has yet to be reconstructed.

4.2.2.3. RAISED BEACH PROCESSES

The fundamental assumption using raised beaches to reconstruct RSL is that once a beach is uplifted above sea level by post-glacial rebound the beach is preserved from further reworking by wave and tidal energy as well as by post-depositional processes. Many beaches around Antarctica contain coarse-clastic (gravel to boulder) deposits due to limited sediment supply, restricted sediment transport, and buffered wave energy by sea ice. Few studies

(Nichols, 1961; Bulter, 1999; Gardner et al., 2006; Fretwell et al., 2010) have determined how Antarctic coarse-clastic beaches form and assessed their reliability for reconstructing past sea level. In general, coarse-clastic beaches are affected by wave energy, presence or absence of intertidal ice, sediment supply, deposit size, local topography/bathymetry, vertical land motion, and tidal range (Butler, 1999; Orford et al., 2002; St. Hilaire-Gravel et al., 2010; Bluck, 2011); however, polar coarse-clastic beach height is controlled predominantly by wave energy and vertical land motion (Bulter, 1999).

Coarse-clastic beaches are built by high-magnitude waves associated with storm events (Nichols, 1961; Carter and Orford, 1984; Oak, 1984; Bulter, 1999; Gardner et al., 2006; Hall, 2010a). Considering Antarctic beaches are typically dominated by cobble-sized sediment and built by storm waves, the relationship between beach height and sea level will vary spatially and temporally. The standard requirement for defining a sea-level index is that the geomorphic feature or material must have a discernible relationship to sea-level defined by tidal datums (van de Plassche, 1986). Contrastingly, Antarctic raised beaches lack a tightly constrained relationship to sea level (Hall, 2010a); however, the scientific community continues to use raised beaches as indicators of past sea-level change.

Sea ice limits wave action on polar beaches resulting in the formation of poorly-sorted deposits (Butler, 1999). Ice processes can form post-depositional features including ice-push ridges, frost heaving, and truncated beaches (Nichols, 1961). The discontinuous nature of ice-pushed ridges and truncated beaches (Nichols, 1961; Gardner et al., 2006) indicates post-depositional forces have altered the integrity of the beach ridges as indicators of past sea levels. The presence of ice on beaches could cause overturning or shifting of cobbles. Frost processes can also destroy the fabric of beach ridges by reworking beach

sediment by frost cracking and sorting. Caution must be used when sampling Antarctic coastal environments for OSL-dating since burial ages derived from sediment affected by post-depositional processes would underestimate the true ages of raised beaches. Suitable beaches for sampling are defined by: (1) exhibiting continuous, shore-parallel extent; (2) containing rounded cobbles; and (3) displaying imbrication (depositional fabric of preferred clast orientation) or boulder pavements formed by the action of ice moving in the intertidal zone (Simms et al., 2011a).

4.2.2.4. MODERN UPLIFT MEASUREMENTS

Along with geologic rates of vertical motion using RSL observations, global positioning system (GPS) monitoring of present-day uplift is vital for testing GIA models. GPS surveys conducted along the Antarctica Peninsula suggest varying rates of present-day vertical motion (Dietrich et al., 2004; Taylor et al., 2008; Bevis et al., 2009; Ivins et al., 2011; Thomas et al., 2011). Of those surveys, Dietrich et al. (2004) and Taylor et al. (2008) report rates of elastic-corrected vertical motion for two GPS stations located within northern Marguerite Bay at Rothera and San Martin (see Figure 11c for locations). Dietrich et al. (2004) suggests insignificant uplift (< + 2 mm a^{-1}) at both stations due to a large measurement uncertainty of 5-6 mm a^{-1}. More recently, Thomas et al. (2011) suggest low vertical velocities of + 1.5 ± 1.9 mm a^{-1} at Rothera and - 0.22 ± 1.93 mm a^{-1} at San Martin. Further north along the western side of the Antarctic Peninsula an elastic-corrected uplift rate of 0.7 ± 0.3 mm a^{-1} is observed at Palmer station (Bevis et al., 2009). GIA model-predicted vertical adjustment for the Antarctic Peninsula as a whole averages to + 2.4 mm a^{-1} (Ivins et

al., 2011). Current vertical motion in Marguerite Bay is lower than the average predicted uplift for the Antarctic Peninsula.

4.3. STUDY AREA

Calmette Bay is located on the mainland of the Antarctic Peninsula east of Adelaide Island in northeastern Marguerite Bay (Figure 11). Calmette Bay is approximately 4 km wide and 5.5 km long with a southwest to northeast orientation. The northern and eastern coasts of the bay are bounded by mountainous terrain and numerous tide-water glaciers with steep calving fronts (Figure 12a-b). The southern coast of Calmette Bay is predominantly ice free with glacial and coastal landforms (Figure 13). A glacial landform, possibly a rock glacier or moraine (Figure 12c-d), is located at the southwestern end of Calmette Bay near the confluence with Marguerite Bay proper and a well-developed spit (Figure 12a) on the southeastern side of the bay. The southern coast of the bay is dominated by raised beaches (Figure 12a-f) that terminate abruptly at steep talus slopes (Figure 12c, e-f) approximately 300 m from the modern beach. The beaches are continuous along the south side of the bay intermittently interrupted by outcrops (Figure 12b-c, e). Thirty-one raised beaches were surveyed between modern sea level and 40.8 masl (Figure 13); however, the number of beach ridges may have been miscounted due to extensive snow cover. Further inspection revealed that one of the identified beaches – originally labeled as beach 29 at 36.1 masl – was most likely not a beach due to our difficulty identifying a distinct ridge; consequently, beach 29 is combined with beach 30 at 36.7 masl. Additionally, beach 25 at 26.8 masl was identified on the first day of field work; however, due to snow cover the remaining days, I could not

Figure 12. (a) Raised beaches along the southern coast of Calmette Bay displaying shore-parallel orientation and a well-developed spit. The eastern coast of the bay is dominated by mountainous cliffs and tide-water glaciers. Taken facing the east. The spit is approximately 300 m long. (b) Lower beaches from modern sea-level to 21.7 masl showing the interruption of beaches by outcrops. (c) Upper beaches that terminate into steep talus slopes approximately 300 m from the modern beach. A prominent scarp is observed along the southern coast and a glacial feature, most likely a moraine or rock glacier, is seen near the confluence of Calmette Bay with Marguerite Bay. (d) Swash zone at Calmette Bay showing coarse-grained nature of deposits and the presence of ice and snow on the lowest beach. The termination of the glacial feature is at the left edge of the image. (e) Upper beaches from 31.7-40.8 masl showing the scarp visible in (c). (f) Parallel, continuous nature of several of the lower beaches showing the tide-water glacier visible in (a). People for scale. (g) Cobble-supported beach deposits show the typical framework for beaches at Calmette Bay with the exception of the 40.8 masl beach. The cobble labelled 31 is approximately 15 cm long. (h) Sandy matrix-supported beach cobbles on the 40.8 masl beach. Sample label is 7.5 cm in length.

relocate the beach thus perhaps a discrete beach is not located at 26.8 masl. The beaches are composed of predominantly poorly-sorted, angular to rounded cobble-sized deposits of plutonic granite to diorite with minor amounts of exotic cobbles not sourced locally but most likely transported to Calmette Bay as ice-rafted debris. The swash zone (Figure 11d) during the majority of our field study was lined with brash ice of varying size that appeared to dampen the swell and buffer wave action. The beaches displayed cobble-supported open frameworks (Figure 12g) with the exception of the upper ridge at 40.8 masl which contained a coarse sand matrix (Figure 12h).

4.4. METHODS

4.4.1. FIELD SAMPLING

Samples were extracted from raised beaches under a light-proof tarpaulin and wrapped in layers of light-proof black plastic for transport to the laboratory. Flashlights with red Lee 106 filters (wavelength of 600-650 nm; Lamothe et al., 1994) were used for sample collection. Prior to extracting samples from beach ridges, rounded cobbles containing visible quartz crystals were identified. Cobbles with diameters < 30 cm were targeted for sampling due to uncertainty of the effectiveness of wave action on larger cobbles. Two to three representative samples surrounding the dated cobbles were collected for dose rate determination.

4.4.2. BEACH ELEVATION

Beach elevations relative to modern sea level at Calmette Bay were determined using a Trimble differential GPS with a vertical error of ± 2 cm. Elevations are reported in meters

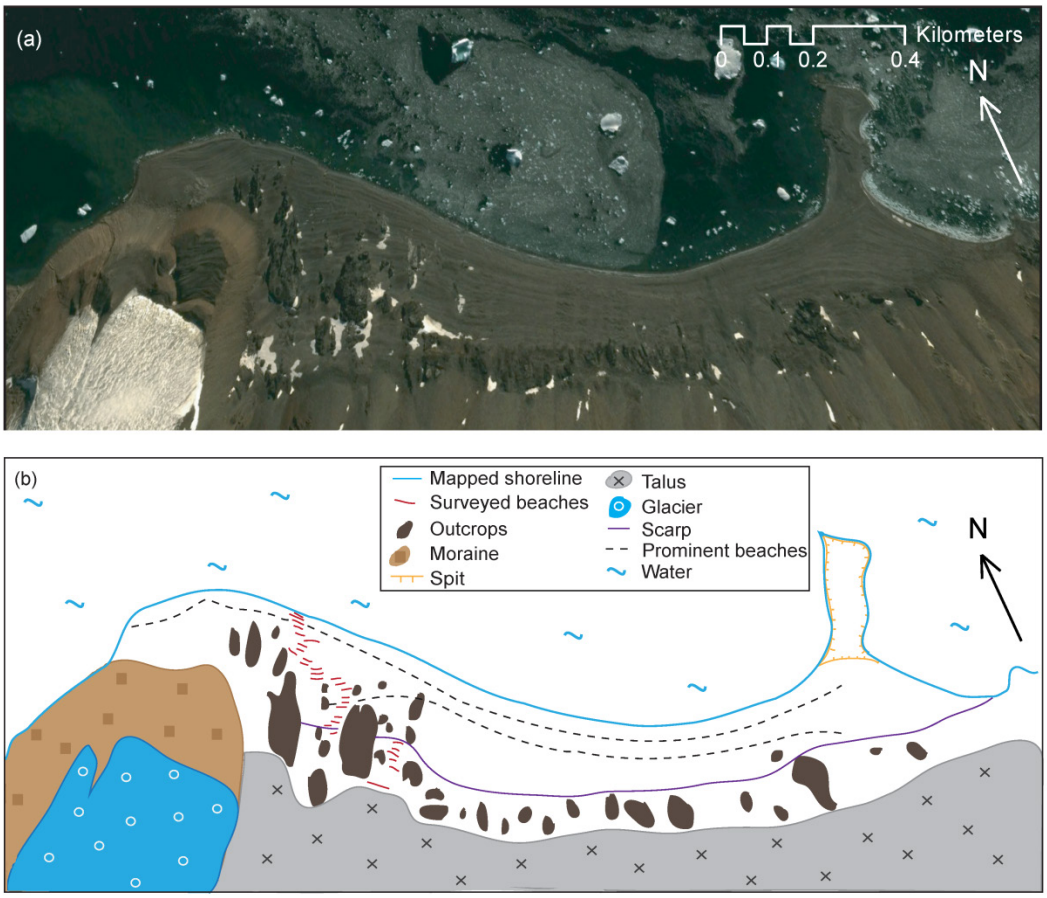

Figure 13. (a) Satellite image of the southern coast of Calmette Bay modified from Google Earth. (b) Schematic of the geomorphology observed at Calmette Bay using the same location and scale as shown in (a).

above sea level (masl) using a single GPS measurement of water height in the swash zone. Sea level was measured at 11.1 m above the IGS08 reference frame. A tide model for the Weddell and Bellingshausen Seas predicts a micro-tidal range of 0.5 m for the majority of the western side of the Antarctic Peninsula including Rothera (Padman et al., 2002). However, Waller (2008) suggests the tidal range for Rothera is 1.7 m. Despite estimates of tidal ranges, robust mean sea level cannot be determined for Marguerite Bay due to limited temporal tide measurements hence our use of water height in the swash zone for elevation reference.

4.4.3. OSL SEDIMENT PREPARATION

Established applications and equipment for OSL dating are suitable for analyzing grains < 250 μm; therefore, quartz crystals ranging in size between 63-250 μm were extracted from buried cobble surfaces. The outer 1 mm (Simms et al.,2011a) of the undersides of sampled beach cobbles were isolated using a series of cuts with rock saws and crushed lightly using a ceramic mortar and pestle. Crushed samples were sieved to isolate grains between 63-250 μm. The sieved samples were treated with 3.75% HCl and 27% H_20_2 to remove carbonates and organics, respectively. Quartz was isolated using density separations of 2.62 and 2.75 g cm^{-3} with lithium heteropolytungstate (LST). The remaining portion of the samples were etched with 48% HF for 40 minutes (Fleming, 1979) to remove feldspar contamination and eliminate the shell affected by alpha radiation that penetrates the outer 20-30 μm surface (Aitken, 1998; Wagner, 1998) of the grains. Quartz separates of ~ 100-200 grains were prepared on stainless steel cups using silicone oil spray (Silkospray). Sample carriers were cleaned following the methods described in Simkins et al. (2013b) to ensure sample carriers were void of contaminant luminescence signals.

4.4.4. OSL MEASUREMENTS

OSL measurements were conducted using a Risø TL/OSL-DA-15 Reader manufactured by Risø National Laboratory with a built-in $^{90}Sr/^{90}Y$ beta source at Oklahoma State University. The internal beta source dose rate ranged from 92.3-94.5 mGy s^{-1} over the duration of this study. Optical stimulation was carried out with blue LEDs (470 nm, 31 mW cm^{-2}) and infrared stimulation with LEDs (~875 nm, 110 mW cm^{-2}) using a UV (Hoya U340, 7.5 mm, 340 nm peak) detection window (Bøtter-Jensen & Murray, 1999) with a heating rate

of 5°C s^{-1} and measurement rate of 1 count s^{-1}. Equivalent doses were determined following the single-aliquot regenerative-dose (SAR) procedure (Murray and Wintle, 2000; Wintle and Murray, 2006). Our specific measurement protocol is outlined in Table 5. High-temperature stimulation was used at the end of each measurement cycle to ensure complete resetting between regenerative doses by emptying deep electron traps (Murray and Wintle, 2003). Appropriate preheat temperature and cut heat temperatures were determined by heat plateau tests. A post-IR blue sequence (Wallinga et al., 2002; Duller, 2003; Wintle and Murray, 2006) eliminates the contribution of contaminant feldspars to the measured quartz signal. Infrared stimulation between samples varied from 20-100 s due to the differences in feldspar contamination. Reliability tests (Murray and Wintle, 2000) conducted include: (1) a recycling ratio test to measure the reproducibility of measurements; (2) a recuperation test that verifies that previous irradiation, stimulation, and heating do not cause unwanted signals

Table 5. OSL measurement sequence

1. Radiation dose D_i
2. Preheat at 200°C for 10 s
3. IRSL at 60°C for t*
4. OSL at 125°C for 100 s
5. Fixed test radiation dose D_t**
6. Preheat at 180°C for 10 s
7. IRSL at 60°C for t*
8. OSL at 125°C for 100 s
9. OSL at 240°C for 40 s
10. Repeat steps 2-9 for cycle 0 and steps 1-8 for cycles 1-7
Cycle 0: Natural signal, D_0
Cycle 1-4: Regenerative doses, D_1, $D_2<D_0<D_3$,D_4
Cycle 5: Dose recovery test, $D_2<D_5<D_3$
Cycle 6: Recycle test, $D_6=D_1$
Cycle 7: Recuperation test, $D_7=0$
* t (time) varies by sample
** D_t=20% D_0

that are not related to the given dose; and (3) a dose recovery test that measures the ability of the SAR procedure to accurately measure the dose. The dose recovery test differs from the dose recovery test suggested by Wintle and Murray (2006) – which refers to the recovery of a dose that was administered to unheated bleached aliquots – by giving a dose between cycles 2 and 3 using thermal treatments as for the regenerative cycles. Passing aliquots used for equivalent dose estimates have recycling ratios < 20 %, recuperation tests with values < 10 %, and dose deviation ratios < 25 %. The fast component (1-2 s) of the OSL decay curve was used for equivalent dose calculations. The slow component of the OSL curve was removed by subtraction of the background signal calculated from the last 10 s of stimulation.

Statistical age models are utilized to obtain the most representative equivalent dose from a population of intra-sample equivalent doses. The common age model is used for samples with grains that received the same dose (Galbraith et al., 1999); thus the common age model is appropriate for samples extracted from buried cobble surfaces that are expected to have received the same dose. Consequently, the common age model is used for the majority of samples to determine the equivalent dose used for age calculations. However, samples with high overdispersion suggest possible mixing of fully bleached (zero stored dose upon burial) and partially bleached (inherent dose upon burial) grains by the inclusion of deeper (> 1μm) portions of the cobble surfaces. The 3-parameter minimum age model places higher weight on lower equivalent doses with the idea that the lower doses are representative of the fully bleached grains prior to burial (Galbraith et al., 1999); therefore, this model was used for samples with overdispersion > 25 % and > 10 passing aliquots.

4.4.5. DOSIMETRY

Water in the pore space between beach sediment absorbs radiation and reduces the effective dose rate; therefore, water content must be considered in the total dose rate. The sample water content of the beach cobbles themselves is negligible. Several factors have an influence on the water content of the material surrounding the dated cobble including: (1) pore volume, (2) snow cover, (3) density of snow, (4) density of the sample, and (5) percentage of filled pores. These factors most likely have not been constant throughout the burial history of our samples; however, reasonable values (Appendix III) are used for the factors according to modern meteorological conditions and field observations to calculate water content.

Using surrounding material and the remaining portion of dated cobbles, ^{238}U and ^{232}Th series and ^{40}K nuclide concentrations were measured with a Reverse Electrode Coaxial Germanium Detector from Canberra Industries, Inc. The open-framework and poorly-sorted nature of the beaches results in heterogeneous dose rates between the dated sample and surrounding material; therefore, the total dose rate was calculated by using dosimetry measurements from both the dated sample and a weighted average of 2-3 representative surrounding cobbles. Beta, gamma, and cosmic radiation of the cobble and surrounding material as well as water content are accounted for in the total dose rate.

To calculate the beta dose rate, half of the beta radiation affecting the buried part of the cobble surface originates from the cobble itself and the other half from surrounding material. The internal beta dose rate from potassium in K-feldspars is approximately 0.067 Gy ky^{-1} based on the average potassium content in K-feldspars of 12% (Mejdahl, 1979). The exact potassium concentration due to feldspar contamination in the measured quartz separates is not known. Thus an additional 5% uncertainty was added to the beta dose rate to

account for variable potassium content. Beta radiation is attenuated during its passage through a grain, so that the beta dose rate depends on grain size (or rather crystal size for this study). The mean quartz crystal size was used instead of the sieved grain size of the measured quartz fraction to correct for beta dose rate attenuation (Mejdahl, 1979). Crystal size was determined using two methods: (1) by manual measurement of quartz in thin section images; and (2) using an image analysis program in Matlab (Trauth, 2010). Both methods, however, have large uncertainty due to sampling bias, pixel resolution, and irregular crystal shape. Consequently, a standard estimate of error equivalent to 50% of the attenuation correction factor was applied.

The cobbles are only partially buried and are themselves smaller than the range of gamma radiation of 30-40 cm (Aitken, 1985). The cobble surface receives the gamma dose rate corresponding to a full half layer of surrounding material. Gamma radiation from above stems from the cobble only which is of finite size and requires a correction factor for the cobble size. Following Simms et al. (2011a), a Monte Carlo simulation was used to determine a correction factor *S* for the irregular shape of individual cobbles approximated using the long and intermediate axes and sample density.

Cosmic flux was estimated for each cobble using a model of intensity and depth of muons dependent on altitude, latitude, burial depth, and sample density following Prescott and Stephan (1982) and Barbouti and Rastin (1983). No variations were applied to the standard calculations for cosmic flux with the exception of rock height used for burial depth. The total dose rate is calculated using the following equation:

$$\frac{DR_{\beta\ cobble}}{2} + \frac{DR_{\beta\ surrounding\ wet}}{2} + S\left(\frac{DR_{\gamma\ cobble}}{2}\right) + \frac{DR_{\gamma\ surrounding\ wet}}{2} + DR_{cosmic} \qquad (1)$$

Table 6. Summary of OSL ages

Sample	RB	Elevation (masl)	Crystal size[a] (μm)	Aliquots[b]	Age model	D_e[c] (Gy)	D_e error (Gy)	σ (Gy)	Overdispersion[d] (%)	DR (Gy ka^{-1})	DR error (Gy ka^{-1})	Age[e] (ka)	Age error (ka)	Age[f] (ky BP)	Relative error (%)
Lower beaches															
CB10-064	1	2.2	140	6	C	15	1.1	9	64	3.7	0.47	3.98	0.59	3.92	15
CB10-025	2	2.7	600	4	C	16	1.6	12	75	3.8	0.26	4.14	0.51	4.08	12
CB10-026	3	3.3	400	3	C	3.6	0.85	2	63	3.4	0.56	1.06	0.3	1	28
CB10-027	3	3.3	600	14	MAM	3.0	0.87	3	39	3.8	0.26	0.79	0.24	0.73	30
CB10-030	5	3.4	400	7	C	24	2.6	11	49	9.0	1.4	2.62	0.51	2.56	19
CB10-069	5	3.4	1000	17	C	11	0.42	2	21	3.5	0.29	3.04	0.28	2.98	9
CB10-033	7	6.5	600	14	MAM	7.0	0.58	6	56	3.5	0.38	1.99	0.27	1.94	14
CB10-039	11	7.4	400	14	MAM	22	0.26	6	26	3.8	0.23	5.78	0.35	5.72	6
CB10-044	13	9.0	600	23	MAM	11	0.96	12	48	3.2	0.18	3.29	0.35	3.23	11
CB10-046	15	11.3	1400	20	MAM	10	0.55	5	36	4.2	0.39	2.43	0.26	2.37	11
CB10-048	16	13.1	1200	14	C	11	1.7	2	21	3.5	0.57	3.16	0.71	3.1	22
CB10-057	24	21.7	300	15	MAM	15	0.42	6	32	3.5	0.33	4.15	0.41	4.09	10
CB10-059	24	21.7	500	1	C	19	4.6	na	na	3.4	0.16	5.61	1.37	5.55	24
Upper beaches															
CB10-003	26	31.8	500	20	MAM	40	0.92	61	74	3.0	0.40	13.2	1.78	13.15	14
CB10-004	26	31.8	600	18	C	33	1.0	6	18	3.5	0.41	9.31	1.12	9.25	12
CB10-006	27	33.8	600	28	C	49	0.87	8	15	3.9	0.68	12.6	2.24	12.57	18
CB10-009	28	34.9	400	6	C	3	0.87	16	498	3.2	0.19	0.98	0.28	0.92	28
CB10-021	31	40.8	500	8	C	46	4.6	102	223	3.1	0.22	14.8	1.8	14.74	12
CB10-022	31	40.8	500	29	MAM	22	1.8	64	69	3.2	0.19	6.83	0.69	6.77	10

RB = raised beach number, C = common age model, MAM = minimum age model, De = equivalent dose, DR = dose rate, σ = standard deviation, ka = thousand years ago, ky = thousand years, ky BP = thousand years before present

[a] Mean quartz crystal size of cobble was used to estimate absorbed beta dose fractions. Crushed and sieved crystal size used for OSL measurements.

[b] Aliquots presented pass all standard SAR procedure tests (see text for details)

[c] Equivalent doses calculated using the common or minimum age model of Galbraith et al. (1999)

[d] Overdispersion was calculated by dividing the standard deviation of all passing aliquots by the simple mean D_e

[e] Ages and age errors were rounded to the nearest ten years

[f] Samples were collected in 2010 thus 60 years was subtracted from the age to allow direct comparison of calibrated radiocarbon ages

where $DR_{\beta\ cobble}$ and $DR_{\beta\ surrounding\ wet}$ are the beta dose rates and $DR_{\gamma\ cobble}$ and $DR_{\gamma\ surrounding\ wet}$ are the gamma dose rates for the dated cobble and surrounding material, respectively. Values for the surrounding material corrected for water content are termed $_{wet}$. DR_{cosmic} is the cosmic dose rate and S is the correction factor for irregular shape and finite size of the cobbles.

4.5. RESULTS

4.5.1. OSL AGES

Although I attempted to date forty-eight samples, twelve samples had no natural signal Possible reasons for samples with no natural signal are petrology and source of the quartz as well as low OSL sensitivity from limited sediment transport histories – depositional cycles lead to a sensitization of quartz (Sawakuchi et al., 2011). Additionally, fourteen samples lacked sufficient quartz to date or failed reliability tests thus these samples were excluded from further dating measurements. Equivalent doses, dose rates, and ages of twenty dated samples from raised beaches at Calmette Bay are reported in Table 6. Unlike radiocarbon ages, calibration curves and additional adjustments are not necessary for OSL ages considering luminescence dating is not based on isotopic decay and ages are in calendar years; therefore, all OSL ages are reported in thousand years ago (ka) as of 1950 CE. Intra-sample dose distribution scatter is quantified by overdispersion (Table 6) which is calculated by dividing the standard deviation by the simple average of equivalent doses. Examples of dose distributions from two samples (CB10-027 and -069) are shown in Figure 14 while all sample dose distributions and OSL decay and dose response curves are available in Appendix IV.

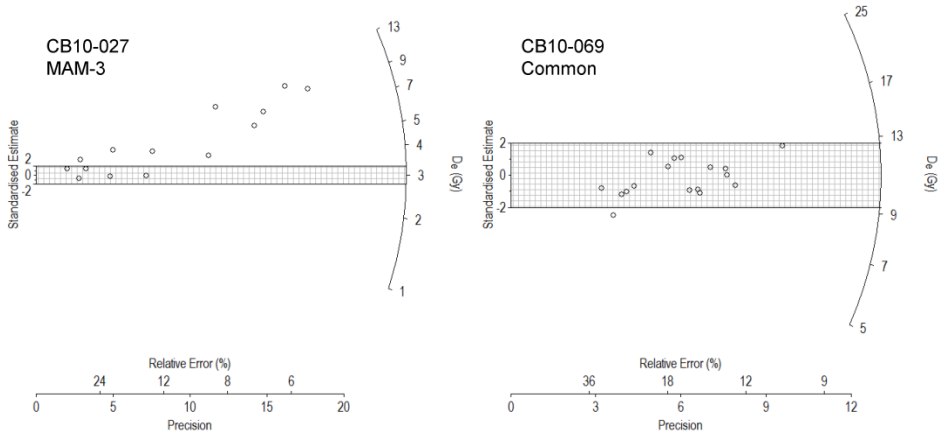

Figure 14. Examples of radial plots of equivalent dose distributions from samples CB10-027 and CB10-069. The 2-sigma error bar represents the representative equivalent dose calculated from the age model. A radial line from the left-hand axis through a point to the right-hand axis gives the equivalent dose of individual aliquots. Relative error and precision of each aliquot are shown along the x-axis where less precise aliquots with larger error will plot toward the left. The three parameter minimum age model (MAM-3) was used to calculate a representative dose for CB10-027 showing the age model is weighted toward the lower equivalent doses. The common age model was used for sample CB10-069. Radial plots for the other dated samples are shown in Appendix IV.

Samples CB10-064 and -025 have high overdispersion (> 60 %) and few aliquots (< 6) due to failure of reliability tests and limited quartz. Age results from the lowest sampled beach at 2.2 m (CB10-064) do not provide insight on whether the 2.2 m beach is the modern beach or an older raised beach. Ages from samples taken at 3.3 masl are congruent within error (CB10-026, 1.00 ± 0.30 ka; CB10-027, 0.730 ± 0.24 ka). Two samples from 3.4 masl (CB10-030 and -069) yield the same age within error with individual ages of 2.56 ± 0.51 and 2.98 ± 0.28 ka. Sample CB10-039 does not fit with other sea-level constraints within Marguerite Bay thus are considered as unreliable for RSL reconstruction most likely due to sample preparation error by the inclusion of deeper parts of the cobble (> 1 mm from surface) not reset during the last bleaching event. Ages from two beaches at 11.3 and 13.1 masl yield the same age within error (CB10-046, 2.37 ± 0.26 ka; CB10-048, 3.10 ± 0.71 ka). Samples from 21.7 masl have the same age within error (CB10-057, 4.09 ± 0.41 ka; CB10-059, 5.55 ±

1.37 ka) despite only one dated aliquot for CB10-059. Although three samples were dated from 31.8 masl (CB10-002, -003, and -004), only one of those ages (CB10-004, 9.25 ± 1.12 ka) occurs during open-marine conditions in Marguerite Bay. Ages from samples CB10-002, -003, -006, and -021 do not fit previous interpretations of RSL within Marguerite Bay with ages between 12.57 and 16.87 ka.

The ages of 0.92 ka from 34.9 masl (CB10-009) and 6.77 ka from 40.8 masl (CB10-022), which are younger than expected, result from cobbles that experienced post-depositional reworking . Cryoturbation, reworking of sediment by frost action, would cause younger-than-expected ages by post-depositional sorting. Alternatively, resetting or partial bleaching of the OSL signal could occur by solar penetration through the top of the cobbles. Vafiadou et al. (2007) suggest bleaching of granitic rocks from Greece, Sweden, and Denmark down to 12-15 mm below the top surface while Simms et al., (2011a) measure partial bleaching only down to 5 mm below the top surface of a granite cobble from the South Shetland Islands. Cobble heights for this study are no smaller than 5 cm; therefore, bleaching of the OSL signal from the top most likely does not influence the OSL signal of the buried cobble surface. Based on observations of frost-circles and frost-cracking on the uppermost beaches, I favor the underestimation of the ages by cryoturbation instead of bleaching from the top. Thus for this reason, samples CB10-009 and -022 are excluded from further discussion.

4.5.2. GEOMORPHOLOGY

The beaches at Calmette Bay are separated into two sets, “upper” and “lower” beaches, by a large scarp (Figure 15a). The sediment in the swash zone consists of angular to

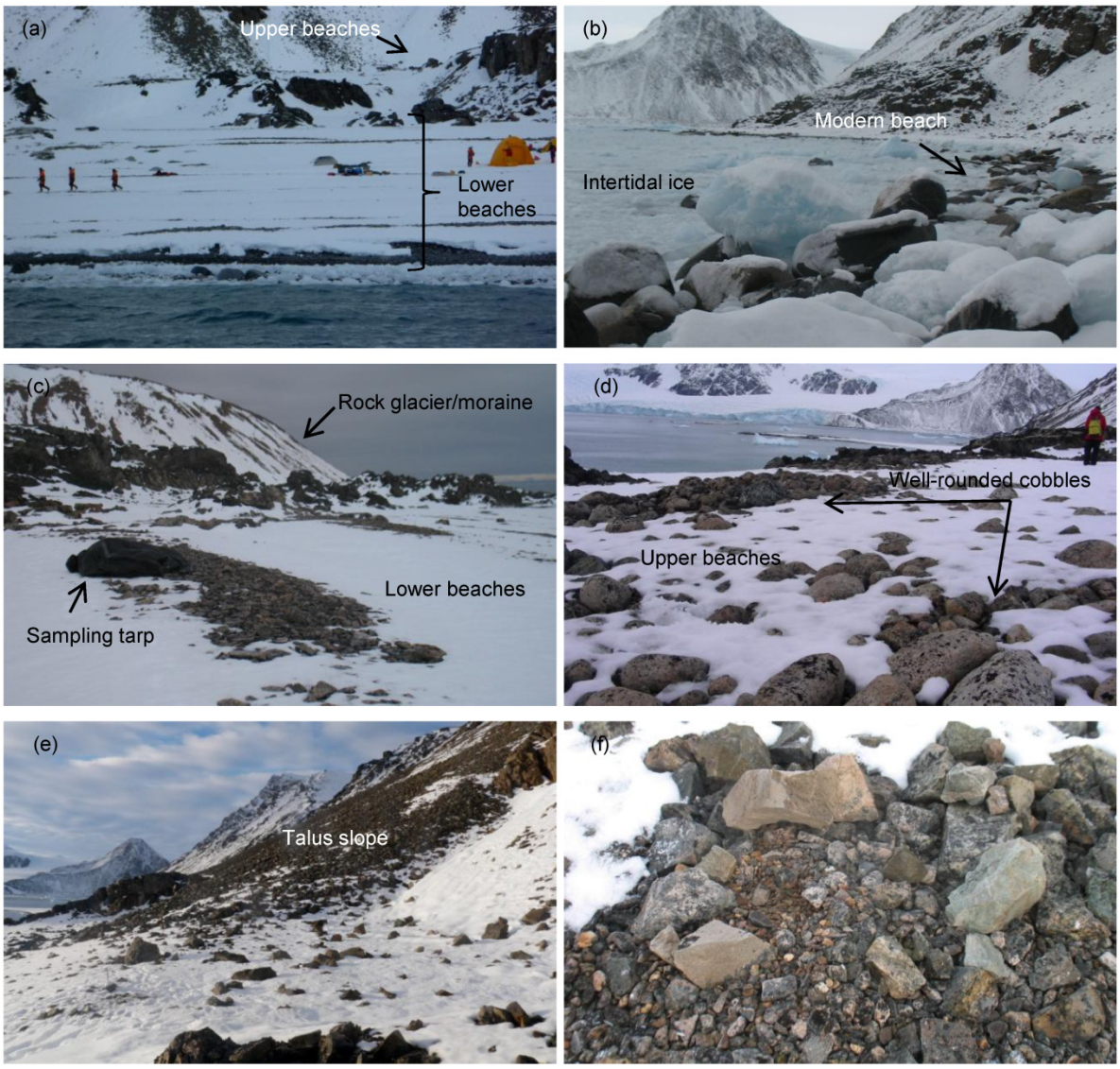

Figure 15. (a) Upper and lower beaches are separated by a large scarp (people for scale). Discrete outcrops are visible in the background. (b) Coarse deposits and intertidal ice boulders along the modern beach. (c) Lower beaches showing cobble-sized sediment with the rock/glacier moraine in the background (~2 m-long sampling tarp for scale). (d) Well-rounded cobbles and boulders on the upper beaches (person for scale). (e) Highest raised beach at 40.8 masl terminating against a talus slope. (f) A frost circle shown along the highest raised beach.

rounded pebbles, cobbles, and boulders as well as intertidal ice boulders (Figure 12d, 15b). The lower beaches (≤ 21.7 masl) are predominantly composed of cobbles (Figure 12f, 14c) with approximately equal distributions of rounded and angular sediment. Similarly, the upper beaches (≥ 31.8 masl) are dominated by cobble-sized deposits; however, large,

extremely well- rounded cobbles and boulders along with angular cobbles are observed on beaches between 31.8-34.9 masl (Figure 15d). The upper beaches are confined to a pocket between outcrops, the scarp separating the upper and lower beaches, and talus slopes. A similar observation on the size and granulometry of these higher beaches was made by Hodgson et al. (2013). The highest beach at 40.8 masl is directly below talus slopes (Figure 15e) and consists of more sub-angular to angular cobbles with a coarse-sand matrix. Cryoturbation of the uppermost beaches is evident by frost circles (Figure 15f) and frost shattering (not shown). Compared to the lower beaches, the breaks between the individual upper beaches are less distinct. In addition, although we were unable to quantify deposit thickness due to extensive snow cover, the upper beach ridges appeared to be composed of less material (e.g. thinner deposits).

4.6. DISCUSSION

4.6.1. AGES CONSTRAINTS FROM CALMETTE BAY RAISED BEACHES

4.6.1.1. LOWER BEACHES

Within the lower beaches, samples at different elevations with congruent ages (Table 6). The simple average was used to calculate beach ages where multiple samples are available. Samples CB10-030 and -069 at 3.4 masl and CB10-033 at 6.5 masl have the same age within error of 2.5 ka. Samples CB10-046 (11.3 masl) and -048 (13.1 masl) also have the same age within error of 2.7 ka. Two samples, CB10-057 and CB10-059 at 21.7 masl, yield an average age of 5.3 ka. The age of 5.3 ka for the beach at 21.7 masl is skewed by sample CB10-057 with an age of 4.09 ± 0.41 ka calculated using the 3-parameter minimum age model (Galbraith et al., 1999). The minimum age model places larger weight on lower

equivalent doses from sample dose distributions; however, if the common age model is used, sample CB10-057 would yield an age of 5.21 ± 0.52 ka which is in better agreement with sample CB10-059 from the same raised beach. Additionally, samples CB10-057 and -059 would all have the same age within error closer to 5.6 ka; thus I suggest this group of ages and the 21.7 m beach to have formed ~ 5.5 ka. The groups of similar ages suggest that raised beaches experienced synchronous exposure and burial cycles in order to reset the OSL "clock" and produce similar OSL ages from beaches at different elevations.

4.6.1.2. UPPER BEACHES

OSL ages from the upper beaches at Calmette Bay do not provide a clear record of RSL change. Four of the ages from the upper beaches (12.6-16.9 ka; Table 6) are older-than-expected for the establishment of Holocene open-water conditions in Marguerite Bay. These ages could be interpreted in one of three ways. First, the safest interpretation is that the upper beaches formed ~ 9.3 ka based on the age from CB10-004 at 31.8 masl. This would be in agreement with earlier studies and the timing of initial open-bay conditions in Marguerite Bay. Second, the ages could be interpreted based on the majority of the OSL ages with ages between 12-17 ka suggesting Marguerite Bay deglaciated earlier than previously thought. However, marine-geophysical and sedimentological work from the continental shelf suggested deglaciation commenced around 14 ka on the outer shelf and continued retreating on the inner continental shelf until 9.2-9.6 ka. Third, the upper beaches could represent pre-LGM beaches reworked during the expansion to or retreat from the LGM. The favored hypothesis is that the upper beaches represent pre-LGM beaches reset during the expansion or retreat of LGM ice. Pre-LGM beaches have been observed at Cape Ross in Southern

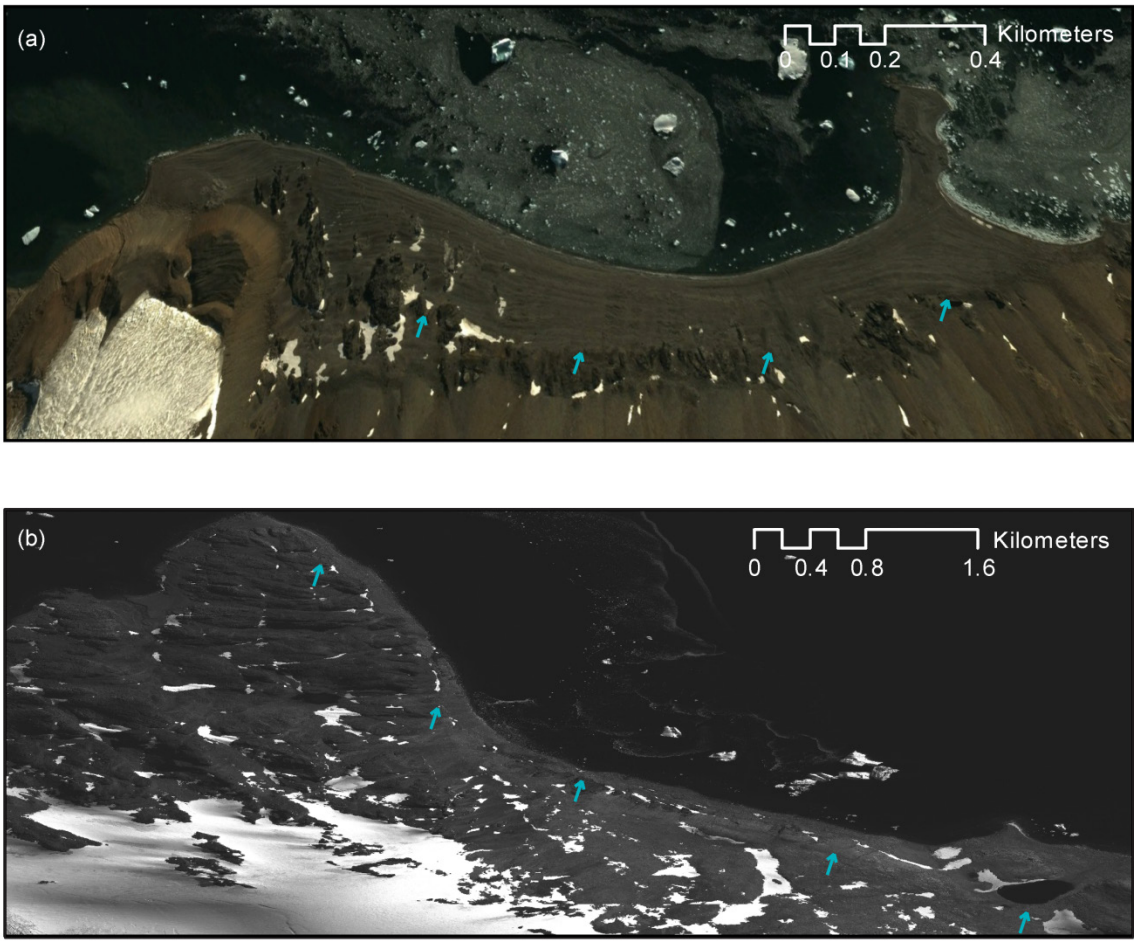

Figure 16. (a) Google Earth image of Calmette Bay (same as in Figure 13a) showing a spatially continuous scarp (denoted by blue arrows) in the land surface. (b) Satellite image of the northern coast of Pourquoi Pas Island showing a similar scarp.

Victoria Land of the Ross Sea Embayment (Gardner and Hall, 2006), the South Shetland Islands (John and Sudgen, 1971; Curl, 1980), and the Sôya Coast in East Antarctica (Igarashi et al., 1995; Maemoku et al., 1997; Miura et al., 1998; Takada et al., 2003).

Indirect support for pre-LGM formation of the upper beaches is provided by the differences in geomorphology between the upper and lower beaches and their separation by a large scarp (Figure 16a). I hypothesize that basal conditions of the LGM ice sheet allowed preservation of the fabric of the upper beaches. The upper beaches are confined by outcrops,

the prominent scarp, and talus slopes. Considering the upper beaches are not as continuous as the lower beaches, we suggest that the observed upper beaches were preserved while it is possible that majority of the upper pre-LGM beaches were reworked by LGM advance and retreat. A similar scarp is observed along the northern coast of Pourquoi Pas Island located ~ 40 km west of Calmette Bay (Figure 16b). The scarp on Pourquoi Pas Island is located at just above a platform at 21.5 masl that extends around an isolation basin (Hodgson et al., 2013) at a similar elevation as the beach at the base of the scarp at Calmette Bay. The scarp possibly formed during a transgressive phase of sea level (Figure 17) in the early Holocene after ice-free conditions were established in Marguerite Bay observed in GIA-modeled RSL curves (Whitehouse et al., 2012a; Briggs et al., 2013). Further work is necessary to confirm the ages of the upper beaches and to make robust interpretations on the importance of the upper beaches with respect to sea level and ice-sheet processes as well as the nature and significance of the scarp.

4.6.1.3. HOLOCENE MARINE LIMIT

If the upper beaches are pre-LGM beaches, the Holocene marine limit would then be placed at 21.7 masl with an age ranging from 5.5-7.3 ka based on our oldest lower beach dates and the isolation basin age from Porquoi Pas Island (Appendix V; Bentley et al., 2005a). A marine limit of 21.7 masl at Calmette Bay coincides with the elevation of the highest beach at 22.1 masl at Gaul Cove on Horseshoe Island and a platform at 21.5 masl that extends around Narrows Lake on Pourquoi Pas Island (Bentley et al., 2005a; Hodgson et al., 2013). A lowered marine limit is in disagreement with higher-elevation, undated beaches previously presumed to represent Holocene marine limits within Marguerite Bay. As

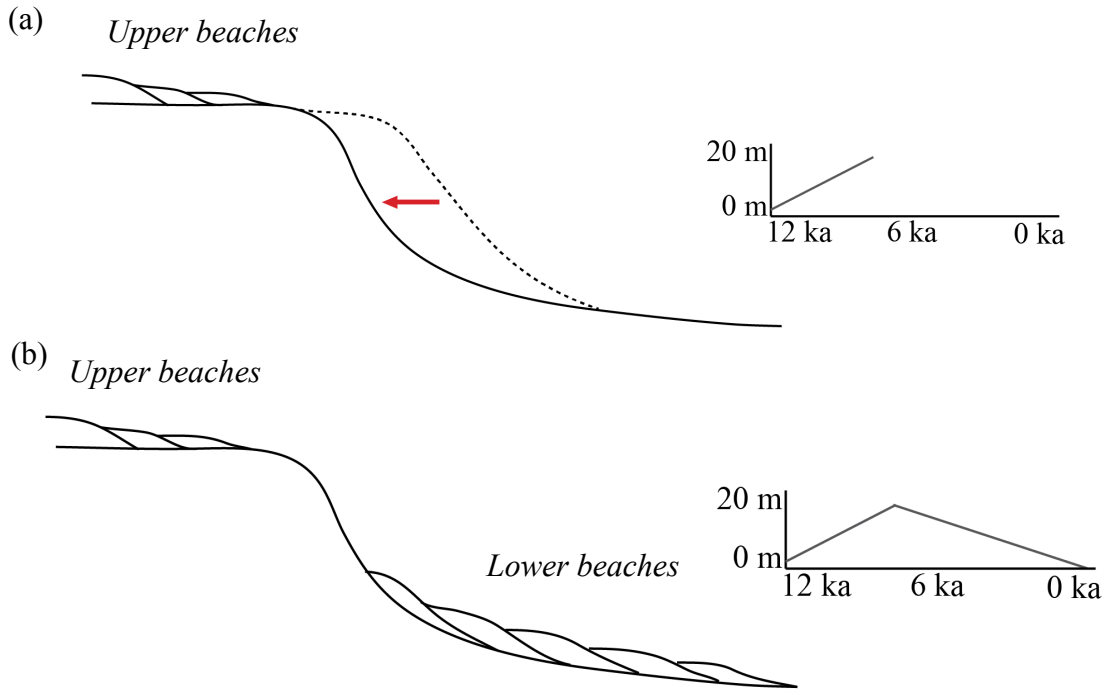

Figure 17. Hypothesized formation of 10-m scarp separating the upper and lower beaches. (a) Pre-LGM beaches exposed above scarp. After ice-free conditions were established in Marguerite Bay around ~9 ka, RSL rose due to eustatic sea-level rise outpacing uplift associated with GIA causing erosion and backstepping of the coastline forming a prominent scarp. (b) As RSL began to fall when GIA outpaced eustatic sea level rise, Holocene beaches formed and were subsequently preserved above sea level by post-glacial rebound.

mentioned earlier, GIA-modeled RSL curves for Marguerite Bay (Whitehouse et al., 2012a) are unable to simultaneously fit both the dated RSL observations and the undated marine limits observed throughout the area. Dated sea-level indices are more appropriate for constraining GIA-model predictions and caution must be taken when making interpretations based on undated sea-level indices. A misestimation of the Holocene marine limit in Marguerite Bay would result in discrepancies in the LGM ice-load model along this portion of the Antarctic Peninsula. The 21.7 masl marine limit inferred from ages within Marguerite Bay suggests half as much RSL fall throughout the Holocene than previously thought using a marine limit of 41 masl. Additional support for a lower Holocene marine limit is supported by the absence of published ages for sea-level indices above ~ 20 masl from Marguerite Bay.

4.6.2. RELATIVE SEA-LEVEL CURVE

OSL-dated RSL indices from the lower beaches (≤ 21.7 masl) at Calmette Bay are shown in Figure18. Three OSL ages from Calmette Bay (Samples CB10-064, -025, -039) are marked as unreliable for reasons discussed in Section 4.5.1. As the age of the lowest surveyed beach at 2.2 masl is not well-constrained due to a lack of aliquots, this beach could potentially represent the modern beach or an older raised beach. Modern beach heights vary from 1.8 m along Livingston Island, South Shetland Islands (Curl, 1980), ~ 2 m at Fildes Peninsula, South Shetland Islands (Fretwell et al., 2010), 2.8 m at Rothera (Bentley et al., 2005a), and 2-3 m at multiple sites on Livingston and King George Islands, South Shetland Islands. In a similar study, Hall et al. (2010a) subtracts 2 m from raised beach elevations to account for the uncertain relationship between beach height and mean sea level. Considering the highest observed modern beach is recorded at 3 m, a vertical error of -3 m is used for OSL-dated raised beaches.

The OSL-dated RSL observations are compared to existing RSL data from various sites within Marguerite Bay (Figure 18a; Appendix V; Horseshoe Island - Wassell and Håkansson, 1992; Ginger and Lagoon Islands - Emslie and McDaniel, 2002; Pourquoi Pas and Anchorage Islands - Bentley et al., 2005a; Alexander Island - Roberts et al., 2009). Although RSL varies spatially, I justify plotting the RSL observations from multiple sites within Marguerite Bay because the sites are no more than 60 km apart with the exception of one age from deltaic sediments on Alexander Island at ~ 200 km from Calmette Bay. Original published marine reservoir corrections from previous studies are used to correct the radiocarbon ages. All previously published RSL data for Marguerite Bay derived from

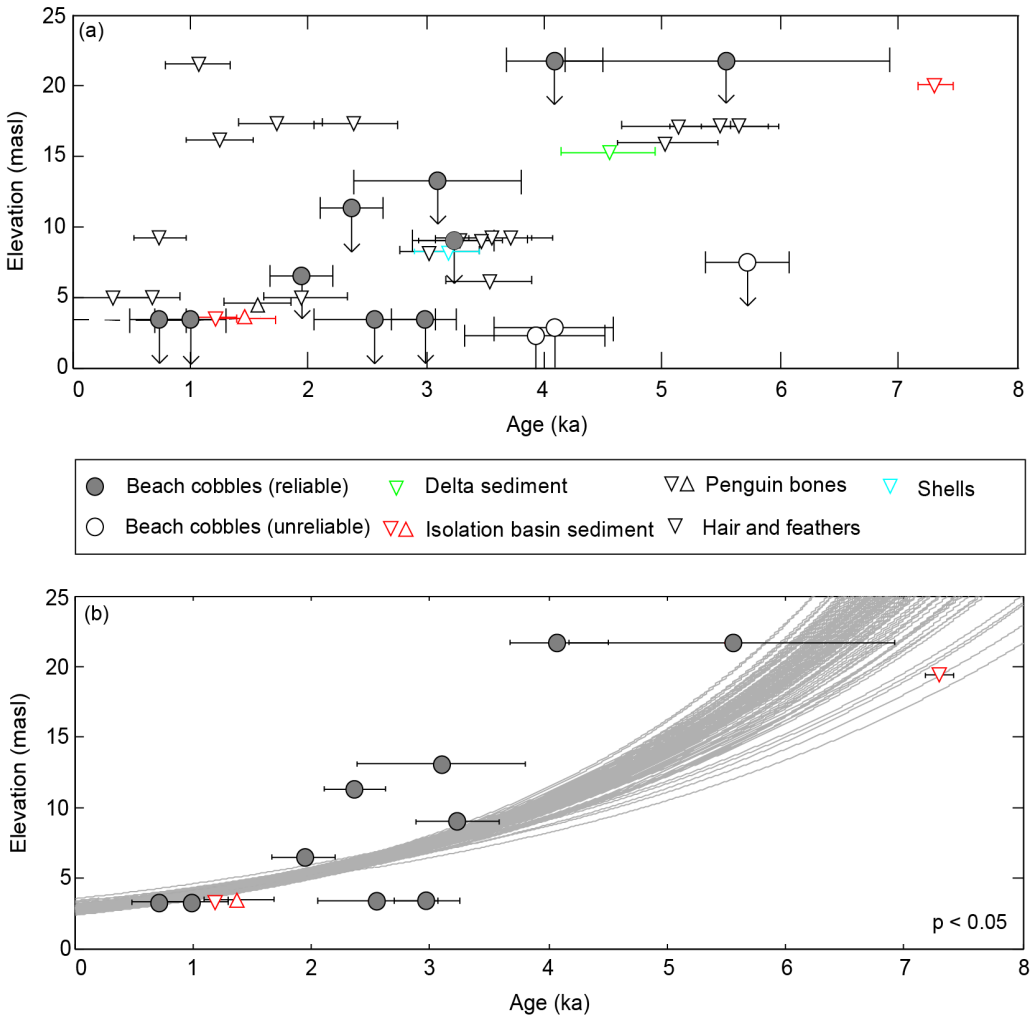

Figure 18a. RSL indicies from Marguerite Bay. (a) OSL-dated beaches at elevations ≤ 21.7 masl from Calmette Bay. A vertical error of – 3 m (black downward arrows) is applied to OSL-dated beaches to account for the uncertain relationship between storm beach height and sea-level. Three OSL ages are labeled as unreliable (open circles) for reasons discussed in Section 4.5.1. Ages from dated sea-level indices from other sites within Marguerite Bay are plotted as well (Appendix V; Wassell and Håkansson, 1992; Emslie and McDaniel, 2002; Bentley et al., 2005a; Roberts et al., 2009). Minimum age constraints are shown as downward facing triangles and maximum ages are shown as upward facing triangles based on interpretations of RSL indices by Bentley et al. (2005a). The age from delta sediment (Roberts et al., 2009) is classified as a minimum age due to the position of the delta relative to the shoreline. OSL ages derived from cobble surfaces provide minimum ages considering coarse-clastic beaches are formed by storm waves. OSL ages are plotted in ka (as of 1950 CE) while ages derived from radiocarbon dating are in cal ky BP; therefore, for simplicity, the x-axis units are labeled as ka since the ages from both methods are referenced to 1950 CE. The dashed line represents that approximate trend in RSL fall for Marguerite Bay throughout the Holocene. (b) OSL-dated sea-level indices from this study and ages from isolation basin sediment in Marguerite Bay fitted using an exponential function derived from Monte-Carlo simulations (n=100 trials).

radiocarbon dating not calibrated for calendar years were calibrated with CALIB 6.0 (Reimer et al., 2009) using the southern hemisphere atmosphere (SH Atmosphere) and marine

(MARINE09) curves depending on the type of material dated. The trend in RSL fall from the combined RSL observations suggests near-linear fall from ~ 5.5-7.3 ka to 2.5 ka and gradual RSL fall from 2.5 ka to present.

The RSL indices derived from OSL-dated cobbles from this study and from isolation basins (n=3) elsewhere in Marguerite Bay closely date the beach formation whereas ages from animal remains provide a range of constraints on beach formation. Therefore, a trend in the RSL fall throughout the Holocene is estimated from the OSL-dated cobble surfaces from Calmette Bay and the ages from isolation basins (Figure 18b). The uncertainty on the fit was evaluated using Monte-Carlo simulations (n=100 trials) which took into consideration the uncertainty in age (horizontal error bars). To do so, we deviated the age within a normal distribution centered about the mean age with a standard deviation inferred from the quoted uncertainty.

From the RSL data, I calculated a conservative rate of RSL fall for Marguerite Bay of 3.3 mm a^{-1} between 7.3 ka (RSL constraint from Pourquoi Pas Island; Bentley et al., 2005a) and 2.5 ka (RSL constraint from Calmette Bay). The platform (Figure 19) between modern sea-level (elevation of swash zone at 0 masl) and 3.4 masl suggests a steady, slow RSL fall in the late Holocene of around 1.4 mm a^{-1} after 2.5 ka. The decrease in RSL rates at 2.5 ka may represent: (1) ice loading or re-advance associated with neoglacial advance within Marguerite Bay; or (2) near-complete relaxation of post-glacial adjustment. RSL data from Marguerite Bay, however, does not indicate a distinct GIA response to a neoglacial advance associated with the Little Ice Age (~0.25-0.5 ka) observed in sea-level records from the South Shetland Islands (Hall, 2007; Hall, 2010a; Simms et al., 2012). The South Shetland

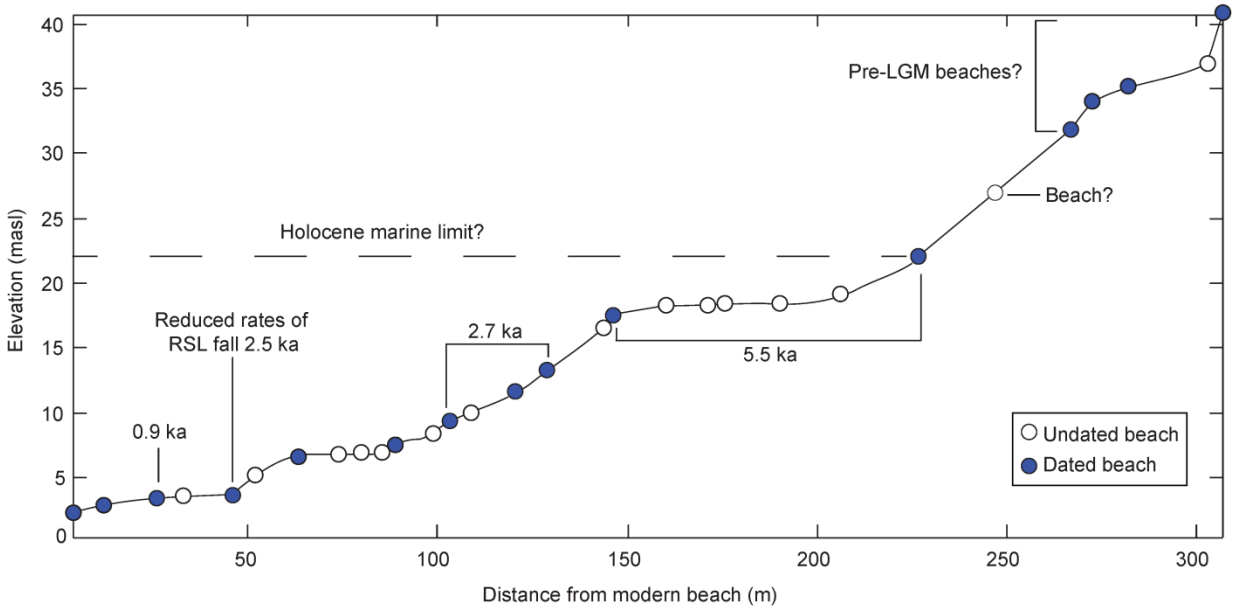

Figure 19. Elevation profile of beaches at Calmette Bay. Dated beaches are marked as blue circles and undated beaches are shown with open circles. Annotations provide a summary of the age results from this study showing the groups of similar ages, inferred Holocene marine limit, and pre-LGM beaches.

Islands have an estimated lithospheric thickness of 15 km and a mantle viscosity of 1-2 x 10^{18} Pa s (Simms et al., 2012), which is much less than the rheological properties estimated for the rest of the Antarctic Peninsula (Ivins and James, 2005). The weak rheology perhaps makes the South Shetland Islands more sensitive to rapid, short-lived ice mass changes than other locations around Antarctica including Marguerite Bay. Contrastingly, perhaps a Little Ice Age signal is not resolved due to smaller magnitude changes in ice advance or loading within Marguerite Bay.

4.6.3. POST-DEPOSITIONAL REWORKING BY WAVES

Antarctic coarse-clastic beaches are formed by high-magnitude storm events. Observed storm wave heights along the coast of Antarctica are between 1.5-3 m (Butler, 1999; Hall, 2010a). Large storm events may be capable of reworking uplifted beach sediment above modern day-to-day swash processes. Additionally, post-depositional sorting

by tsunamis triggered by iceberg calving could produce waves large enough to rework raised beaches. This phenomenon was observed by the second author of this study at Andvord Bay along the northern Antarctic Peninsula where modern beach cobbles were reworked by small tsunami caused by ice-calving. OSL-ages from Calmette Bay display similar ages at different elevations (Figure 18a; Table 6) as well as plateaus of beaches with similar ages separated by scarps (Figure 19). Reworking by storm waves and/or ice-calving tsunamis could explain mechanisms responsible for producing congruent ages at different elevation beaches in Calmette Bay. Ages from beach cobble surfaces, therefore, provide minimum age constrains for RSL curves due to the likely possibility of post-depositional sorting by high-magnitude waves.

4.7. CONCLUSIONS

The use of a relatively novel application of OSL to date cobble surfaces is provides further constraints on RSL within Marguerite Bay along the Antarctic Peninsula. Our new ages suggest the Holocene marine limit for Marguerite Bay is 21.7 masl with an age of ~ 5.5-7.3 ka. Our favored hypothesis for the age of the beaches from 21.7-40.8 masl is that the beaches formed prior to the LGM. A pre-LGM interpretation is supported by: (1) the distinct geomorphology of the upper beaches compared to the lower beaches; (2) the late Pleistocene ages of the beaches; and (3) the geomorphologic separation of the upper and lower beaches at Calmette Bay by a large scarp as well as the observation of a similar scarp on Pourquoi Pas Island. A marine limit of 21.7 masl suggests half as much RSL fall throughout the Holocene than previously thought. Congruent ages (2.5, 2.7, and 5.5 ka) are observed from beaches at different elevations in Calmette Bay. The beach profile from Calmette Bay contains breaks

in elevation between beaches of similar ages. The lower raised beaches at Calmette Bay with similar ages at different elevations likely experienced post-depositional reworking by storm waves following RSL fall. Although potential problems associated with using raised beaches as proxies for RSL reconstructions are highlighted, the ages provided by this study contribute to better understanding the timing and nature of RSL change in Marguerite Bay.

CHAPTER 5

ASSESSING THE LINK BETWEEN COASTAL MORPHOLOGY, WAVE ENERGY, AND SEA ICE THROUGHOUT THE HOLOCENE FROM ANTARCTIC RAISED BEACHES

5.1. INTRODUCTION

Antarctic beaches offer a unique record of coastal environmental change as beaches are preserved above present sea level due to post-glacial rebound following the Last Glacial Maximum (LGM). Consequently, Antarctic beaches have been extensively utilized for Holocene relative sea-level (RSL) reconstructions providing constraints on glacial isostatic adjustment and ice-sheet models (Baroni and Orombelli, 1991; Adamson and Colhoun, 1992; Maemoku et al., 1997; Baroni and Hall, 2004; Hall et al., 2004; Bentley et al., 2005; Hall, 2010; Simms et al., 2011; Simms et al., 2012; Simkins et al., 2013a). Additionally, variations in ice-rafted debris (Hall and Perry, 2004) and the remains of marine species (Baroni and Orombelli, 1994; Berkman et al., 1998; Del Valle et al., 2002; Hall et al., 2006) incorporated in raised beaches provide insight on Antarctic paleoclimate throughout the

---

A version of this chapter is in a paper currently in review for publication in the Journal of Quaternary Science titled "Assessing the link between coastal morphology, wave energy, and sea ice throughout the Holocene from Antarctic raised beaches" by Simkins, Lauren, Simms, Alexander, and DeWitt, Regina.

Holocene. Few studies have focused on the processes that influence coastal evolution around Antarctica (Nichols, 1961; Butler, 1999; Gardner et al., 2006; Fretwell et al., 2010; Lindhorst and Schutter, 2014).

Only ~5% of the Antarctic coastline is ice free (Berkman et al., 1998); however, beaches prevail where sediment cover is present and less extensive ice conditions allow wave and tidal energy to rework coastal deposits (Butler, 1999). The collective influence of restricted sediment supplies and buffering of wave energy by sea ice (Nichols, 1961; Butler, 1999; Gardner et al., 2006) commonly results in beaches comprised of gravel- to boulder-sized deposits. Coarse-clastic beaches across the globe are built by high wave-energy conditions (Carter and Orford, 1984; Forbes et al., 1994; Bluck, 2011; Tamura, 2012) including high-latitude raised beaches in northern Norway (Fletcher et al., 1993), northwestern Russia (Møller et al., 2002), and the Canadian Arctic Archipelago (St.Hilaire-Gravel et al., 2010). Similar to Northern Hemisphere high-latitude beaches, Antarctic beach ridges are built by heightened wave energy generally associated with high magnitude, low frequency storm events (Butler, 1999; Baroni and Hall, 2004; Gardner et al., 2006; Hall, 2010; Lindhorst and Schutter, 2014).

The dominant controls on Antarctic beach formation are wave energy and vertical land motion (Butler, 1999). Though post-glacial rebound is responsible for uplifting the coastline and preserving beaches above sea level, wave energy is the likely control of discrete beach ridge formation. Wave energy is the combination of swash, fair-weather, and storm waves; however, coarse-clastic beaches are built by high-magnitude waves that exceed the influence of swash processes (Carter and Orford, 1984; Butler, 1999). The absence or

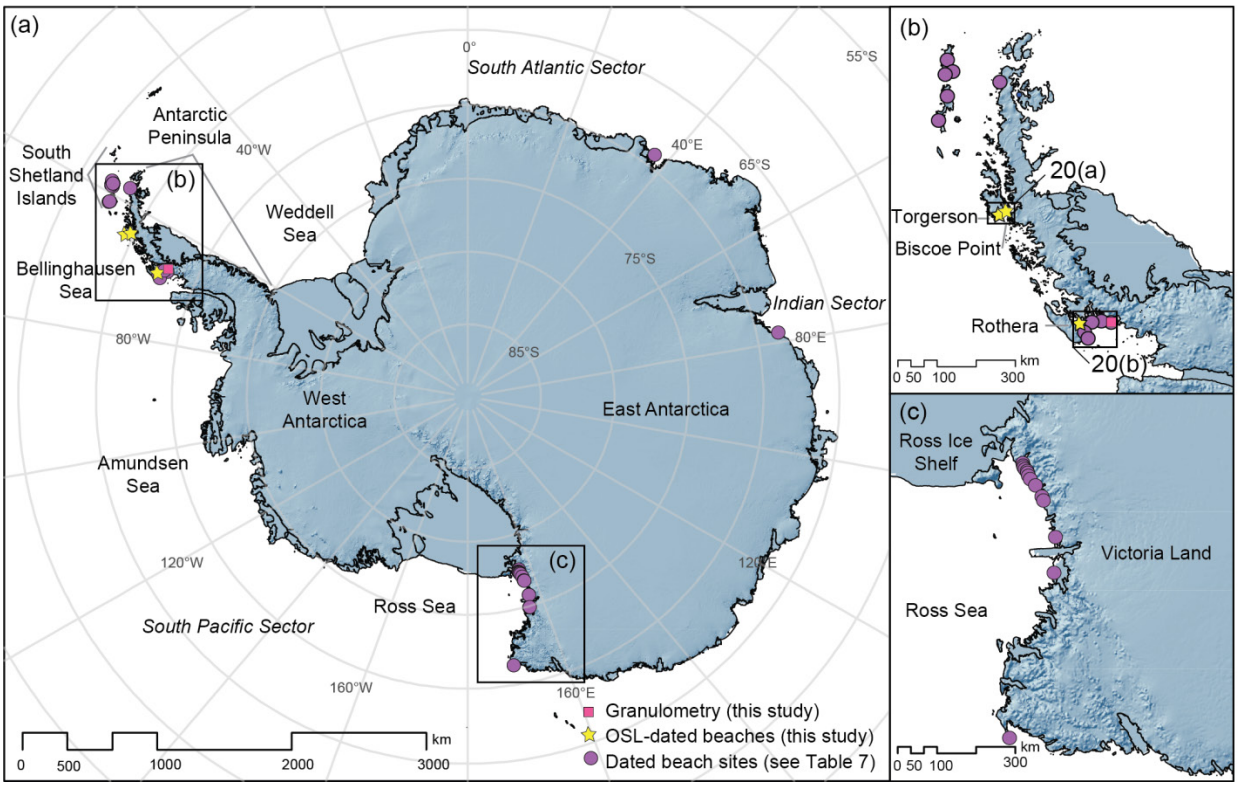

Figure 20. Maps of (a) Antarctica, (b) the Antarctic Peninsula, and (c) Ross Sea showing major geographic locations and referenced sites. The locations of maps shown in Figure 21 are noted in (b). Dated beach sites from previously published studies used in the age compilation are denoted with purple circles. Beaches dated using optically stimulated luminescence (OSL) from this study are shown by yellow stars. The site of granulometry measurements of clast roundness is marked with a pink square.

presence of sea ice determines the extent of open-water conditions around Antarctica and hence the efficiency of storm waves to create coarse-clastic beach ridges. A recent study by Lindhorst and Schutter (2014) on the architecture of gravel beaches at Potter Peninsula, King George Island in the South Shetland Islands independently suggests periods of increased storminess and/or reduced sea ice based on the elevation distribution of raised beaches. When sea ice is limited wave energy is more effective at reworking coastal sediment due to increased wave exposure. Based on the relationship between wave energy and beach formation, the temporal distribution of beaches from around Antarctica should provide insight on wave exposure in the past. I hypothesize that beach formation occurs when sea ice

is limited and increased open water allows waves to more frequently rework beach material. Conversely, beach formation is inhibited during periods of extensive sea ice and thus limited wave exposure.

The ages of beaches derived from radiocarbon and OSL dating around Antarctica (Figure 20) were compiled in two ways. First, two-hundred eighty nine beach ages were compiled from previously published studies (Table 7) and ages provided by this study derived from optically stimulated luminescence-dated cobble surfaces regardless of indicative meaning of ages for beach formation to allow for the observation of general trends. Second, the dataset is limited to representative ages for each dated beach – resulting in one-hundred fifty two unique beaches – to avoid sampling bias of beaches that have been dated multiple times. The temporal distributions of raised beaches are compared to sea-ice proxies from around Antarctica to determine the relationship between sea ice, wave energy, and beach formation. Granulometry measurements of beach deposit roundness from Marguerite Bay, western Antarctic Peninsula are used as an independent proxy for wave-energy conditions. This study provides insight on the possible links between the anti-phasing of climate forcing and beach formation around Antarctica.

Table 7. Original sources for published beach ages

Region	Sources for beach ages
South Shetland Islands	Sudgen and John (1973), Hansom (1979), Curl (1980), Barsch and Mäusbacher (1986), Del Valle et al. (2002), Hall and Perry (2004), Hall (2010), Simms et al. (2011), Simms et al. (2012)
Antarctic Peninsula	Emslie and McDaniel (2002), Bentley et al. (2005a), Simkins et al. (2013a)
Ross Sea	Stuiver et al. (1976), Stuiver et al. (1981), Baroni and Orombelli (1994), Hall and Denton (2000a,b), Lambert et al. (2002), Hall et al. (2004), Baroni and Hall (2004)
East Antarctica	Adamson and Colhoun (1992), Maemoku et al. (1997), Omoto (1977)

5.2. BACKGROUND

5.2.1. ANTARCTIC RAISED BEACHES

Early work on Antarctic beaches focused on modern coastal processes (Nichols, 1961; Kirk, 1966) and characterization of coastal marine and glacial features (Nichols, 1968; Hansom, 1983; Adie, 1964). Attempts to date raised beaches and reconstruct RSL histories began in the 1970s and 1980s (Sudgen and John, 1973; Stuiver et al., 1976; Hansom, 1979; Curl 1980; Stuiver er al., 1981; Barsch and Mäusbacher, 1986). Whereas the Ross Sea, South Shetland Islands, and Marguerite Bay are relatively well-studied (Baroni and Orombelli, 1991; Baroni and Hall, 2004; Hall et al., 2004; Bentley et al., 2005; Hall, 2010; Simms et al., 2012; Simkins et al., 2013a), few studies have focused on East Antarctic beaches (Adamson and Colhoun, 1992; Hayashi and Yoshida, 1994; Maemoku et al., 1997; Miura et al., 1998) while beaches have not been observed in West Antarctica outside of the Antarctic Peninsula. The vast majority of explored raised beaches around Antarctica date to the Holocene resulting from the preservation of beaches above swash processes due to post-glacial rebound accompanied by open-water, ice-free conditions since the LGM. Older beaches are most likely reworked by glacial activity thus preservation of beaches that formed prior to the LGM is limited. However, emergent pre-LGM beaches have been observed at Cape Ross in Southern Victoria Land of the Ross Sea Embayment (Gardner et al., 2006), the South Shetland Islands (John and Sudgen, 1971; Curl, 1980), the Sôya Coast in East Antarctica (Igarashi et al., 1995; Maemoku et al., 1997; Miura et al., 1998; Takada et al., 2003), and possibly Marguerite Bay (Simkins et al., 2013a). Berkman et al. (1998) provide a compilation of raised beach ages between 20-35 ky BP from the Sôya Coast and McMurdo

Sound. Modeling studies have utilized RSL histories derived from raised beaches to constrain glacial isostatic adjustment since the LGM (Payne, 1989; Pallas et al., 1997; Fretwell et al., 2010; Whitehouse et al., 2012; Gomez et al., 2013, Okuno and Miura, 2013).

5.2.2. GEOCHRONOLOGY

Antarctic beaches are most commonly dated using radiocarbon analysis of inorganic calcium carbonate and organic remains incorporated within beach deposits (Baroni and Orombelli, 1991; Adamson and Colhoun (1992); Maemoku et al., 1997; Baroni and Hall, 2004; Hall et al., 2004; Bentley et al., 2005; Hall, 2010). Common materials dated include shells, whale bones, guano, snow petrel stomach oil, and seal and penguin remains. Mobile marine species (e.g. birds and seals) are not limited to sea level (Berkman et al., 1998) and thus provide minimum age constraints for beach formation. For example, crabeater seals have been observed more than 50 km inland at elevations >1000 m (Péwé et al. 1959), snow petrels have been found >300 km from the coastline (Hiller et al. 1988), and penguin rookeries can be tens of meters above sea level (Volkman and Trivelpiece, 1981). Ages from shells provide minimum ages for beach formation if deposited by waves after initial beach formation, maximum ages if reworked or sampled from a facies below beach sediment, and ages that date the beach if found *in situ*. Despite the common interpretation of radiocarbon-dated materials as minimum age constraints (Baroni and Orombelli, 1991; Bentley et al., 2005; Hall, 2010), more resistant materials such as bones and shells may be reworked into younger beaches providing maximum ages for beaches (Bentley et al., 2005). Debate continues on how to interpret materials buried deep within beaches where Hall (2010) suggest buried materials (> 30 cm) represent ages near the timing of beach formation while

Bentley et al. (2005) suggest buried materials (> 10 cm) are reworked providing maximum ages.

Alternatively, optically stimulated luminescence (OSL) has recently been used to date Antarctic beaches (Simms et al., 2011; Simms et al., 2012). OSL dating determines the time elapsed since minerals were last exposed to sunlight (Lian and Roberts, 2006; Rhodes, 2011). Established applications and equipment for OSL dating are suitable for analyzing quartz and feldspar grains < 250 μm in diameter. However, Simms et al. (2011) applied OSL dating to buried cobble surfaces from raised beaches of the South Shetland Islands showing agreement with previously published radiocarbon ages. The authors use the assumption that the last time the buried cobbles were reset by sunlight was in the swash zone thus OSL ages provide constraints on the timing of uplift above swash and storm processes. OSL-dated beach cobbles provide ages that closely constrain beach formation by dating burial since the last reworking event by waves.

5.3. METHODS

5.3.1. OSL AGES

Buried cobbles were extracted from raised beaches at Rothera (65°26'S 65°30'W), Torgersen Island (64.7°46'S 64°05'W), and Biscoe Point (64°49'S 63°49'W) under a light-proof tarpaulin and wrapped in layers of light-proof black plastic (see Figure 21 for locations). Material surrounding the dated cobbles was collected for dosimetry measurements used for dose rate determination. The outer 1 mm was extracted from the buried portion of sampled cobble using rock saws then crushed and sieved to obtain grains between 63-250 μm in diameter. The sieved samples were treated with 3.75% HCl and 27% H_2O_2 followed by

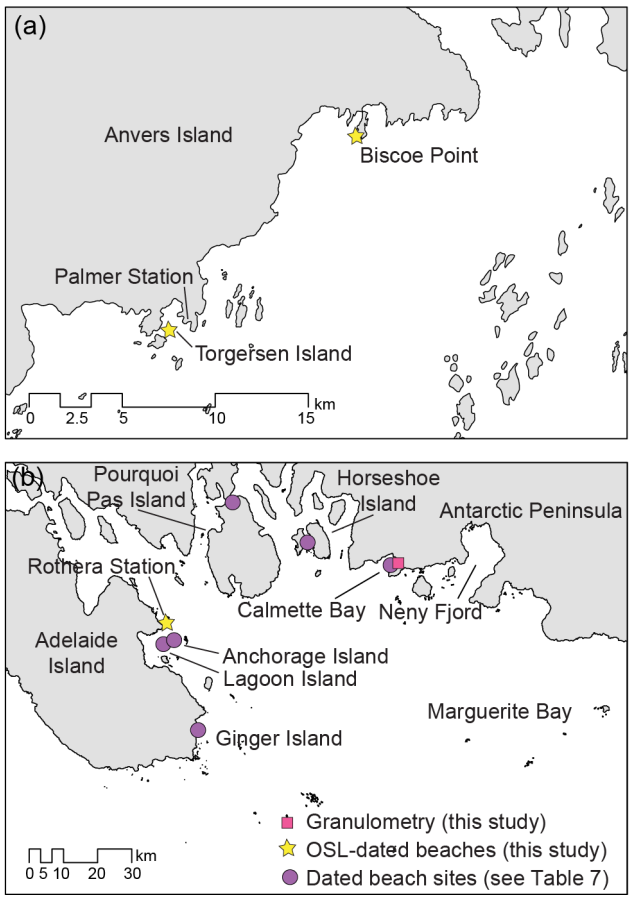

Figure 21. (a) Anvers Island along the central western Antarctic Peninsula showing the sampling locations for OSL dating. (b) Northern Marguerite Bay along the western Antarctic Peninsula showing the locations of previously dated beaches, OSL-dated beaches, and granulometry measurements from this study.

density separations of 2.62 and 2.75 g cm^{-3} with lithium heteropolytungstate to isolate the quartz fraction. The remaining quartz fractions were etched with 48% HF for 40 minutes (Fleming, 1979). Quartz separates of ~100-200 grains were prepared on sample carriers using silicone oil spray. Sample carriers were cleaned following the methods described in Simkins et al. (2013b) to prevent sediment signal contamination by variable, dose-dependent signals produced by the sample carriers themselves.

OSL measurements were conducted using a Risø TL/OSL-DA-15 Reader manufactured by Risø National Laboratory with a built-in $^{90}Sr/^{90}Y$ beta source at Oklahoma

State University. Optical stimulation was carried out with blue LEDs (470 nm, 31 mW cm^{-2}) and infrared stimulation with LEDs (~875 nm, 110 mW cm^{-2}) using a UV (Hoya U340, 7.5 mm, 340 nm peak) detection window (Bøtter-Jensen and Murray, 1999) with a heating rate of 5°C s^{-1} and measurement rate of 1 count s^{-1}. Equivalent doses were determined following the single-aliquot regenerative-dose (SAR) procedure (Murray and Wintle, 2000; Wintle and Murray, 2006) using the specific measurement protocol outlined in Table 5 (Section 4.4.4) with high-temperature stimulation (Murray and Wintle, 2003) and a post-IR blue sequence (Wallinga et al., 2002; Duller, 2003; Wintle and Murray, 2006). The common age model (Galbraith et al., 1999) was used to determine equivalent doses used for age calculation from a population of aliquots. Using surrounding material and the remaining portion of dated cobbles, ^{238}U and ^{232}Th series and ^{40}K nuclide concentrations were measured with a Reverse Electrode Coaxial Germanium Detector from Canberra Industries, Inc. Beta, gamma, and cosmic radiation and the influence of water content were accounted for in the total dose rate following the methodology of Section 4.4.5.

5.3.2. AGE COMPILATION

Two-hundred eighty nine ages derived from radiocarbon and OSL-dated beaches were compiled from previously published studies around Antarctica (Table 7). Five of the ages are new from this study and are derived from OSL-dated cobble surfaces. The OSL ages are treated as ages that closely constrain the timing of beach formation. Latitudes and longitudes of the dated beach sites are shown in Appendix VIII. Published ages were excluded if: (1) samples were not taken from beach ridges; (2) sample location, elevation, or material was not provided; (3) samples were derived from windblown material, orthogenic

soils on top of beaches, or reworked slope material; and/or (4) the ages predate the Holocene. Radiocarbon ages were corrected using a marine radiocarbon reservoir age of 1144 ± 120 years corresponding to a delta-R value (regional deviation from the global average reservoir age) of 791 ± 121 years (Hall et al., 2010). All radiocarbon ages were calibrated for calendar years using Calib 6.0 (Reimer et al., 2009) with the marine (MARINE09) calibration curve and reported with two-sigma error. OSL ages are reported as originally published and presented in thousand years before present (ky BP; as of 1950) with two-sigma error to allow for direct comparison with radiocarbon ages in calendar thousand years before present.

5.3.3. STATISTICAL METHODS

The temporal distribution of beach ages were calculated two different ways. The first method includes compiling all radiocarbon and OSL ages from raised beaches around Antarctica that follow our criteria discussed in Section 5.3.2. Appendix VI provides details of radiocarbon ages including sample sites, materials, elevations, raw ^{14}C ages, calibrated ages, original sources, and indicative meaning for beach formation. Appendix VII includes sample locations, elevations, equivalent doses, dose rates, and ages of OSL-dated raised beaches. This includes all ages regardless of indicative meaning for beach formation and, in some cases, multiple ages from the same beaches. Compiling the ages this way allows for the observation of general trends in beach ages from around Antarctica without biasing toward interpreted indicative meaning in terms of beach formation of the dated materials. As some individual beaches have been dated multiple times and could bias the record with a few beaches that have been dated multiple ages, I also compiled the ages to remove sampling biases. The second method includes determining a representative age for individual beaches

from specific sites around Antarctica (Appendix IX). The representative ages were calculated by averaging ages in the case where multiple ages are provided for the same beach. The indicative meaning of the dated materials as minimum and maximum ages as well as ages that closely date beach formation were determined using the interpretations of the authors who published the ages. Ages that closely date beach formation were preferentially used over minimum or maximum ages. Only three beach ages were calculated using maximum ages (3.5-m beach at Dunlop Island, Ross Sea; 3.5-m and 4-m beaches at Potter Cove and Potter Peninsula). For the other beaches without ages that closely date beach formation, individual beaches ages were calculated by averaging minimum ages.

For both methods, histograms of the compiled ages were separated into groups by region including the South Shetland Islands, the Antarctic Peninsula, Ross Sea, and East Antarctica. The distribution of beach ages were sub-divided further by individual site for the second method using representative ages for individual beaches at each site. For the first method, in addition to the histogram, probability distribution functions were utilized to include the error space of individual ages and determine overlap between the ages. Probability distribution functions for radiocarbon ages were calculated using Calib 6.0

Table 8. Summary of new OSL ages from the western Antarctic Peninsula

Location	Sample	Elevation (masl)	Aliquots[a]	D_e (Gy)	DR (Gy ka^{-1})	Age	(ka)[b]
Rothera	R07	5.5	3	3.94 ± 1.23	3.47 ± 0.10	1.13 ± 0.72	
Torgerson Is	T10-06	5.0	14	1.18 ± 0.08	1.48 ± 0.14	0.79 ± 0.18	
Torgerson Is	T10-03	7.2	15	3.42 ± 0.14	2.32 ± 0.13	1.48 ± 0.20	
Torgerson Is	T10-01	7.2	8	2.43 ± 0.21	1.11 ±0.14	2.18 ± 0.68	
Biscoe Point	BP10-09	7.0	11	1.43 ± 0.12	2.47 ± 0.10	0.58 ± 0.1	

masl = meters above sea level, D_e = equivalent dose, DR = dose rate, ka BP = thousand years before present

[a] Number of aliquots that pass all standard SAR procedure tests

[b] Ages are rounded to the nearest ten years with 2-sigma uncertainties. Samples were collected in 2010 thus 60 years was subtracted to obtain ages before present (as of 1950) for direct comparison with radiocarbon ages

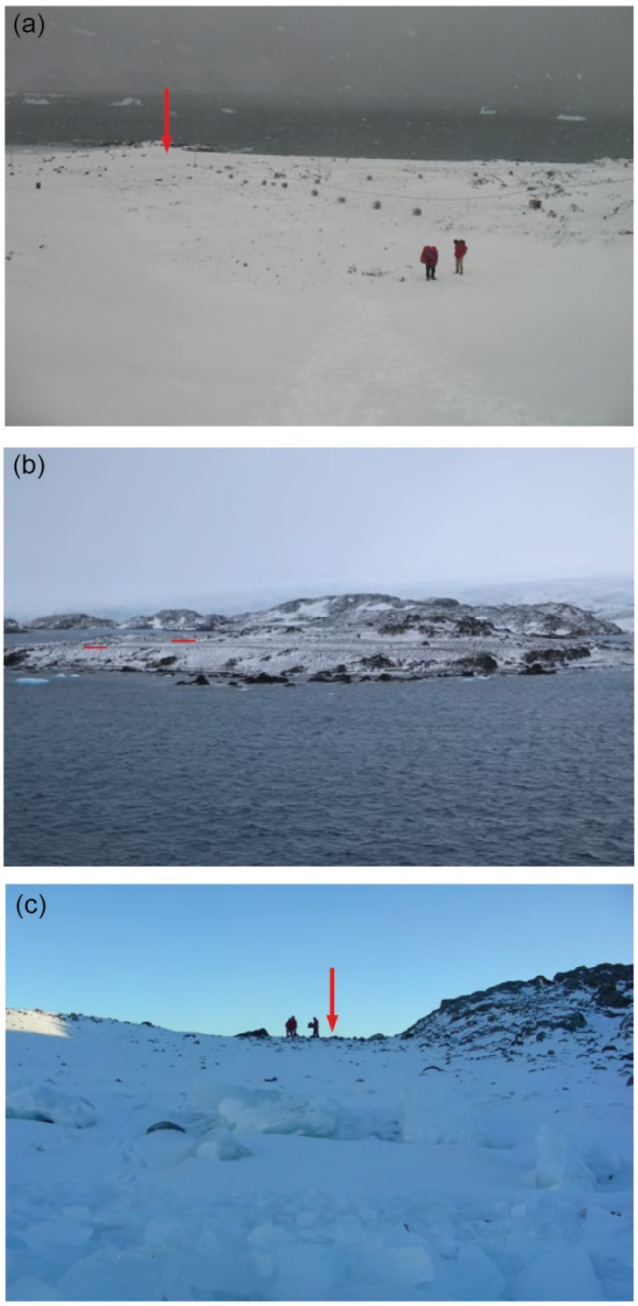

Figure 22. (a) Sampling location at Rothera showing the approximate site where sample R07 was taken. (b) Torgerson Island showing the sample sites along two prominent raised beaches. (c) Sample location from Biscoe Point at the top of the scarp (photograph was taken from the modern beach looking up at the scarp).

(Reimer et al., 2009). Where radiocarbon age uncertainty predominantly stems from calibration of ages from radiocarbon years to calendar years, OSL age uncertainty is

propagated from analytical uncertainty, statistical spread of aliquot measurements, and assumptions used in age calculations and reported as standard error. Therefore, I apply equal probability between the upper and lower age error bars for the OSL ages. The probabilities of individual ages were summed over the last 10 ky at 1-year intervals to obtain a single probability curve per region. The composite probability curves were standardized by the number of dated beaches for each region to avoid spatial sampling bias.

5.3.4. GRANULOMETRY

Measurements of clast roundness were collected from raised beaches at Calmette Bay within Marguerite Bay along the western side of the Antarctic Peninsula (Figure 21). Granulometry was measured for one-hundred cobbles within an area of ~ $1m^2$ as rounded, sub-rounded, sub-angular, and angular from twenty-three beach ridges ranging from 0-22 meters above sea level (masl). As not all beach ridges were previously dated, the age interpretations from Simkins et al. (2013a) were used from the same site to provide chronological constraints. Where two ages were provided for the same raised beach, I use the mean and the lowest and highest values of standard error as the error range.

5.4. RESULTS

5.4.1. OSL AGES

Five OSL ages are provided from raised beaches along the western Antarctic Peninsula with one age from Adelaide Island near Rothera Station and four from the southern end of Anvers Island at Torgerson Island (n=3) and Biscoe Point (n=1). The equivalent doses, dose rates, and ages are summarized in Table 8. The four ages from the southern end

of Anvers Island provide the first dated constrains on RSL and beach formation along the western Antarctic Peninsula outside of the South Shetland Islands and Marguerite Bay. The sampled beach at Rothera contained a primitive organic soil that filled the matrices between beach cobbles. Cobbles were extracted from > 30 cm below the surface to avoid sampling cobbles that could have potentially been reset by anthropogenic activity. Field sampling at Rothera (Figure 22a) was hindered by extensive snow cover and frozen ground. An age of 1.13 ± 0.36 ky BP from 5.5-m asl at Rothera is in agreement with dated beaches between 3.4 and 6.5 masl at Calmette Bay, 60 km east of Rothera (Simkins et al., 2013a). Samples from Torgerson are from well-defined raised beaches (Figure 22b). The ages (0.79 ± 0.09 ky BP at 5.0 m asl; 1.48 ± 0.10 and 2.18 ± 0.34 ky BP at 7.0 m asl) from Torgerson Island show a normal succession of increasing age with increasing elevation while two samples from the beach at 7.2 m provide similar ages. At Biscoe Point, the dated sample was taken at the top of a composite beach ramp that extended from modern sea level to 7 masl in a small embayment filled with brash ice (Figure 22c). Interpretation is difficult from the single age (0.58 ± 0.05 ky BP at 7 m) at Biscoe Point; however, equivalent-elevation beaches within the South Shetland Islands have similar ages to the beach at Biscoe Point (Simms et al., 2012). The ages provided by this study except those from Torgerson Island should be regarded as preliminary age constrains for two reasons: (1) a limited number of dated beaches is provided for each site; and (2) the absence of independent ages constraints on other geomorphic features at these sites, especially for the sites offshore of Anvers Island.

5.4.2. TEMPORAL DISTRIBUTIONS

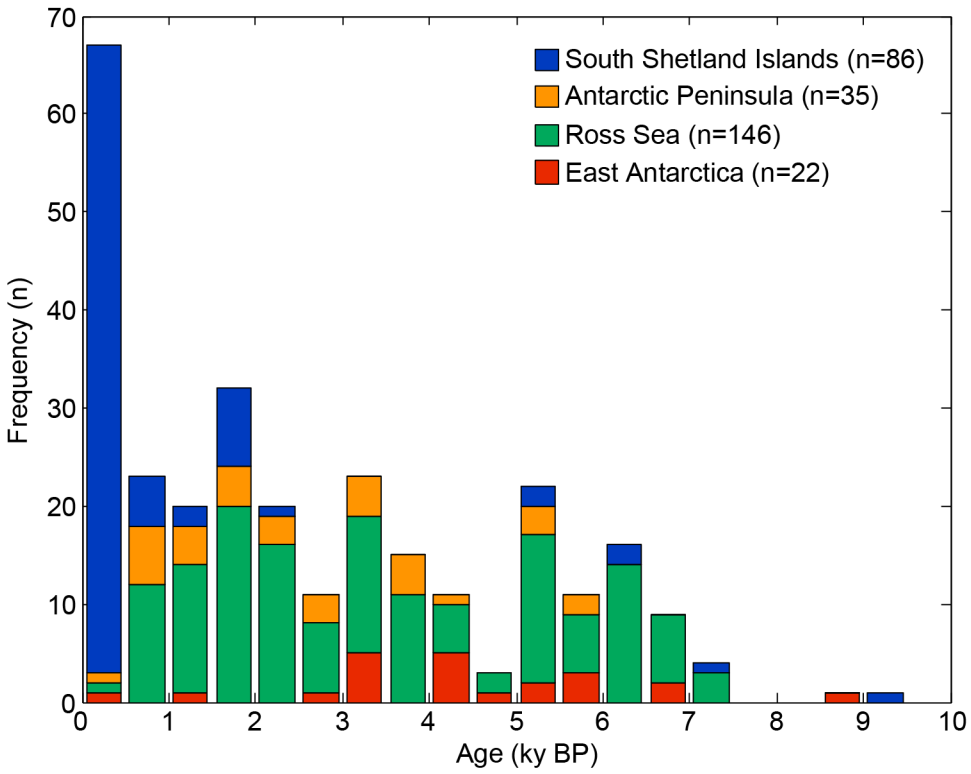

Figure 23. Distribution of all ages from Antarctic beaches separated by region. The bin width is 500 years and the frequency (n) is the ages that fall within the 500-year bins.

The distribution of all previously dated raised beach ages (Table 7) and new ages provided by this study (Table 8) are shown graphically in a histogram (Figure 23). Composite probability distributions are used for each region to account for age uncertainty within the dataset (Figure 24). A large number of ages between 0.2-0.7 ky BP from the South Shetland Islands most likely reflect a period of enhanced uplift from the Little Ice Age unique to the South Shetland Islands due to the rheological properties of the islands overlying an active subduction zone. The South Shetland Islands have a weaker rheology (Simms et al., 2012) than estimated for the Antarctic Peninsula (Ivins and James, 2005) and elsewhere around Antarctica. The weak rheology perhaps makes the South Shetland Islands more sensitive to rapid, short-lived ice-mass changes. Simms et al. (2012) suggest the South Shetland Islands experienced ice-cap advance during the Little Ice Age (1400-1700 CE; 0.3-

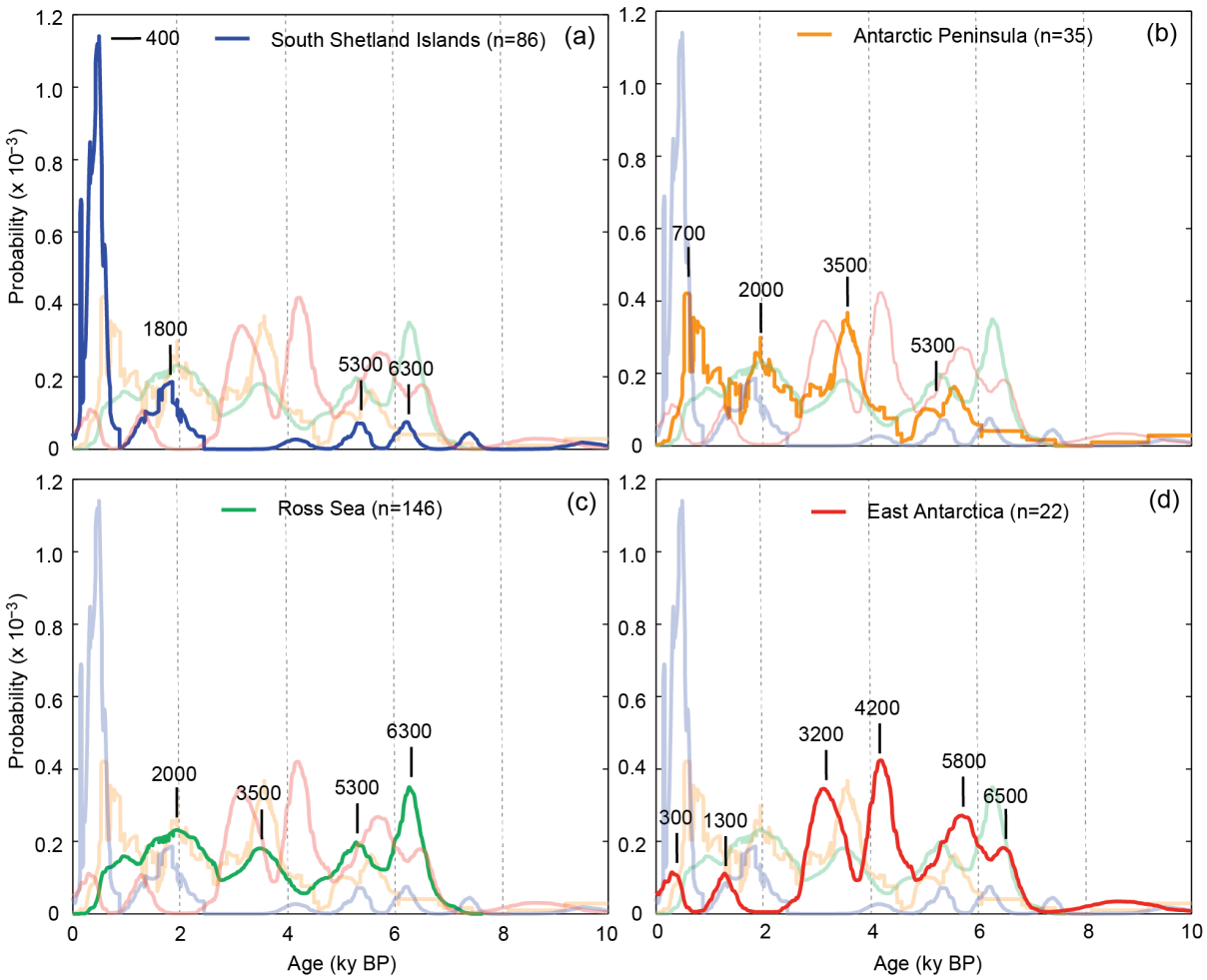

Figure 24. Composite probability distributions for all ages from beaches for the (a) South Shetland Islands, (b) Antarctic Peninsula, (c) Ross Sea, and (d) East Antarctica standardized by the number of dated beaches per region. Peaks in beach occurrence are labeled in years while the peak widths are noted in the text.

0.6 ky BP). Subsequent rapid rates of post-glacial rebound (up to 12.5 mm yr^{-1}) after the ice cap retreated at the termination of the Little Ice Age resulted in the preservation of numerous young beaches. Consequently, the South Shetland Islands are considered as a separate system from the rest of Antarctica for the purposes of this study as the majority of ages are limited to < 1 ky BP. However, the distribution from the South Shetland Islands also has minor peaks centered at 1.8, 5.3, and 6.3 ky BP (Figure 24).

The temporal distributions of beaches from the Antarctic Peninsula, Ross Sea, and East Antarctica show distinct peaks in beach occurrence (Figure 23). These periods are centered at 0.7 (0.5-1.2), 2 (1.6-2.5), 3.5 (3.3-3.9), and 5.3 (4.9-5.9) ky BP in the Antarctic Peninsula and 2 (1.4-2.5), 3.5 (3.2-3.8), 5.3 (5.0-5.6), and 6.3 (6.0-6.5) ky BP within the Ross Sea (Figure 24). The minor peaks in beach occurrence in the South Shetland Islands are generally synchronous with the distributions from the Antarctic Peninsula and Ross Sea excluding the younger peak centered at 0.4 ky BP. The distribution of beach ages in East Antarctica shows peaks in beach occurrence at 0.3 (0.1-0.5), 1.3 (1.1-1.4), 3.2 (2.8-3.5), 4.2 (4.0-4.5), 5.8 (5.4-5.9), and 6.5 (6.3-6.9) ky BP (Figure 24).

To account for potential bias in the record created by multiple ages from single beaches, the number of individual beaches of a given age was used to determine the temporal distribution of beaches was determined for the South Shetland Islands, Antarctic Peninsula, Ross Sea, and East Antarctica. As the representative beach ages are derived from specific sites, the distribution of individual sites allows for a closer examination at the temporal distribution in beach occurrence within the four major regions (Figure 26). The histograms from both methods of age compilation – all ages (Figures 23-24) versus individual beaches of given ages (Figures 25-26) – show similar trends in beach occurrence despite the reduced number of data points. We suggest the changes in the temporal distribution of beach occurrence reflect periods when either more or less beaches are formed. Beach formation within the Antarctic Peninsula and Ross Sea is generally synchronous while beach formation in East Antarctic during periods of limited beach formation elsewhere in Antarctica. The synchronous timing of beach formation along the Antarctic Peninsula and Ross Sea suggests a large-scale control on the processes that shape beach preservation along

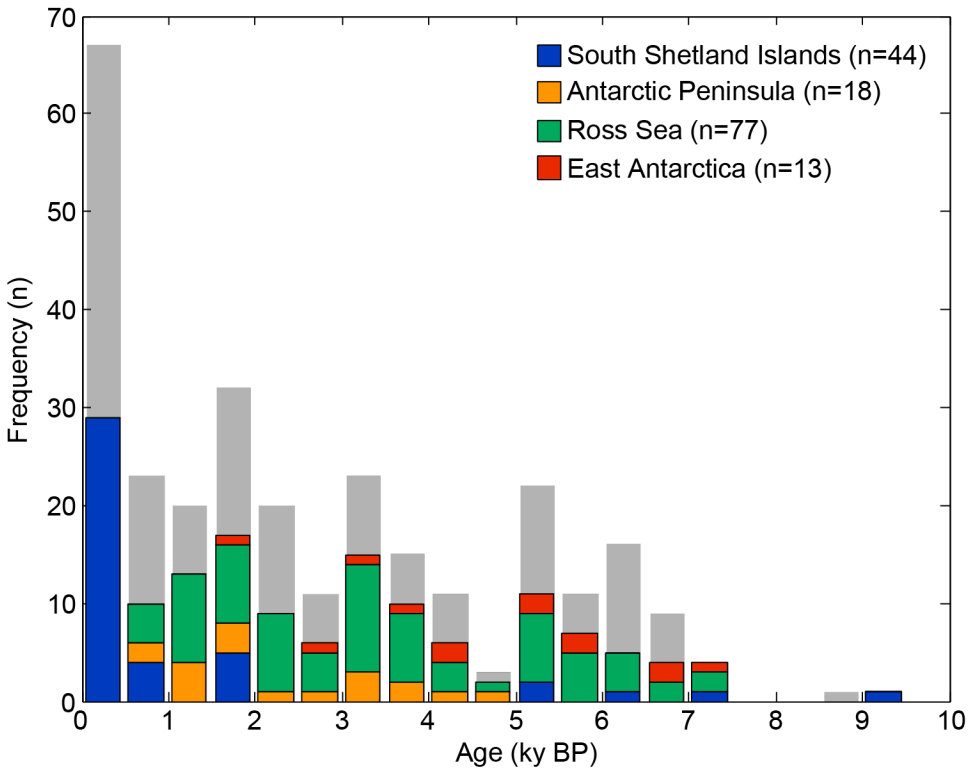

Figure 25. Distribution of the number of dated beaches for a given time period separated by region. The bin width is 500 years and the frequency (n) is the number of beaches that fall within the 500-year bins. The histogram of all ages from beaches (Figure 23) is shown in the background (gray bars).

the coastline between the two regions rather than local variations in wave climate and rates of post-glacial rebound.

5.4.3. GRANULOMETRY

After counting 100 clasts from each beach ridge, beach ridges at Calmette Bay show a wide range of rounded material varying from 0- 36% clasts characterized as round (Figure 27). In the absence of fluvial transport, wave energy is responsible for rounding beach deposits thus a larger abundance of rounded material represents increased periods of reworking by wave action signifying more frequent periods of open-water conditions. Although the age constraints provided by Simkins et al. (2013a) contain large uncertainties,

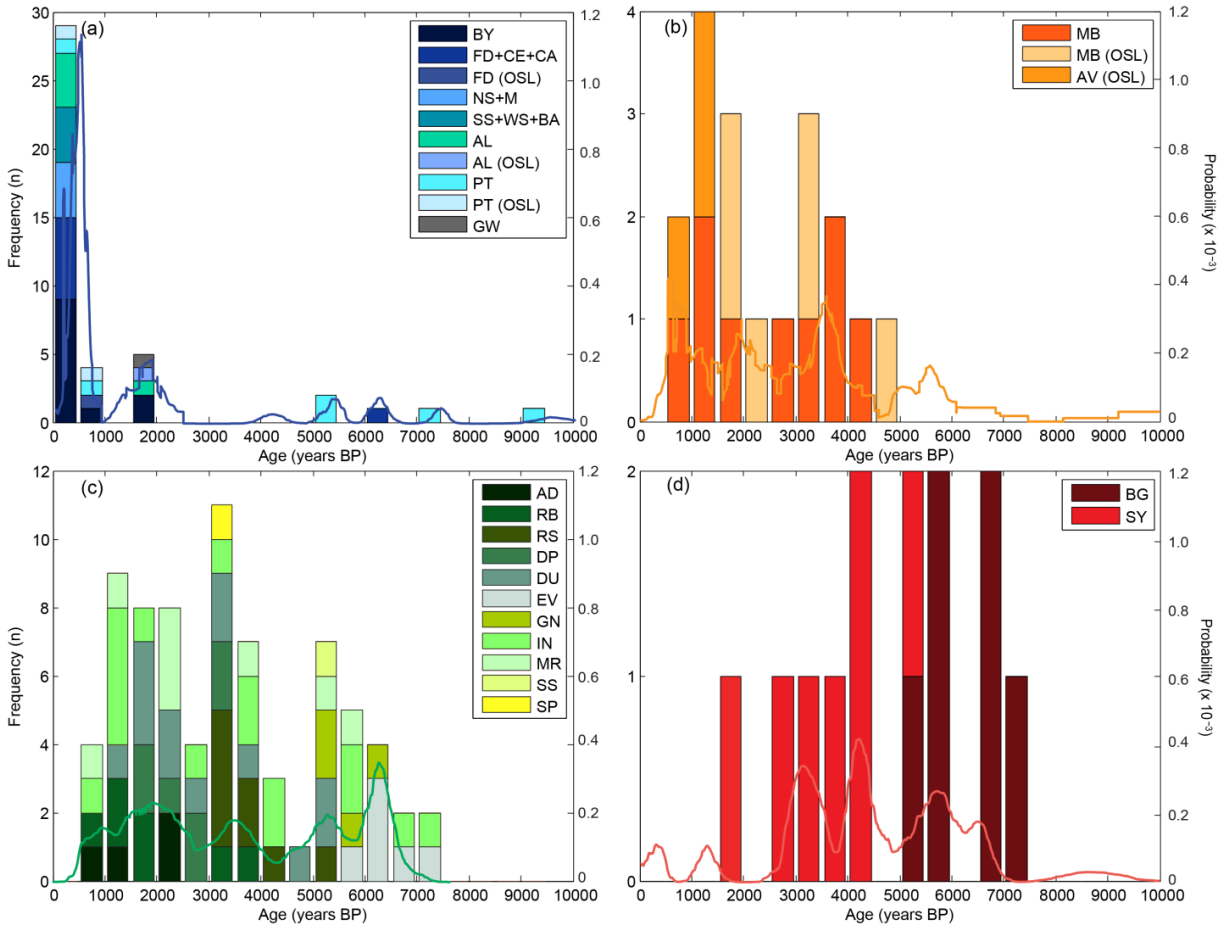

Figure 26. Histograms showing the distribution of individual beach ages by specific site group by region including (a) the South Shetland Islands, (b) Antarctic Peninsula, (c) Ross Sea, and (d) East Antarctica. The composite probability distribution functions from Figure 24 are shown for each region. Frequency of beaches is on the left-hand y-axis and probability of ages on the right-hand y-axis for (a)-(d).

the abundance of rounded beach deposits (>10%) indicates more frequent wave exposure along the coastline of Calmette Bay at approximately 1, 2, and 5-6 ky BP (Figure 27).

5.5. DISCUSSION

5.5.1. BEACHES AS A PROXY FOR WAVE EXPOSURE

Periods of enhanced beach occurrence are observed from the temporal distribution of raised beaches indicating periods of enhanced beach formation due to increased wave exposure along the coastline of Antarctica. The granulometry measurements independently

suggest increased wave exposure at Calmette Bay around 1, 2, and 5-6 ky BP (Figure 27). Bentley et al. (2005) also identified periods of increased wave exposure from clast roundness at Anchorage Island and Rothera Station within Marguerite Bay between 2.2-3.5 ky BP. Additionally, Hodgson et al. (2013) indicate a period of increased wave energy due to reduced summer sea-ice extent between 2.0 and 6.0 ky BP at Horseshoe Island, Marguerite Bay. Thus granulometry measurements from multiple sites provide an independent means of assessing wave-energy conditions to test the use of temporal distribution of beaches as a proxy for beach formation associated with variable wave exposure. The periods of increased wave-induced reworking derived from clast roundness are generally synchronous with the periods of enhanced beach formation along the Antarctic Peninsula from 0.7, 2, 3.5, and 5.3 ky BP.

The ability of wave action to rework coastal sediment around Antarctica is severely limited by the presence of sea ice. Due to the lack of independent proxies for wave-energy conditions, Antarctic sea-ice proxies provide independent insight on wave energy where extensive sea ice correlates to more frequent wave action. Several studies provide insight on sea ice derived from marine sediment cores throughout the Holocene offshore of the Antarctic Peninsula and East Antarctica and along the Antarctic Polar Front (Kanfoush et al., 2002; Nielsen et al., 2004; Crosta et al., 2007; Allen et al., 2010; Denis et al., 2010; Divine et al., 2010; Etourneau et al., 2013). Here I compare the temporal distribution of raised beaches from the Antarctic Peninsula to a sea-ice proxy from the Palmer Deep Basin, western Antarctic Peninsula (Etourneau et al., 2013) derived from highly branched isoprenoid alkenes diene and triene used as diatom-specific biomarkers for sea ice and open water indicators, respectively, in the Southern Ocean (Figure 28). During periods of beach formation at 2, 3.5,

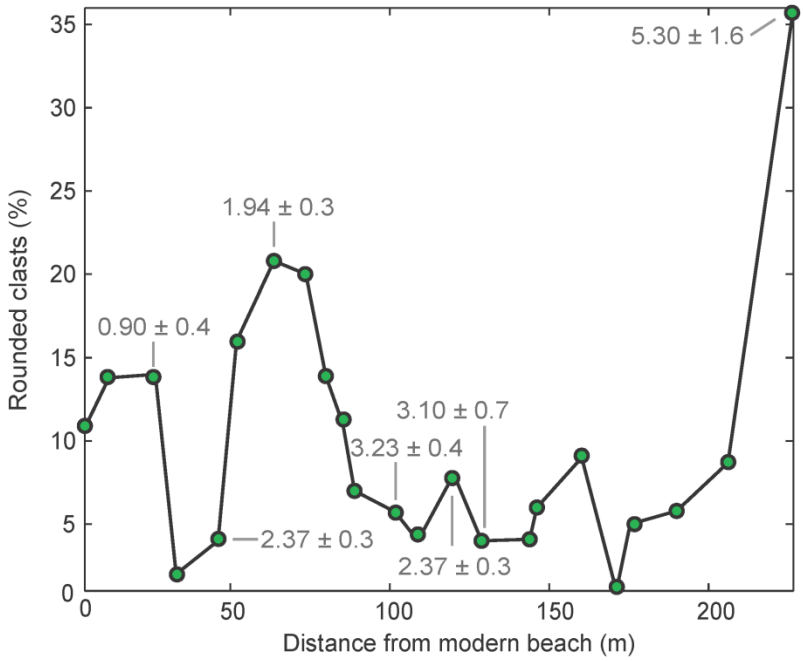

Figure 27. Granulometry of beach deposits at Calmette Bay showing roundness in percent as a function of distance from the modern beach. The age constraints are the mean ages between the lowest and highest uncertainties from Simkins et al. (2013a).

and 5.3 ky BP, an observed decrease in diene/triene ratios is used to infer periods of relatively limited sea-ice conditions. The correlation between periods of enhanced beach formation in the Antarctic Peninsula and less sea ice in the Antarctic Peninsula suggests coastal evolution is influenced by sea-ice conditions. Crosta et al. (2007) provide a sea-ice proxy derived from sea-ice diatom species, *F. curta* and *F. cylindrus,* offshore of Adélie Land, East Antarctica showing an overall trend of less sea ice from the early Holocene to 3.5 ky BP followed by increased sea ice in the late Holocene occurring near the timing of little Holocene beach formation in East Antarctica at 3.2 ky BP (Figure 29a-b). Additionally, Kanfoush et al., (2002) provide a proxy for ice-rafted debris (IRD) along the Antarctic Polar Front in the South Atlantic sector of the Southern Ocean (53°S) as an indicator of the survival of icebergs and sea ice traveling clockwise around the continent in the Antarctic

Circumpolar Current from the Weddell Sea. When comparing the distribution of East Antarctic beaches to the IRD proxy of Kanfoush et al. (2002), periods of beach formation correspond to periods of limited IRD indicating warmer sea-surface temperatures (Figure 29c). Warmer sea-surface temperatures would lead to reduced survival of icebergs as well as shorter periods of sea-ice growth and more open-water conditions. The sea-ice record proximal to Adélie Land, East Antarctica derived from the abundance of *F. curta* and *F. cylindrus* may represent either local sea-ice conditions or meltwater pulses considering *F. cylindrus* is an indicator of glacial meltwater as well as sea ice (Pike et al., 2008; Allen et al., 2010). The inverse relationship between IRD at the Antarctic Polar Front and beach formation in East Antarctica suggests the IRD record represents a regional record of marine ice conditions.

5.5.2. IMPLICATIONS FOR COASTAL RESPONSE TO CLIMATE

Periods of heightened wave exposure along the coast control the efficiency of beach formation around Antarctica with periods of increased wave exposure (i.e. decreased sea ice) centered at 2, 3.5, and 5.3 ky BP in the Antarctic Peninsula and Ross Sea and 3.2, 4.2, 5.8, and 6.5 ky BP around East Antarctica outside of the Ross Sea. The out-of-phase relationship between beach formation in East Antarctica compared to the Antarctic Peninsula and Ross Sea resembles the anti-phasing of climate forcing around Antarctica (Mayewski et al., 2004, 2009; Nielsen et al., 2004; Yuan, 2004; Schneider et al., 2006). Monien et al. (2014) infer maximums in penguin populations from 6.1-5.2, and 4.3-3.4, 2.0-1.4 ka from penguin guano traces in lake sediment on Ardley Island, South Shetland Islands. Enhanced beach formation centered at 3.5 ky BP observed in the distributions from the Antarctic Peninsula and Ross

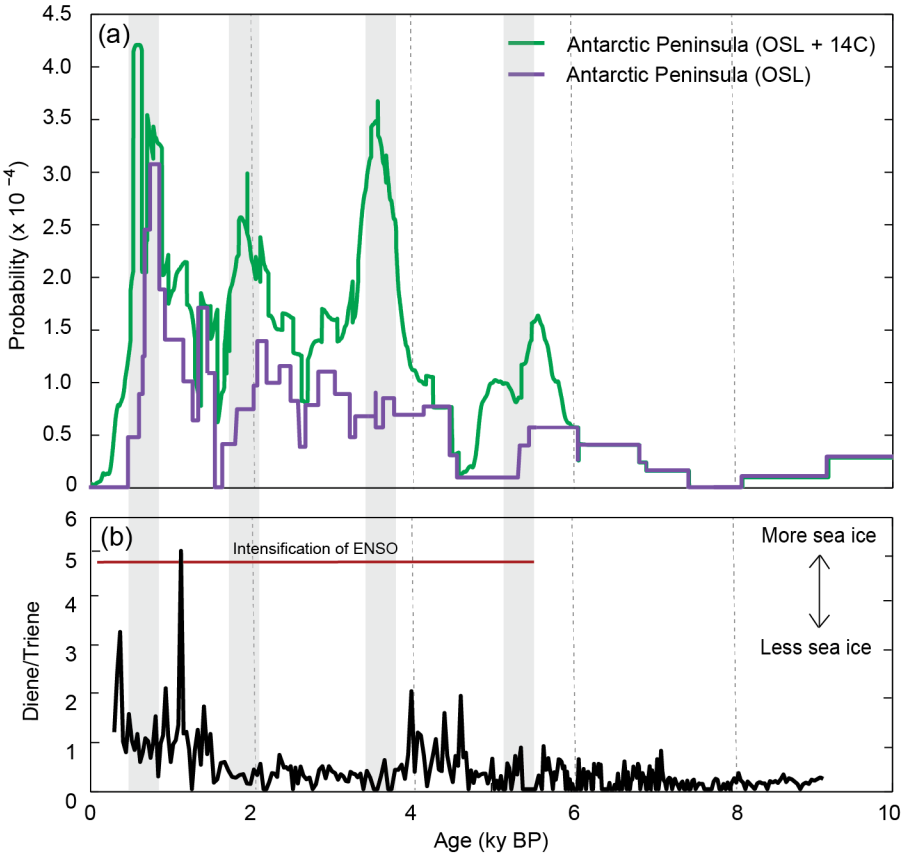

Figure 28. (a) Distribution of Antarctic Peninsula beaches derived from OSL and radiocarbon ages (green line) and OSL ages alone (purple line). (b) Sea-ice proxy of Etourneau et al. (2013) from the Palmer Deep Basin, western Antarctic Peninsula derived from highly branched isoprenoid alkenes diene and triene used as diatom-specific biomarkers for sea ice and open water indicators, respectively.

Sea occurs during the "Penguin Optimum" in the Ross Sea between 3-4 ky BP when warmer climate conditions and less sea ice are inferred from the distribution of abandoned penguin rookeries along the coast of Victoria Land, Ross Sea (Baroni and Orombelli, 2004). Additionally, an expansion of seal populations from ~1.0-2.5 ky BP has been observed from the distribution of dated seal skin and hair incorporated into beaches of Victoria Land suggesting decreased coastal sea ice (Baroni and Orombelli, 2004). The timing of Penguin and Seal Optimums and beach ages are both based on radiocarbon ages of penguin and seal remains incorporated into raised beaches; therefore, the timing of optimums and peaks in beach formation are inherently linked. However, the OSL ages from the Antarctic Peninsula

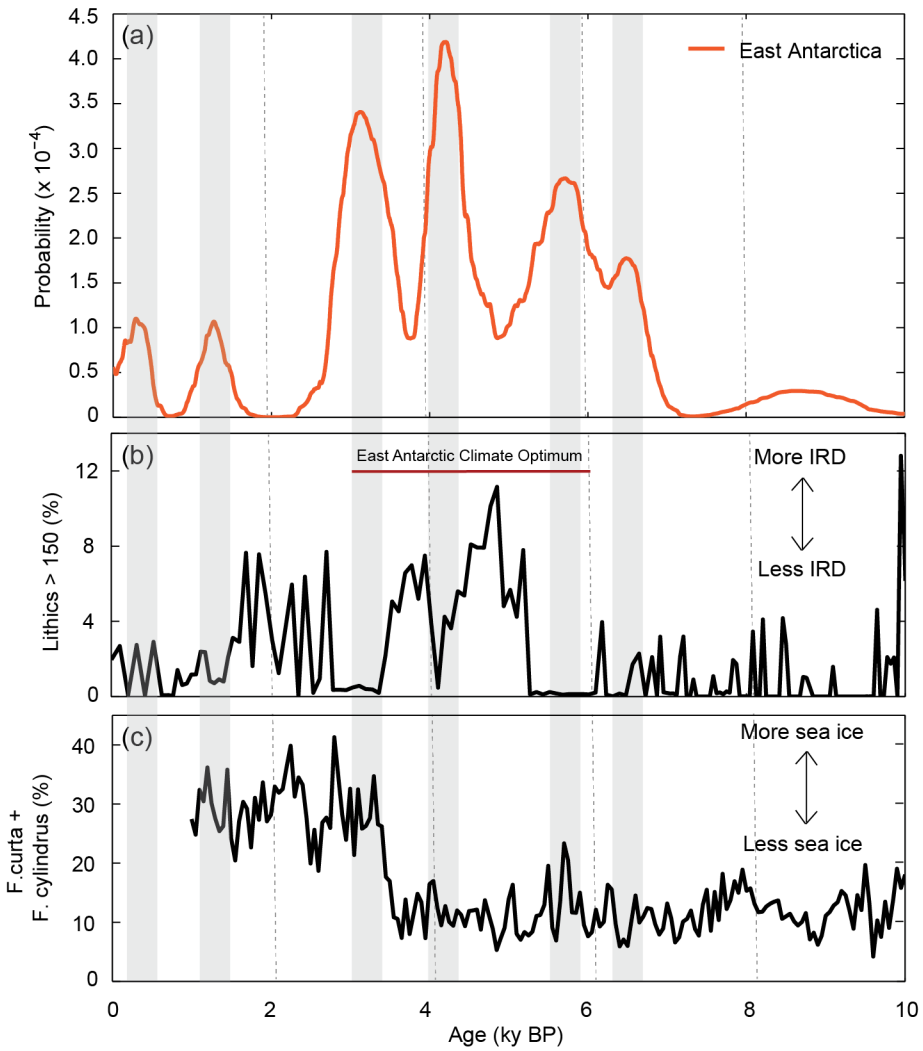

Figure 29. (a) Distribution of beaches in East Antarctica. (b) Proxy for ice-rafted debris (IRD) from along the Antarctic Polar from in the South Atlantic sector of the Southern Ocean (53°S) from Kanfoush et al. (2002). (c) Sea-ice proxy of Crosta et al. (2007) from offshore of Adélie Land, East Antarctica derived from sea-ice diatom species.

provide an independent record of beach formation and can be used to rule out bias in the temporal distribution of beach ages due to radiocarbon availability. The OSL ages from the Antarctic Peninsula independently show the same peaks as the composite distribution derived from both OSL- and radiocarbon-dated beaches (Figure 28a) supporting the use of the temporal distribution of beach ages as an indicator of beach formation rather the radiocarbon availability.

An intensification of El Niño Southern Oscillation (ENSO) at 5 ky BP has been observed in low-latitude paleoclimate records in the Southern Hemisphere (Moy et al., 2002; Conroy et al., 2008; Donders et al., 2008) generally coincident with the initiation of enhanced beach formation in the Antarctic Peninsula and Ross Sea. Southern circumpolar westerlies weakened around 5.2 ky BP resulting in milder temperatures over the West Antarctic ice sheet (Yan et al., 2005). In East Antarctica a weak climate optimum occurs between 3 and 6 ky BP and a late climate optimum at 3.0 ky BP occurs in some ice cores most likely due to maximum summer insolation in the southern hemisphere (Masson et al., 2000). The timing of climate optimums in East Antarctica is coincident with periods of enhanced beach formation with the exception of the peak in beach formation centered at 6.8 ky BP.

Wave energy is buffered by sea ice thus the factors that control sea-ice formation directly influence beach formation around Antarctica. Studies on sea ice and its relationship to oceanic and atmospheric climate forcing suggest a strong link to ENSO which causes shifts in the position of the westerlies and variations in sea-surface temperature that control sea-ice extent and duration (Simmonds and Jacka, 1995; Yuan and Martinson, 2000; Martinson and Iannuzzi, 2003; Yuan, 2004; Bertler et al., 2004; Stammerjohn et al, 2008; Sasgen et al., 2010; Etourneau et al., 2013). Yuan (2004) find historical warm ENSO (El Niño) events generate warm temperatures and reduced sea ice in the South Pacific sector while the South Atlantic sector experiences colder temperatures and increased sea ice. Nielsen et al. (2004) suggest an out-of-phase relationship between the Holocene climate dynamics of the Ross Sea/Antarctic Peninsula and East Antarctica. Similar to circum-Antarctic climate and sea ice patterns, a similar pattern of anti-phasing of beach formation is observed in the Antarctic Peninsula and Ross Sea when compared to East Antarctica.

5.6. CONCLUSIONS

The temporal distribution of raised beaches around Antarctica show synchronous periods of beach formation in the Antarctic Peninsula and the Ross Sea centered at 2.0, 3.5, and 5.3 ky BP while East Antarctic (outside of the Ross Sea) beach formation is out-of-phase with the rest of the Antarctica at 3.2, 4.2, 5.8, and 6.5 ky BP. The distribution of beaches in the South Shetland Islands is dominated by enhanced beach formation between 0.2 and 0.7 ky BP most likely due to rapid post-glacial rebound associated with the Little Ice Age with minor peaks in beach formation from 1.3-2.2, 5.1-5.6, and 6.0-6.5 ky BP. The similar timing of beach formation within the Antarctic Peninsula and Ross Sea suggest a regional control on the processes responsible for building beach ridges rather than local variations in wave climate, ice-sheet dynamics, and rates of post-glacial rebound. Antarctic raised beaches, commonly used as sea-level indices, also provide insight on wave energy throughout the Holocene as beach ridges are formed during periods of limited sea-ice and increased open water allowing high-magnitude waves to rework sediment. Granulometry measurements from Marguerite Bay, Antarctic Peninsula provide an independent record of wave-energy conditions showing similar timing to periods of enhanced beach formation in the Antarctica Peninsula. Beach formation results from higher wave exposure during periods of reduced sea ice observed from comparison with Holocene sea-ice proxies. The anti-phasing of beach formation in the Antarctic Peninsula and Ross Sea compared to East Antarctica is markedly similar to the phasing of modern and Holocene climate forcing around Antarctica. Holocene coastal response to oceanographic and climate forcing provides a link between marine and terrestrial records around Antarctica.

CHAPTER 6

FINAL REMARKS

A lack of geochronological constraints on raised beaches limits our understanding of Antarctic RSL change since the LGM. Optically stimulated luminescence dating of quartz extracted from raised beach cobbles provides an alternate means of constraining RSL in settings where material for radiocarbon dating is limited. The studies presented here highlight the poor luminescence behavior of Antarctic cobble surfaces including low OSL signals, tendency to fail standard measurement reliability tests, and equivalent dose scatter. Typically small sources of error stemming from sample carriers used for OSL measurements have a relatively large influence on quartz with low OSL sensitivities. Methods to reduce signals from sample carriers were established by testing cleaning methods capable of removing the luminescent film (Schmidt et al., 2011) and neutralizing the contaminant variable, dose-dependent signals. To further improve the methods of dating cobble surfaces, I attempt to provide insight on the poor luminescence behavior of OSL measurements on quartz extracted from cobble surfaces. The analysis reveals a lack of discernable relationship between OSL and CL characteristics and petrology; however, the petrographic analysis shows the majority of samples contain limited quartz that often occurs as anhedral intergrowths in feldspars. Based on modeling of dose-rate parameters, estimating the size of

these poorly-formed quartz crystals is the most important factor for determining beta dose attenuation and ultimately OSL ages.

Using the novel approach of Simms et al. (2011a) to date Antarctic cobble surfaces using OSL, the RSL history of Marguerite Bay, Antarctic Peninsula is reconstructed from OSL-dated cobble surfaces buried in raised beaches. GIA-modeled RSL for Marguerite Bay (Whitehouse et al., 2012a) are not able to simultaneously fit both the dated RSL observations and the undated marine limits observed throughout the area. Dated sea-level indices are more appropriate for constraining GIA-model predictions and caution must be taken when making interpretations based on undated sea-level indices. Based on the sedimentology, geomorphology, and OSL age constraints, I observe a distinct difference between the upper ($\geq$ 31.8 masl) and lower ($\leq$ 21.7 masl) beaches separated by a 10-m scarp. The upper beaches including the marine limit at 41 masl commonly used to constrain GIA models likely formed prior to the LGM and are not associated with post-glacial rebound since the LGM. The highest raised beach of the lower beaches at 21.7 masl would then represent the marine limit associated with post-glacial rebound since the LGM suggesting half as much RSL fall throughout the Holocene than previously. Further evidence of a lowered marine limit is supported by the marine to freshwater transition at ~20 m with an age of 7.3 ka from an isolation basin at Pourquoi Pas Island, ~40 km northwest of Calmette Bay (Bentley et al., 2005).

In addition to providing further constraints on GIA models, the ages from raised beaches in Marguerite Bay show similar ages at different elevations suggesting beaches are reworked by storm waves after uplifted by post-glacial rebound. Age constraints from raised beaches provide insight on the last reworking event rather than initial beach formation or on

the timing of uplift above sea level. I investigate whether these populations of ages are observed elsewhere around Antarctica and what processes are responsible for reworking Antarctic coastal deposits. The temporal distribution of circum-Antarctic raised beaches throughout the Holocene is utilized to determine the relationship between wave-energy, sea ice, and coastal evolution. The temporal distribution of raised beaches reflects periods of enhanced beach formation throughout the Holocene where synchronous beach formation occurs in the Antarctic Peninsula and Ross Sea and enhanced beach formation in East Antarctica is anti-phased with the rest of Antarctica. Wave energy is responsible for building coarse-clastic beaches; however, that energy is buffered by the presence of sea ice. Beach formation results from higher wave exposure during periods of reduced sea ice observed from comparison with Holocene sea-ice proxies providing a link between marine and terrestrial records.

The findings of the studies presented here have implications for understanding sea-level, GIA, ice-sheet histories, and climate since the LGM. Future work should focus on testing GIA models with dated RSL constraints excluding potentially reworked material and materials that lack a discernable relationship to sea level and/or beach formation. Many locations around Antarctica have poorly constrained RSL histories. Additionally, GIA models show discrepancies in modeled and observed RSL in other locations other than Marguerite Bay; therefore, these locations are targets for future sea-level studies derived from OSL-dated beach deposits. The temporal distribution of Antarctic beach formation shows a strong link to sea-ice conditions that determine the effectiveness of wave energy at reworking coastal sediment. As the extent and duration of sea ice is controlled by oceanographic and climate variability, new reconstructions of sea ice throughout the

Holocene could provide further insight on the link between circum-Antarctic marine and terrestrial records. The application of OSL to date Antarctic cobble surfaces could potentially be extended to date other coarse deposits found across the globe where other dating methods are insufficient.

REFERENCES

Adamson, D.A., Colhoun, E.A., 1992. Late Quaternary glaciation and deglaciation of the Bunger Hills, Antarctica. Antarctic Science 4, 435-435.

Adie, R.J., 1964. Stratigraphic correlation in West Antarctica. Proceedings of the First International Symposium on Antarctic Geology, 307-313.

Aitken, M.J., 1985. Thermoluminescence dating: London, Academic.

Aitken, M.J., 1998. An Introduction to Optical Dating: The Dating of Quaternary Sediments by the Use of Photon-stimulated Luminescence: New York, Oxford University Press.

Allen, C.S., Oakes-Fretwell, L., Anderson, J.B., Hodgson, D.A., 2010. A record of Holocene glacial and oceanographic variability in Neny Fjord, Antarctic Peninsula. The Holocene 20(4), 551-564.

Anderson, J., Shipp, S., Siringan, F., 1992. Preliminary seismic stratigraphy of the northeastern Weddell Sea continental shelf. In: Yoshida, Y., Kaminuma, K., Shiraishi, K. (Eds.), Recent Progress in Antarctic Earth Sciences. Terra Scientific Publishing, Tokyo, 603-612.

Anderson, J.B., Shipp, S.S., Lowe, A.L., Wellner, J.S., Mosola, A.B., 2002. The Antarctic Ice Sheet during the Last Glacial Maximum and its subsequent retreat history: a review. Quaternary Science Reviews 21, 49-70.

Anderson, J.B., Fretwell, P.T., 2008. Geomorphology of the onset area of a paleo-ice stream, Marguerite Bay, Antarctic Peninsula. Earth Surface Processes and Landforms 33, 503-512.

Auclair, M., Lamothe, M., Huot, S., 2003. Measurement of anomalous fading for feldspar IRSL using SAR. Radiation Measurements 37, 487-493.

Banfield, L., Anderson, J., 1995. Seismic facies investigation of the late Quaternary glacial history of Bransfield Basin, Antarctica. Antarctic Research Series 68, 123-140.

Barbouti, A., Rastin, B., 1983. A study of the absolute intensity of muons at sea level and under various thicknesses of absorber. Journal of Physics G: Nuclear Physics 9, 1577-1595.

Baroni, C., Orombelli, G., 1991. Holocene raised beaches at Terra Nova Bay, Victoria Land, Antarctica. Quaternary Research 36, 157-177.

Baroni, C., Orombelli, G., 1994. Abandoned penguin rookeries as Holocene paleoclimatic indicators in Antarctica. Geology 22, 23-26.

Baroni, C., Hall, B.L., 2004. A new Holocene relative sea-level curve for Terra Nova Bay, Victoria Land, Antarctica. Journal of Quaternary Science 19, 377-396.

Barsch, D., Mäusbacher, R., 1986. New data on the relief development of the South Shetland Islands, Antarctica. Interdisciplinary Science Reviews 11, 211-218.

Bassett, S.E., Milne, G.A., Bentley, M.J., Huybrechts, P., 2007. Modelling Antarctic sea-level data to explore the possibility of a dominant Antarctic contribution to meltwater pulse IA. Quaternary Science Reviews 26, 2113-2127.

Bentley, M.J., Anderson, J.B., 1998. Glacial and marine geological evidence for the ice sheet configuration in the Weddell Sea; Antarctic Peninsula region during the Last Glacial Maximum. Antarctic Science 10, 309-325.

Bentley, M.J., Hodgson, D.A., Smith, J.A., Cox, N.J., 2005a. Relative sea level curves for the South Shetland Islands and Marguerite Bay, Antarctic Peninsula. Quaternary Science Reviews 24, 1203-1216.

Bentley, M.J., Hodgson, D.A., Sugden, D.E., Roberts, S.J., Leng, M.J., Bryant, C., 2005b. Early Holocene retreat of the George VI Ice Shelf, Antarctic Peninsula. Geology 33, 173-176.

Bentley, M.J., Johnson, J.S., Hodgson, D.A., Dunai, T., Freeman, S.P.H.T., Ó Cofaigh, C., 2011. Rapid deglaciation of Marguerite Bay, western Antarctic Peninsula in the Early Holocene. Quaternary Science Reviews 30, 3338-3349.

Berkman, P.A., Andrews, J.T., Björck, S., Colhoun, E.A., Emslie, S.D., Goodwin, I.D., Hall, B.L., Hart, C.P., Hirakawa, K., Igarashi, A., Ingólfsson, O., López-Martínez, J., Lyons, W.B., Mabin, M.C.G., Quilty, P.G., Taviani, M., and Yoshida, Y., 1998. Circum-Antarctic coastal environmental shifts during the late Quaternary reflected by emerged marine deposits. Antarctic Science 10, 345–362.

Bertler, N. A., Barrett, P. J., Mayewski, P. A., Fogt, R. L., Kreutz, K. J., and Shulmeister, J., 2004. El Nino suppresses Antarctic warming. Geophysical Research Letters 31, L15207, 4 p.

Bevis, M., Kendrick, E., Smalley, R., Jr., Dalziel, I., Caccamise, D., Sasgen, I., Helsen, M., Taylor, F.W., Zhou, H., Brown, A., Raleigh, D., Willis, M., Wilson, T., Konfal, S., 2009. Geodetic measurements of vertical crustal velocity in West Antarctica and the implications for ice mass balance. Geochemisty, Geophysics, Geosystems 10, p. Q10005.

Bluck, B.J., 2011. Structure of gravel beaches and their relationship to tidal range. Sedimentology 58, 994-1006.

Bøtter-Jensen, L., Murray , A.S., 1999, Developments in Optically Stimulated Luminescence Techniques for Dating and Retrospective Dosimetry. Radiation Protection Dosimetry 84, 307-315.

Bøtter-Jensen, L., McKeever, S.W.S., Wintle, A.G., 2003, Optically Stimulated Luminescence Dosimetry: Amsterdam, Elsevier Science B.V.

Briggs, R.D., Tarasov, L., 2013. How to evaluate model-derived deglaciation chronologies: a case study using Antarctica. Quaternary Science Reviews *63*, 109-127.

Butler, E.R.T., 1999. Process environments on modern and raised beaches in McMurdo Sound, Antarctica. Marine Geology 162, 105-120.

Canals, M., Casamor, J.L., Urgeles, R., Calafat, A.M., Domack, E.W., Baraza, J., Farran, M., De Batist, M., 2002. Seafloor evidence of a subglacial sedimentary system off the northern Antarctic Peninsula. Geology 30, 603-606.

Clapperton, C.M., Sugden, D.E., 1982. Late quaternary glacial history of George VI Sound area, West Antarctica: Quaternary Research 18, 243-267.

Conroy, J.L., Overpeck, J.T., Cole, J. E., Shanahan, T.M., Steinitz-Kannan, M., 2008. Holocene changes in eastern tropical Pacific climate inferred from a Galápagos lake sediment record. Quaternary Science Reviews 27, 1166-1180.

Crosta, X., Debret, M., Denis, D., Courty, M. A., Ther, O., 2007. Holocene long-and short-term climate changes off Adelie Land, East Antarctica. Geochemistry, Geophysics,Geosystems 8, Q11009.

Curl, J.E., 1980. A glacial history of the South Shetland Islands, Antarctica. Institude of Polar Sudies Report 63, Ohio State University, Columbus, OH.

del Valle, R.A., Montalti, D., Inbar, M., 2002. Mid-Holocene macrofossil-bearing raised marine beaches at Potter Peninsula, King George Island, South Shetland Islands. Antarctic Science 14, 263-269.

Denis, D., Crosta, X., Barbara, L., Massé, G., Renssen, H., Ther, O., Giraudeau, J., 2010. Sea ice and wind variability during the Holocene in East Antarctica: insight on middle–high latitude coupling. Quaternary Science Reviews 29, 3709-3719.

Dennen, W.H., Blackburn, W.H., Quesada, A., 1970. Aluminum in quartz as a geothermometer. Contributions to Mineralogy and Petrology 27, 332-342.

Dietrich, R., Rülke, A., Ihde, J., Lindner, K., Miller, H., Niemeier, W., Schenke, H.-W., Seeber, G., 2004. Plate kinematics and deformation status of the Antarctic Peninsula based on GPS. Global and Planetary Change 42, 313-321.

Divine, D.V., Koç, N., Isaksson, E., Nielsen, S., Crosta, X., Godtliebsen, F., 2010. Holocene Antarctic climate variability from ice and marine sediment cores: insights on ocean–atmosphere interaction. Quaternary Science Reviews 29, 303-312.

Domack, E., 2006. Continental Shelves and Slopes. In: Riffenburgh, B. (Ed.), Encycolpedia of the Antarctic: Routledge, New York, pp. 286-290.

Donders, T.H., Wagner-Cremer, F., Visscher, H., 2008. Integration of proxy data and model scenarios for the mid-Holocene onset of modern ENSO variability. Quaternary Science Reviews 27, 571-579.

Dowdeswell, J.A., Cofaigh, C.Ó., Pudsey, C.J., 2004. Thickness and extent of the subglacial till layer beneath an Antarctic paleo–ice stream. Geology 32, 13-16.

Duller, G.A.T., 2003. Distinguishing quartz and feldspar in single grain luminescence measurements. Radiation Measurements 37, 161-165.

Emslie, S.D., McDaniel, J.D., 2002. Adélie penguin diet and lcimat change during the middle to late Holocene in northern Marguerite Bay, Antarctic Peninsula. Polar Biology 25, 222-229.

Etourneau, J., Collins, L., Willmott, V., Kim, J.-H., Barbara, L., Leventer, A., Schouten, S., Sinninghe Damsté, J., Bianchini, A., Klein, V., 2013. Holocene climate variations in the western Antarctic Peninsula: evidence for sea ice extent predominantly controlled by changes in insolation and ENSO variability. Climate of the Past 9, 1431-1446.

Evans, J., Pudsey, C.J., ÓCofaigh, C., Morris, P., Domack, E., 2005. Late Quaternary glacial history, flow dynamics and sedimentation along the eastern margin of the Antarctic Peninsula Ice Sheet. Quaternary Science Reviews, 24, 741-774.

Fairbanks, R.G., 1989. A 17,000-year glacio-eustatic sea level record: influence of glacial melting rates on the Younger Dryas event and deep-ocean circulation. Nature 342, 637-642.

Fitzsimmons, K.E., Rhodes, E.J., Barrows, T.T., 2009, OSL dating of southeast Australian quartz: a preliminary assessment of the luminescence characteristics and behaviour. Quaternary Geochronology 5: 91-95.
Fleming, S.J., 1979. Thermoluminescence Techniques in Archaeology: Clarendon Press, Oxford.
Fretwell, P.T., Hodgson, D.A., Watcham, E.P., Bentley, M.J., Roberts, S.J., 2010. Holocene isostatic uplift of the South Shetland Islands, Antarctic Peninsula, modelled from raised beaches. Quaternary Science Reviews 29, 1880-1893.
Galbraith, R.F., Roberts, R.G., Laslett, G.M., Yoshida, Y., Olley, J.M., 1999. Optical dating of single and multiple grains of quartz from Jinmium rock shelter, northern Australia: part 1, experimental design and statistical models. Archaeometry 41, 339-364.
Gardner, N., Hall, B., Wehmiller, J., 2006. Pre-Holocene raised beaches at Cape Ross, Southern Victoria Land, Antarctica. Marine Geology 229, 273-284.
Gomez, N., Pollard, D., Mitrovica, J.X., 2013. A 3-D coupled ice sheet–sea level model applied to Antarctica through the last 40 ky. Earth and Planetary Science Letters 384, 88-99.
Götze, J., Plötze, M., Habermann, D., 2001. Origin, spectral characteristics and practical applications of the cathodoluminescence (CL) of quartz – a review. Mineralogy and Petrology 71, 225-250.
Hall, B.L., Denton, G.H., 1999. New relative sea-level curves for the southern Scott Coast, Antarctica: evidence for Holocene deglaciation of the western Ross Sea: Journal of Quaternary Science 14, 641-650.
Hall, B.L., Baroni, C., Denton, G.H., 2004. Holocene relative sea-level history of the Southern Victoria Land Coast, Antarctica. Global and Planetary Change 42, 241-263.
Hall, B.L., Perry, E.R., 2004. Variations in ice rafted detritus on beaches in the South Shetland Islands: a possible climate proxy. Antarctic Science 16, 339-344.
Hall, B.L., Hoelzel, A.R., Baroni, C., Denton, G.H., Le Boeuf, B.J., Overturf, B., and Töpf, A.L., 2006. Holocene elephant seal distribution implies warmer-than-present climate in the Ross Sea. Proceedings of the National Academy of Sciences 103, 10213-10217.
Hall, B.L., 2007. Late-Holocene advance of the Collins Ice Cap, King George Island, South Shetland Islands: The Holocene 17, 1253-1258.
Hall, B.L., 2010a. Holocene relative sea-level changes and ice fluctuations in the South Shetland Islands. Global and Planetary Change 74, 15-26.
Hall, B.L., Henderson, G.M., Baroni, C., Kellogg, T.B., 2010b. Constant Holocene Southern-Ocean 14C reservoir ages and ice-shelf flow rates: Earth and Planetary Science Letters 296, 115-123.
Hanebuth, T.J.J., Stattegger, K., Bojanowski, A., 2009. Termination of the Last Glacial Maximum sea-level lowstand: The Sunda-Shelf data revisited. Global and Planetary Change 66, 76-84.
Hansom, J.D., 1979. Radiocarbon dating of a raised beach at 10 m in the South Shetland Islands. British Antarctic Survey Bulletin 49, 287.
Hansom, J.D., 1983. Shore-platform development in the South Shetland islands, Antarctica. Marine Geology 53, 211-229.

Hayashida, M., Yoshida, Y., 1994. Holocene raised beaches in the Lutzow-Holm Bay region, East Antarctica. National Institute of Polar Research Memorandum Special Issue 50, 49-84.
Heroy, D.C., Anderson, J.B., 2005. Ice-sheet extent of the Antarctic Peninsula region during the Last Glacial Maximum (LGM)—Insights from glacial geomorphology. Geological Society of America Bulletin 117, 1497-1512.
Heroy, D.C., Anderson, J.B., 2007. Radiocarbon constraints on Antarctic Peninsula Ice Sheet retreat following the Last Glacial Maximum (LGM). Quaternary Science Reviews 26, 3286-3297.
Hiller, A., Wand, U., Kämpf, H., and Stackebrandt, W., 1988. Occupation of the Antarctic continent by petrels during the past 35 000 years: inferences from a 14C study of stomach oil deposits. Polar Biology 9, 69-77.
Hjort, C., Ingólfsson, Ó., Möller, P., Lirio, J.M., 1997. Holocene glacial history and sea-level changes on James Ross Island, Antarctic Peninsula. Journal of Quaternary Science 12, 259-273.
Hodgson, D.A., Roberts, S.J., Smith, J.A., Verleyen, E., Sterken, M., Labarque, M., Sabbe, K., Vyverman, W., Allen, C.S., Leng, M.J., 2013. Late Quaternary environmental changes in Marguerite Bay, Antarctic Peninsula, inferred from lake sediments and raised beaches: Quaternary Science Reviews 68, 216-236.
Huntley, D.J., Lamothe, M., 2001. Ubiquity of anomalous fadin in K-feldspars and the measurement and correction for it in optical dating. Canadian Journal of Earth Science 38, 1093-1106.
Huybrechts, P., 2002. Sea-level changes at the LGM from ice-dynamic reconstructions of the Greenland and Antarctic ice sheets during the glacial cycles. Quaternary Science Reviews 21, 203-231.
Igarashi, A., Harada, N., Moriwaki, K., 1995. Marin fossils of 30-40ka in raised beach deposits, and latePleistocene glacial history around Lutzow-Holm Bay, East Antarctica. Proceedings of the NIPR Symposium on Antarctic Geosciences 8, 219-229.
Ingólfsson, Ó., 2004, Quaternary glacial and climate history of Antarctica. In: Ehlers, J., Gibbard, P.L. (Eds.), Developments in Quaternary Science, Volume 2, Part 3: Elsevier, pp. 3-43.
Ivins, E.R., James, T.S., 2005. Antarctic glacial isostatic adjustment: a new assessment. Antarctic Science 17, 541-553.
Ivins, E.R., Watkins, M.M., Yuan, D.-N., Dietrich, R., Casassa, G., Rülke, A., 2011. On-land ice loss and glacial isostatic adjustment at the Drake Passage: 2003-2009. Journal of Geophysical Research 116, B02403.
Jakobsson, M., Anderson, J.B., Nitsche, F.O., Gyllencreutz, R., Kirshner, A.E., Kirchner, N., O'Regan, M., Mohammad, R., Eriksson, B., 2012. Ice sheet retreat dynamics inferred from glacial morphology of the central Pine Island Bay Trough, West Antarctica. Quaternary Science Reviews 38, 1-10.
John, B., Sugden, D., 1971. Raised marine features and phases of glaciation in the South Shetland Islands: British Antarctic Survey Bulletin 24, 45-111.
Kanfoush, S.L., Hodell, D.A., Charles, C.D., Janecek, T.R., Rack, F.R., 2002. Comparison of ice-rafted debris and physical properties in ODP Site 1094 (South Atlantic) with the

Vostok ice core over the last four climatic cycles. Palaeogeography, Palaeoclimatology, Palaeoecology 182, 329-349.
Kennedy, D.S., Anderson, J., 1989. Quaternary glaical history of Marguerite Bay, Antarctic Peninsula. Quaternary Research 31, 255-276.
Kenworthy, M. K., Rittenour, T. M., Pierce, J. L., Sutfin, N. A., Sharp, W. D, 2014. Luminescence dating without sand lenses; An application of OSL to coarse-grained alluvial fan deposits of the Lost River Range, Idaho, USA. Quaternary Geochronology.
Kilfeather, A.A., Cofaigh, C.Ó., Lloyd, J.M., Dowdeswell, J.A., Xu, S., Moreton, S.G., 2011. Ice-stream retreat and ice-shelf history in Marguerite Trough, Antarctic Peninsula: Sedimentological and foraminiferal signatures. Geological Society of America Bulletin 123, 997-1015.
Kirk, R.M., 1966. Beach observations at Cape Royds, Ross Island, McMurdo Sound, Antarctica 1965–1966. Unpublished Report, Geography Department, University of Canterbury.
Kretz, R., 1983. Symbols for rock-forming minerals. American mineralogist 68, 277-279.
Lian, O.B., Rhodes, R.G., 2006. Dating the Quaternary: progress in luminescence dating of sediments. Quaternary Science Reviews 25, 2449-2468.
Lambeck, K., Chappell, J., 2001. Sea Level Change through the Last Glacial Cycle: Science 292, 679-686.
Lambeck, K., Yokoyama, Y., Purcell, T., 2002. Into and out of the Last Glacial Maximum: sea-level change during Oxygen Isotope Stages 3 and 2. Quaternary Science Reviews 21(1), 343-360.
Lamothe, M., Balescu, S., Auclair, M., 1994. Natural IRSL intensities and apparent luminescence ages of single feldspar grains extracted from partially bleached sediments: Radiation Measurements 27, 555-562.
Le Maitre, R. W. (Ed.), 2002. Igneous Rocks: A Classification and Glossary of Terms: A Classification and Glossary of Terms: Recommendations of the International Union of Geological Sciences, Subcommission on the Systematics of Igneous Rocks. Cambridge University Press.
Madsen, A.T., Murray, A.S., 2009. Optically stimulated luminescence dating of young sediments: A review. Geomorphology 109, 3-19.
Maemoku, H., Miura, H., Saigusa, S., Moriwaki, K., 1997. Stratigraphy of the lat Quaternary raised beach deposits in the norther part of Langhovde, Lutzow-Holm Bay, East Antarctica. Proceedings of the NIPR Symposium on Antarctic Geosciences 10, 178-186.
Marshall., D.J., 1988. Cathodoluminescence of geological materials: RELION Industries, 146 p.
Martinson, D. G.,Iannuzzi, R. A., 2003. Spatial/temporal patterns in Weddell gyre characteristics and their relationship to global climate. Journal of Geophysical Research: Oceans (1978–2012) 108 C4.
Masson, V., Vimeux, F., Jouzel, J., Morgan, V., Delmotte, M., Ciais, P., Hammer, C., Johnsen, S., Lipenkov, V.Y., Mosley-Thompson, E., Petit, J.R., Steig, E.J., Stievenard, M., and Vaikmae, R., 2000. Holocene climate variability in Antarctica based on 11 ice-core isotopic records. Quaternary Research 54, 348-358.

Mayewski, P.A., Rohling, E.E., Stager, J.C., Karlén, W., Maasch, K.A., Meeker, L.D., Meyerson, E.A., Gasse, F., van Kreveld, S., Holmgren, K., Lee-Thorp, J., Rosqvist, G., Rack, F., Staubwasser, M., Schneider, R.R., Steig, E.J., 2004. Holocene climate variability. Quaternary Research 62, 243-255.

Mayewski, P.A., Meredith, M.P., Summerhayes, C.P., Turner, J., Worby, A., Barrett, P.J., Casassa, G., Bertler, N.A.N., Bracegirdle, T., Naveira Garabato, A.C., Bromwich, D., Campbell, H., Hamilton, G.S., Lyons, W.B., Maasch, K.A., Aoki, S., Xiao, C., van Ommen, T., 2009. State of the Antarctic and Southern Ocean climate system. Reviews of Geophysics 47, R1003, 38 p.

Mejdahl, V., 1979. Thermoluminescence dating: Beta-dose attenuation in quartz grains. Archaeometry 21, 61-72.

Milne, G. A., Mitrovica, J. X., Schrag, D. P., 2002. Estimating past continental ice volume from sea-level data. Quaternary Science Reviews 21(1), 361-376.

Miura, H., Moriwaki, K., Maemoku, H., Hirakawa, K., 1998. Fluctuations of the East Antarctic ice-sheet margin since the last glaciation from stratigraphy of raised beach deposits along the Sôya coast. Annals of Glaciology 27, 297-301.

Monien, P., Roberts, S. J., Loftfield, J., Schnetger, B., Hocking, E. P., Hodgson, D. A., Bentley, M.J.,Fretwell, P., Ochvra, R., Heye, A.R., Allen C.S., Morenton, S., Brumsack, H. J., 2014. Penguin colony expansion on the western Antarctic Peninsula during Holocene warm phases curtailed by volcanic activity.

Moy, C.M., Seltzer, G.O., Rodbell, D.T., and Anderson, D.M., 2002. Variability of El Niño/Southern Oscillation activity at millennial timescales during the Holocene epoch. Nature 420, 162-165.

Murray, A. S., Roberts, R. G., 1997. Determining the burial time of single grains of quartz using optically stimulated luminescence. Earth and Planetary Science Letters 152(1), 163-180.

Murray, A.S., Wintle, A.G., 2000. Luminescence dating of quartz using an improved single-aliquot regenerative-dose protocol. Radiation Measurements 32, 57-73.

Murray, A.S., Olley, J.M., 2002. Precision and accuracy in the optically stimulated luminescence dating of sedimentary quartz: A status review. Geochronometria 21, 1-16.

Murray, A.S., Wintle, A.G., 2003. The single aliquot regenerative dose protocol: potential for improvements in reliability. Radiation Measurements 37, 377-381.

Nakada, M., Kimura, R., Okuno, J., Moriwaki, K., Miura, H., Maemoku, H., 2000. Late Pleistocene and Holocene melting history of the Antarctic ice sheet derived from sea-level variations. Marine Geology 167, 85-103.

Nichols, R.L., 1961. Characteristics of beaches formed in polar climates: American Journal of Science 259, 694-708.

Nichols, R.L., 1968. Coastal geomorphology, McMurdo Sound, Antarctica: Journal of Glaciology 7, 31, 449-477.

Nielsen, S.H., Koç, N., Crosta, X., 2004. Holocene climate in the Atlantic sector of the Southern Ocean: Controlled by insolation or oceanic circulation? Geology 32, 317-320.

Nielsen A,Murray AS, Pejrup M, Elberling B, 2006. Optically stimulated luminescence dating of a Holocene beach ridge plain in Northern Jutland, Denmark: Quaternary Geochronology 1, 305-312.

Noormets, R., Dowdeswell, J.A., Larter, R.D., Ó Cofaigh, C., Evans, J., 2009. Morphology of the upper continental slope in the Bellingshausen and Amundsen Seas—implications for sedimentary processes at the shelf edge ofWest Antarctica. Marine Geology 258, 100–114.

Ó Cofaigh, C., Pudsey, C.J., Dowdeswell, J.A., Morris, P., 2002. Evolution of subglacial bedforms along a paleo-ice stream, Antarctic Peninsula continental shelf. Geophysical Research Letters 29, 41-1-41-4.

Ó Cofaigh, C., Dowdeswell, J.A., Allen, C.S., Hiemstra, J., Pudsey, C.J., Evans, J., Evans, D.J.A., 2005. Flow dynamics and till genesis associated with a marine-based Antarctic palaeo-ice stream. Quaternary Science Reviews 24, 709-740.

Ó Cofaigh, C., Dowdeswell, J.A., Evans, J., Larter, R.D., 2008. Geological constraints on Antarctic palaeo-ice-stream retreat. Earth Surface Processes and Landforms 33, 513-525.

Okuno, J.I., Miura, H., 2013. Last deglacial relative sea level variations in Antarctica derived from glacial isostatic adjustment modeling. Geoscience Frontiers 4, 623-632.

Omoto, K., 1977. Geomorphic Development of the Soya Coast, East Antarctica-Chronological Interpretation of Raised Beaches based on Levellings and Radiocarbon Datings. Scientific Reports of Tohoku University 7th Series 27, 95-148.

Padman, L., Fricker, H.A., Coleman, R., Howard, S., Erofeeva, L., 2002. A new tide model for the Antarctic ice shelves and seas.Annals of Glaciology 34, 247-254.

Pallas, R., James, T.S., Sabat, F., Vilaplana, J.M., and Grant, D.R., 1997. Holocene uplift in the South Shetland Islands: evaluation of tectonics and glacio-isostasy. The Antarctic region: geological evolution and processes, 861-868.

Payne, A.J., Sugden, D.E., Clapperton, C.M., 1989. Modeling the growth and decay of the Antarctic Peninsula Ice Sheet. Quaternary Research 31(2), 119-134.

Peltier, W.R., 2002. On eustatic sea level history: Last Glacial Maximum to Holocene. Quaternary Science Reviews 21, 377-396.

Peltier, W.R., 2004. Global glacial isostasy and the surface of the ice-age Earth: The ICE-5G (VM2) Model and GRACE: Annual Reviews of Earth Planetary Science 32, 111–149.

Péwé, T.L., Rivard, N.R., Llano, G.A., 1959. Mummified seal carcasses in the McMurdo Sound region. Antarctica. Science 130, 716-716.

Pietsch, T.J., Olley, J.M., Nanson, G.C., 2008, Fluvial transport as a natural luminescence sensitiser of quartz. Quaternary Geochronology 3: 365-376.

Pike, J., Allen, C.S., Leventer, A., Stickley, C.E., Pudsey, C.J., 2008. Comparison of contemporary and fossil diatom assemblages from the western Antarctic Peninsula shelf. Marine Micropaleontology 67(3), 274-287.

Pope, P.G., Anderson, J., 1992. Late Quaternary glacial history of the northern Antarctic Peninsula's western contiental shelf. Antarctic Research Series 57. In: Elliot, D.H. (Ed.), Evidence from the Marine Record, Contribution to Antarctic Research III: American Geophysical Union, Washington, D.C..

Prescott, J.R., Stephan, L.G., 1982. The contribution of cosmic radiation to the environmental dose for thermoluminescence dating. Latitude, altitude, and depth dependences. PACT 6, 17-25.

Preusser, F., Ramseyer, K., Schlüchter, C., 2006 Characterisation of low OSL intensity quartz from the New Zealand Alps: Radiation Measurements 41, 871-877.

Preusser, Frank, Makaiko L. Chithambo, Thomas Götte, Marco Martini, Karl Ramseyer, Emmanuel J. Sendezera, George J. Susino, Ann G. Wintle, 2009. Quartz as a natural luminescence dosimeter. Earth-Science Reviews 97 (1), 184-214.

Pudsey, C.J., Evans, J., 2001. First survey of Antarctic sub–ice shelf sediments reveals mid-Holocene ice shelf retreat. Geology 29, 787-790.

Reimer, P.J., Baillie, M.G.L., Bard, E., Bayliss, A., Beck, J.W., Blackwell, P.G., Bronk Ramsey, C., Buck, C.E., Burr, G.S., Edwards, R.L., Friedrich, M., Grootes, P.M., Guilderson, T.P., Hajdas, I., Heaton, T.J., Hogg, A.G., Hughen, K.A., Kaiser, K.F., Kromer, B., McCormac, F.G., Manning, S.W., Reimer, R.W., Richards, D.A., Southon, J.R., Talamo, S., Turney, C.S.M., van der Plicht, J., Weyhenmeyer, C.E., 2009, IntCal09 and Marine09 radiocarbon age calibration curves, 0–50,000 years cal BP. Radiocarbon 51, 4, 1111–1150.

Rhodes, E.J., 2011. Optically Stimulated Luminescence Dating of Sediments over the Past 200,000 Years. Annual Review of Earth and Planetary Sciences 39, 461-488.

Roberts, S.J., Hodgson, D.A., Bentley, M.J., Sanderson, D.C.W., Milne, G., Smith, J.A., Verleyen, E., Balbo, A., 2009. Holocene relative sea-level change and deglaciation on Alexander Island, Antarctic Peninsula, from elevated lake deltas. Geomorphology 112, 122-134.

Roberts, S.J., Hodgson, D.A., Sterken, M., Whitehouse, P.L., Verleyen, E., Vyverman, W., Sabbe, K., Balbo, A., Bentley, M.J., Moreton, S.G., 2011. Geological constraints on glacio-isostatic adjustment models of relative sea-level change during deglaciation of Prince Gustav Channel, Antarctic Peninsula: Quaternary Science Reviews 30, 3603-3617.

Sasgen, I., Dobslaw, H., Martinec, Z., Thomas, M., 2010. Satellite gravimetry observation of Antarctic snow accumulation related to ENSO. Earth and Planetary Science Letters 299, 352-358.

Sawakuchi, A.O., Blair, M.W., DeWitt, R., Faleiros, F.M., Hyppolito, T., Guedes, C.C.F., 2011, Thermal history versus sedimentary history: OSL sensitivity of quartz grains extracted from rocks and sediment. Quaternary Geochronology 6: 261-272.

Schmidt, C., Kreutzer, S., Fattahi, M., Bailey, R., Zander, A., Zöller, L., 2011, On the luminescence signals of empty sample carriers. Ancient TL 29: 65-74.

Schneider, D.P., Steig, E.J., van Ommen, T.D., Dixon, D.A., Mayewski, P.A., Jones, J.M., Bitz, C.M., 2006. Antarctic temperatures over the past two centuries from ice cores. Geophysical Research Letters 33, L16707, 5 p.

Shipp, S., Anderson, J., Domack, E., 1999. Late Pleistocene–Holocene retreat of the West Antarctic Ice-Sheet system in the Ross Sea: Part 1—Geophysical results. Geological Society of America Bulletin 111, 1486-1516.

Siivola, J., Schmid, R., 2007. List of mineral abbreviations. Metamorphic Rocks: A Classification and Glossary of Terms. Recommendations of the International Union of Geological Sciences Subcommission on the Systematics of Metamorphic Rocks, 93-110.

Simkins, L.M., Simms, A.R., DeWitt, R., 2013a. Relative sea-level history of Marguerite Bay, Antarctic Peninsula derived from optically stimulated luminescence-dated beach cobbles. Quaternary Science Reviews 77, 141-155.

Simkins, L.M., DeWitt, R., Simms, A.R., 2013b. Methods to reduce sample carrier contamination for luminescence measurements. Ancient TL 31, 19-27.

Simmonds, I., and Jacka, T.H., 1995. Relationships between the interannual variability of Antarctic sea ice and the Southern Oscillation. Journal of Climate 8, 637-647.
Simms, A.R., DeWitt, R., Kouremenos, P., Drewry, A.M., 2011a. A new approach to reconstructing sea levels in Antarctica using optically stimulated luminescence of cobble surfaces. Quaternary Geochronology 6, 50-60.
Simms, A.R., Milliken, K.T., Anderson, J.B., Wellner, J.S., 2011b. The marine record of deglacitionof the South Shetland Islands, Antarctica since the Last Glacial Maximum: Quaternary Science Reviews 30, 1538-1601.
Simms, A.R., Ivins, E.R., DeWitt, R., Kouremenos, P., Simkins, L.M., 2012. Timing of the most recent Neoglacial advance and retreat in the South Shetland Islands, Antarctic Peninsula: insights from raised beaches and Holocene uplift rates. Quaternary Science Reviews 47, 41-55.
Sloan, B.J., Lawver, L.A., Anderson, J., 1995. Seismic stratigraphy of the Palmer Basin. In: Cooper, A.K., Barker, P.F., Brncolini, G. (Eds.), Geology and Seismic Stratigraphy of the Antarctic Margin, Antarctic Research Series: American Geophysical Union, Washington, D.C., pp. 235-260.
Smith, R.T., Anderson, J.B., 2010. Ice-sheet evolution in James Ross Basin, Weddell Sea margin of the Antarctic Peninsula: The seismic stratigraphic record. Geological Society of America Bulletin 122, 830-842.
Sohbati, R., Murray, A.S., Jain, M., Buylaert, J.P., Thomsen, K.J., 2011. Investigating the resetting of OSL signals in rock surfaces. Geochronometria 38 (3), 249-258.
Stammerjohn, S.E., Martinson, D.G., Smith, R.C., and Iannuzzi, R.A., 2008. Sea ice in the western Antarctic Peninsula region: Spatio-temporal variability from ecological and climate change perspectives. Deep Sea Research Part II: Topical Studies in Oceanography 55, 2041-2058.
St.Hilaire-Gravel, D., Bell, T.J., Forbes, D.L., 2010. Raised gravel beaches as proxy indicators of past sea-ice and wave conditions, Lowther Island, Canadian Arctic Archipelago. Arctic 63, 213-226.
Strelin, J.A., Sone, T., Mori, J., Torielli, C.A., Nakamura, T., 2006. New Data Related to Holocene Landform Development and Climatic Change from James Ross Island, Antarctic Peninsula: Antarctica: Contributions to Global Earth Sciences, 455.
Stuiver, M., Yang, I.C., Denton, G.H., 1976. Permafrost oxygen isotope ratios and chronology of three cores from Antarctica.
Stuiver, M., Denton, G.H., Hughes, T.J., Fastook, J.L., 1981. History of the marine ice sheet in West Antarctica during the last deglaciation: a working hypothesis. In Denton, G.H., Hughes, T.J., eds., The Last Great Ice Sheets: New York, Wiley, 319-436.
Sugden, D.E., John, B.S., 1973. The ages of glacier fluctuations in the South Shetland Islands, Antarctica. In: van Zinderen Bakker, E.M. (Ed.), Palaeoecology of Africa, the Surrounding Islands and Antarctica, Volume 8: Balkema, Cape Town, pp. 141-159.
Takada, M., Tani, A., Miura, H., Moriwaki, K., Nagatomo, T., 2003. ESR dating of fossil shells in the Lützow-Holm Bay region, East Antarctica: Quaternary Science Reviews 22, 1323-1328.
Taylor, F.W., Bevis, M.G., Dalziel, I.W.D., Smalley, R.J., Frochlich, C., Kendrick, E., Foster, J., Phillips, D., Gudipati, K., 2008. Kinematics and segmentation of the South

Shetland Islands - Bransfield basin system, northern Antarctic Peninsula. Geochemistry, Geophysics, Geosystems 9, Q04035.
Thomas, I.D., King, M.A., Bentley, M.J., Whitehouse, P.L., Penna, N.T., Williams, S.D.P., Riva, R.E.M., Lavallee, D.A., Clarke, P.J., King, E.C., Hindmarsh, R.C.A., Koivula, H., 2011. Widespread low rates of Antarctic glacial isostatic adjustment revealed by GPS observations. Geophysical Research Letters 38, L22302.
Trauth, M.H., 2010. Image Processing, MATLAB® Recipes for Earth Sciences – Third Edition: Springer, Berlin, pp. 255-290.
Vandenberghe, D.A.G., Jain, M., Murray, A.S., 2008, A note on spurious luminescence from silicone oil. Ancient TL 26: 29-32.
van de Plassche, O, 1986. Sea-level research: a manual for the collection and evaluation of data: Geo Books, Norwich, UK, pp.1-26.
Vafiadou, A., Murray, A.S., Liritzis, I., 2007. Optically stimulated luminescence (OSL) dating investigations of rock and underlying soil from three case studies. Journal of Archaeological Science 34, 1659-1669.
Verleyen, E., Hodgson, D.A., Milne, G.A., Sabbe, K., Vyverman, W., 2005. Relative sea-level history from the Lambert Glacier region, East Antarctica, and its relation to deglaciation and Holocene glacier readvance. Quaternary Research 63, pp. 45-52.
Volkman, N.J., Trivelpiece, W., 1981. Nest-site selection among Adelie, chinstrap and gentoo penguins in mixed species rookeries. The Wilson Bulletin, 243-248.
Wagner, G.A., 1998. Age determination of young rocks and artifacts: physical and chemical clocks in Quaternary geology and archaeology: Springer, New York City.
Waller, C., 2008. Variability in intertidal communities along a latitudinal gradient in the Southern Ocean. Polar Biology 31, 809-816.
Wallinga, J., 2002. Optically stimulated luminescence dating of fluvial deposits: a review. Boreas 31, 303-322.
Wassell, A., Håkansson, H., 1992. Diatom stratigraphy in a lake on Horseshoe Island, Antarctica. Diatom Research 7, 157-194.
Watanuki, T., Murray, A.S., Tsukamoto, S., 2005. Quartz and polymineral luminescence dating of Japanese loess over the last 0.6 Ma: Comparison with an independent chronology. Earth and Planetary Science Letters 240, 774-789.
Watcham, E.P., Bentley, M.J., Hodgson, D.A., Roberts, S.J., Fretwell, P.T., Lloyd, J.M., Larter, R.D., Whitehouse, P.L., Leng, M.J., Monien, P., Moreton, S.G., 2011. A new Holocene relative sea level curve for the South Shetland Islands, Antarctica. Quaternary Science Reviews 30, 3152-3170.
Wellner, J.S., Heroy, D.C., Anderson, J.B., 2006. The death mask of the Antarctic ice sheet: Comparison of glacial geomorphic features across the continental shelf. Geomorphology 75, 157-171.
Whitehouse, P.L., Bentley, M.J., Milne, G.A., King, M.A., Thomas, I.D., 2012a. A new glacial isostatic adjustment model for Antarctica: calibrated and tested using observations of relative sea-level change and present-day uplift rates. Geophysical Journal International 190, 1464-1482.
Whitehouse, P.L., Bentley, M.J., Le Brocq, A.M., 2012b. A deglacial model for Antarctica: geological constraints and glaciological modelling as a basis for a new model of Antarctic glacial isostatic adjustment. Quaternary Science Reviews 32, 1-24.

Wintle, A.G., Murray, A.S., 2006. A review of quartz optically stimulated luminexcence characteristics and their relevance in single-aliquot regeneration dating protocols. Radiation Measurements 41, 369-391.
Yan, Y., Mayewski, P.A., Kang, S., Meyerson, E., 2005. An ice-core proxy for Antarctic circumpolar zonal wind intensity. Annals of Glaciology 41, 121-130.
Yokoyama, Y., Lambeck, K., De Deckker, P., Johnston, P., Fifield, L.K., 2000, Timing of the Last Glacial Maximum from observed sea-level minima. Nature 406, 713-716.
Yuan, X., 2004. ENSO-related impacts on Antarctic sea ice: a synthesis of phenomenon and mechanisms. Antarctic Science 16, 415-425.
Zheng, C.X., Zhou, L.P., Qin, J.T., 2009. Difference in luminescence sensitivity of coarse-grained quartz from deserts of northern China: Radiation Measurements 44, 534-537.
Zwartz, D., Bird, M., Stone, J., Lambeck, K., 1998. Holocene sea-level change and ice sheet history in the Vestfold Hills, East Antarctica. Earth and Planetary Science Letters 155, 131-145.

APPENDIX I – CLEANING METHOD PROCEDURES

Detailed procedures for the cleaning methods applied to empty stainless steel cups are described below.

Ethanol

(1) Rinse cups with DI water

(2) 30-minute ultrasonic bath with dish soap and DI water at room temperature

(3) Repeat step (1)

(4) Repeat step (2)

(5) Repeat step (1)

(6) Individual cleaning with ethanol

NOTE: “Ethanol” is our standard carrier cleaning method used on stainless steel cups prior to the application of our modified cleaning methods from this study.

Acetone

(1) Follow steps (1) through (5) of ethanol sequence

(2) Individual cleaning with acetone

Methanol

(1) Follow steps (1) through (5) of ethanol sequence

(2) Individual cleaning with methanol

Sand paper

(1) Follow steps (1) through (5) of ethanol sequence

(2) Individual scrubbing with sand paper

NOTE: “Sand paper” includes scrubbing with sand paper in addition to the standard cleaning method “Ethanol”

HF

(1) Follow steps (1) through (5) of ethanol sequence

(2) Etch cups for 5 min with 48% HF

(3) Rinse with DI water

(4) Individual cleaning with methanol

Alconox (10 min)

(1) Rinse cups with DI water

(2) 10-minute ultrasonic bath with Alconox and DI water at ~70°C

(3) Repeat step (1)

(4) Repeat step (2)

(5) Repeat step (1)

Alconox (30 min) and Alconox (30 min), new cups

(1) Rinse cups with DI water

(2) 30-minute ultrasonic bath with Alconox and DI water at ~70°C

(3) Repeat step (1)

(4) Repeat step (2)

(5) Repeat step (1)

New cups

No cleaning procedure was applied to new cups

Rust Remover

(1) Rinse cups with DI water

(2) 1-hour ultrasonic bath with Rust Stain Remover and DI water at room temperature

(3) Repeat step (1)

NOTE: Rust Stain Remover contains 3 % HF

APPENDIX II – DOSE RESPONSE CURVES FOR CLEANING METHODS

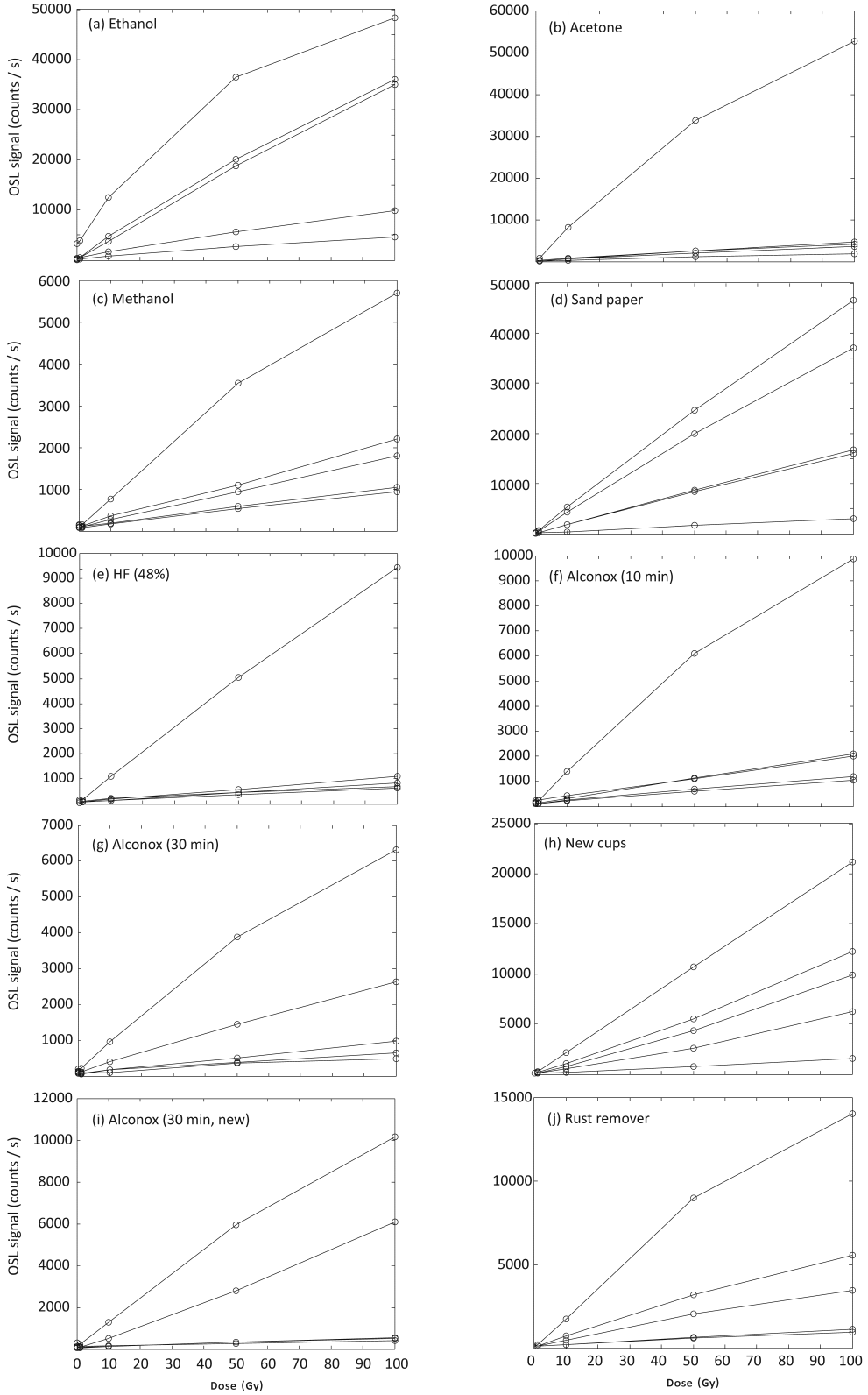

APPENDIX III – WATER CONTENT PARAMETERS FOR DOSE-RATE CALCULATIONS

Pore volume, snow cover, density of snow, density of the sample, and percentage of filled pores are factors that contribute to the overall water content surrounding sampled beach cobbles. We used a pore volume of 20 ± 5 %, the volume of rhombohedral packing of identical spheres (Graton and Fraser, 1935). Closer packing is unlikely due to the open framework of the beaches. Using modern snow fall (Fox and Cooper, 1998) and air temperature records (Harangozo, 1997), we estimate the temporal snow cover at 8 months per year. We use a snow-ice density of 0.8 ± 0.1 g cm^{-3} and measured cobble densities range between 2.3-3.0 g cm^{-3}. The volume of pores filled with ice and snow was estimated at 60 ± 10% from field observations. Using these parameters, the water content (*wc*) of the surrounding material was calculated to account for the absorption of radiation by water using equation (1):

$$\frac{\rho_{snow} v_{pores} s f}{\rho_{surrounding} v_{surrounding}} \quad (1)$$

where ρ_{snow} is the snow-ice density, v_{pores} is the volume of pores, s is duration of snow cover per year, f is the amount of filled pores, $\rho_{surrounding}$ is the surrounding material density, $v_{surrounding}$ is the volume of cobbles. Water content values were used to correct for the absorption of radiation by water, $DR_{\beta\ surrounding\ wet}$ and $DR_{\gamma\ surrounding\ wet}$, using equations (2) for the beta dose rate and (3) for the gamma dose rate, respectively:

$$\frac{DR_{\beta\ surrounding\ dry}}{(1+1.25wc)} \quad (2)$$

$$\frac{DR_{\gamma\ surrounding\ dry}}{(1+1.14wc)} \quad (3)$$

where $DR_{\beta\ surrounding\ dry}$ and $DR_{\gamma\ surrounding\ dry}$ are the dry beta and gamma dose rates of the surrounding material.

References

Fox, A.J., Cooper, A.P.R., 1998. Climate change indicators from archival aerial photography of the Antarctic Peninsula: Annals of Glaciology 27, 636-642.

Graton, L.C., Fraser, H.J., 1935. Systematic Packing of Spheres: With Particular Relation to Porosity and Permeability. The Journal of Geology 43, 785-909.

Harangozo, S.A., Colwell, S.R., King, J.C., 1997. An analysis of a 34-year air temperature record from Fossil Bluff (71S, 68W), Antarctica. Antarctic Science 9, 355-363.

APPENDIX IV – RADIAL PLOTS, DOSE RESPONSE, AND DECAY CURVES

Equivalent dose distributions, OSL decay curves, and dose response curves for dated samples from Calmette Bay are shown in Table B.1. Radial plots (a) show distributions of equivalent doses for aliquots that pass standard reliability tests. The dose for each point can be determined using a radial line from zero on the left-hand y-axis to the right y-axis. The hatched bar shows the 95% confidence interval for the equivalent dose estimation determined by either the common age model (denoted as common; Galibraith et al., 1999) or 3-parameter minimum age model (denoted as MAM-3; Galbraith et al., 1999) noted under the sample name. Unlike histograms, the relative error and the precision of each aliquot is shown along the x-axis thus aliquots with larger error plot to the left. Dose response curves (a) display the dose in time (s) along the x-axis and corrected OSL signal on the y-axis. The dose response curves show the regenerated signals from various doses and are used to determine the dose represented by the natural signal. OSL decay curves (c) from the natural signals are shown for dated samples. The x-axis displays simulation time (s) and the y-axis shows OSL counts per 1 s.

References

Galbraith, R.F., Roberts, R.G., Laslett, G.M., Yoshida, Y., Olley, J.M., 1999. Optical dating of single and multiple grains of quartz from Jinmium rock shelter, northern Australia: part 1, experimental design and statistical models. Archaeometry 41, 339-364.

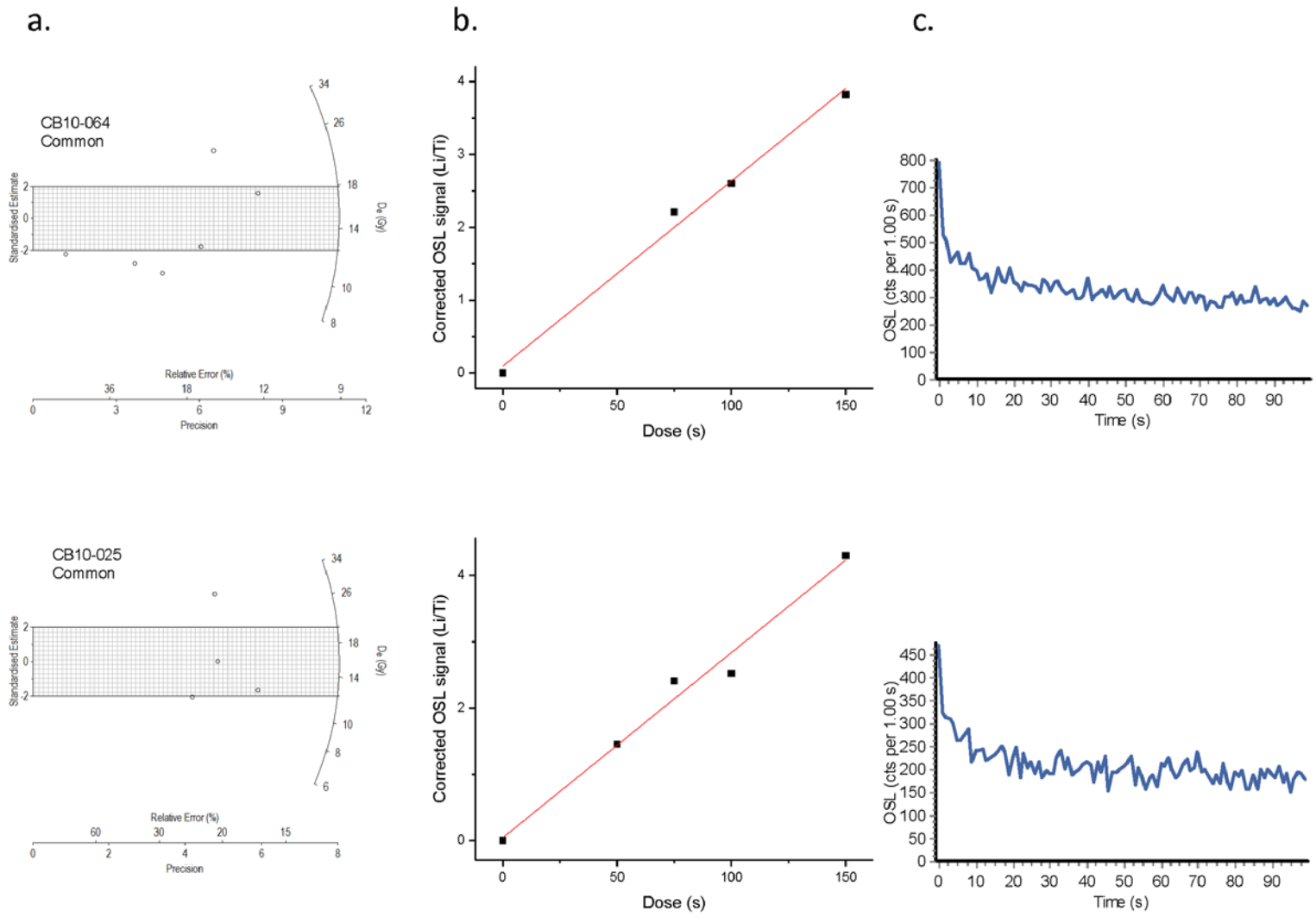
a.
b.
c.
CB10-064
Common
Standardised Estimate
De (Gy)
Relative Error (%)
Precision
Corrected OSL signal (Li/Ti)
Dose (s)
OSL (cts per 1.00 s)
Time (s)
CB10-025
Common
Standardised Estimate
De (Gy)
Relative Error (%)
Precision
Corrected OSL signal (Li/Ti)
Dose (s)
OSL (cts per 1.00 s)
Time (s)

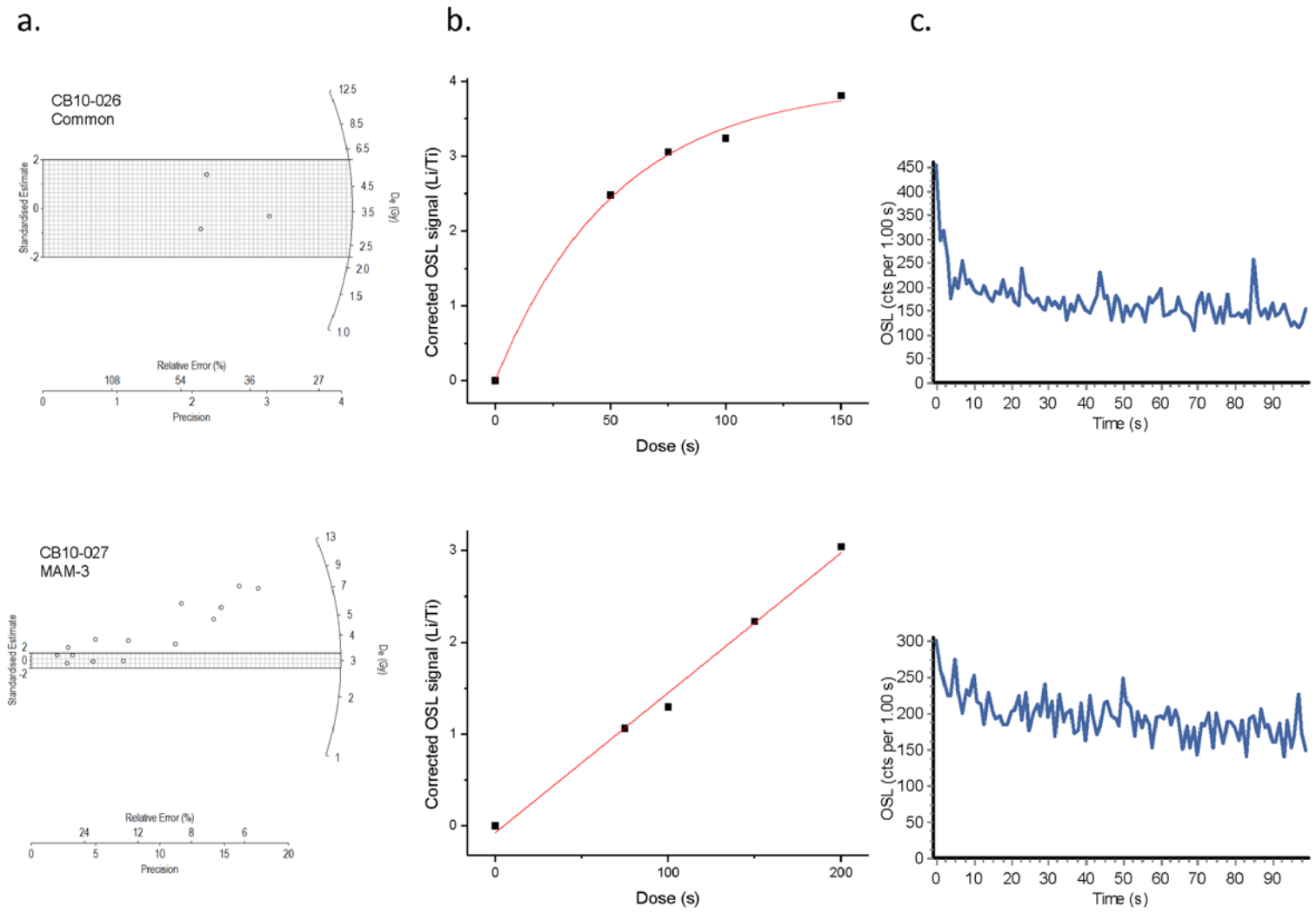
a.
b.
c.
CB10-026
Common
Standardised Estimate
De (Gy)
Relative Error (%)
108
54
36
27
Precision
Corrected OSL signal (Li/Ti)
Dose (s)
OSL (cts per 1.00 s)
Time (s)
CB10-027
MAM-3
Standardised Estimate
De (Gy)
Relative Error (%)
24
12
8
6
Precision
Corrected OSL signal (Li/Ti)
Dose (s)
OSL (cts per 1.00 s)
Time (s)

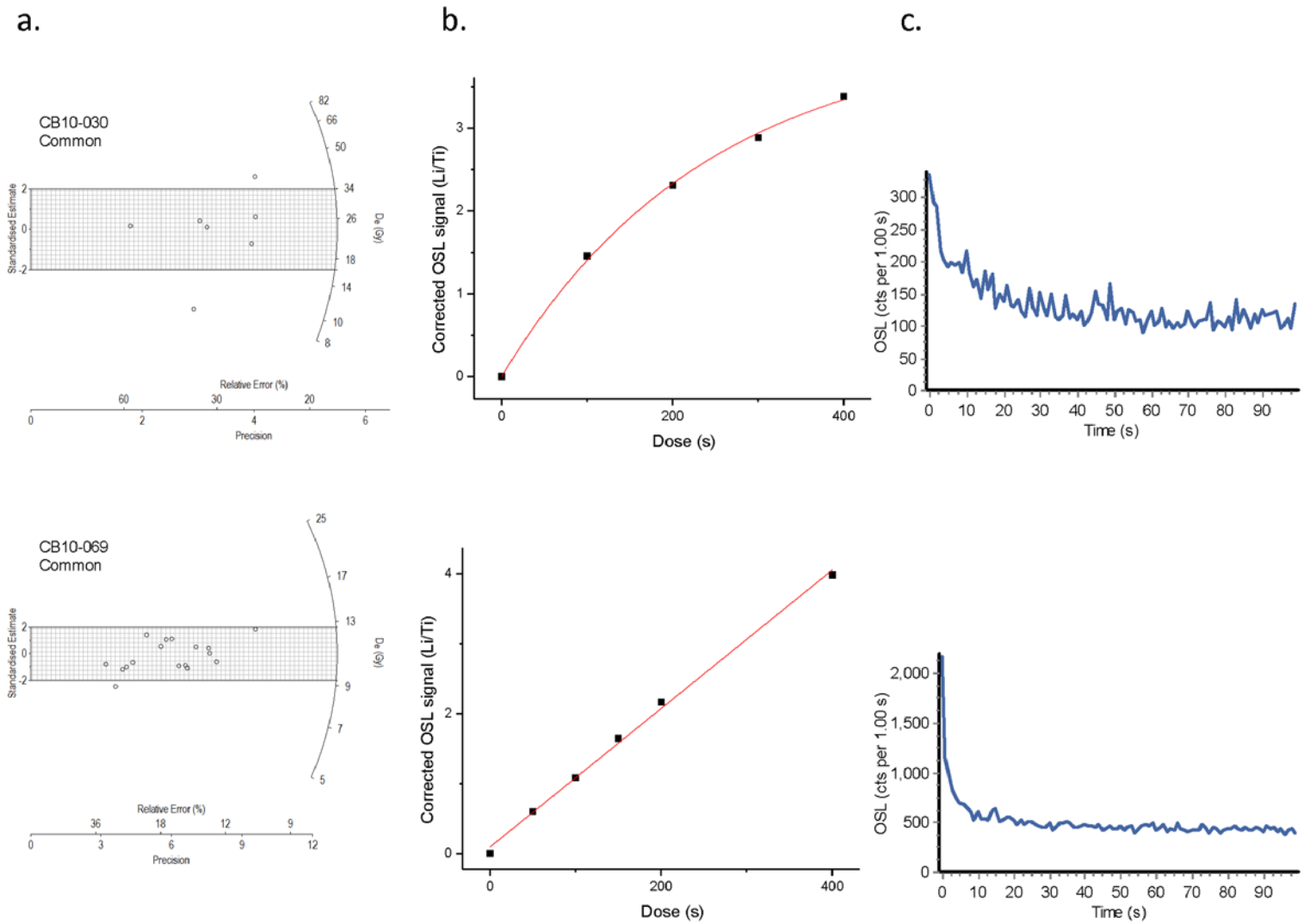
a.
b.
c.
CB10-030
Common
Standardised Estimate
De (Gy)
Relative Error (%)
Precision
Corrected OSL signal (Li/Ti)
Dose (s)
OSL (cts per 1.00 s)
Time (s)
CB10-069
Common
Standardised Estimate
De (Gy)
Relative Error (%)
Precision
Corrected OSL signal (Li/Ti)
Dose (s)
OSL (cts per 1.00 s)
Time (s)

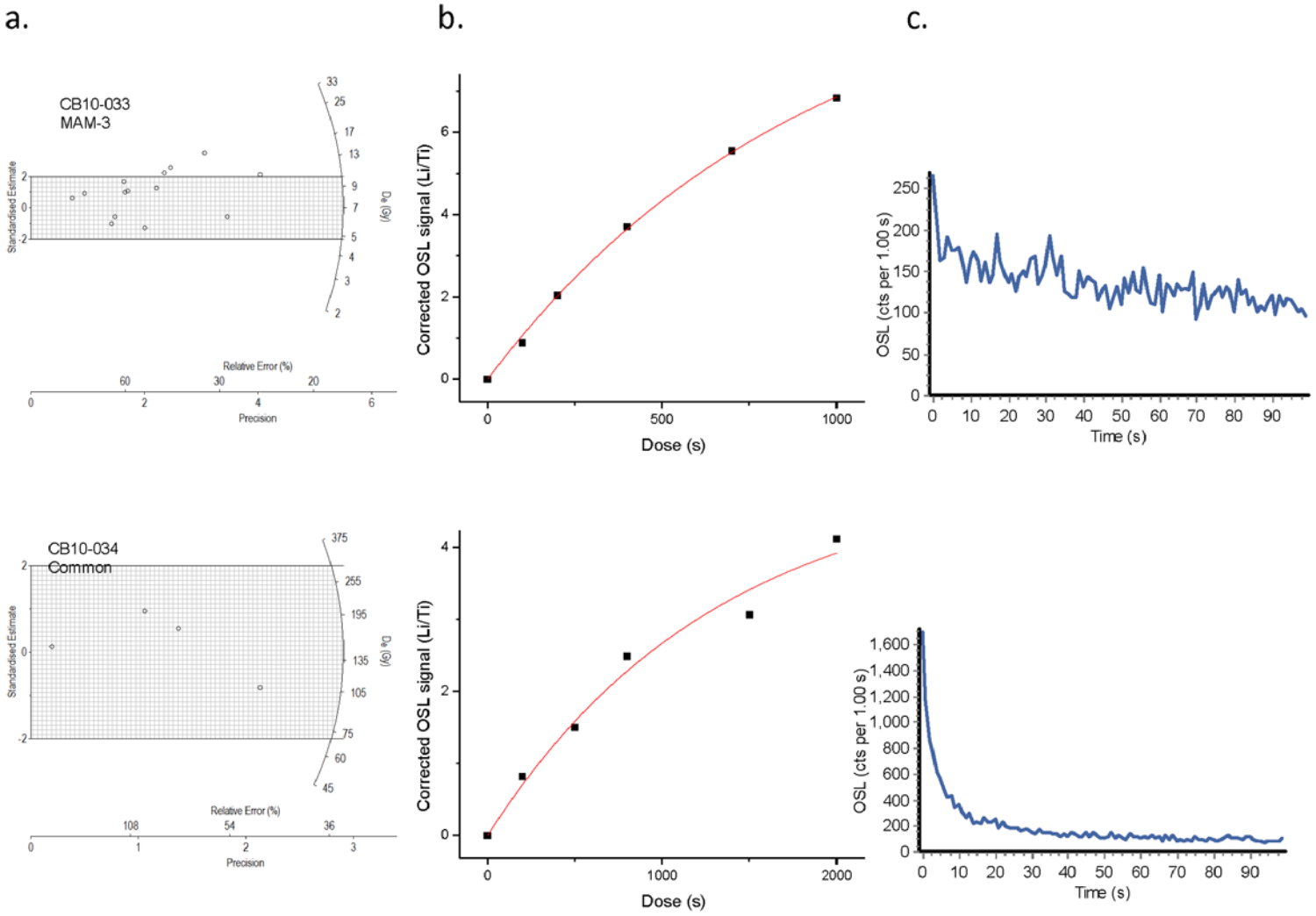
a.
b.
c.
CB10-033
MAM-3
Standardised Estimate
De (Gy)
Relative Error (%)
Precision
Corrected OSL signal (Li/Ti)
Dose (s)
OSL (cts per 1.00 s)
Time (s)
CB10-034
Common
Standardised Estimate
De (Gy)
Relative Error (%)
Precision
Corrected OSL signal (Li/Ti)
Dose (s)
OSL (cts per 1.00 s)
Time (s)

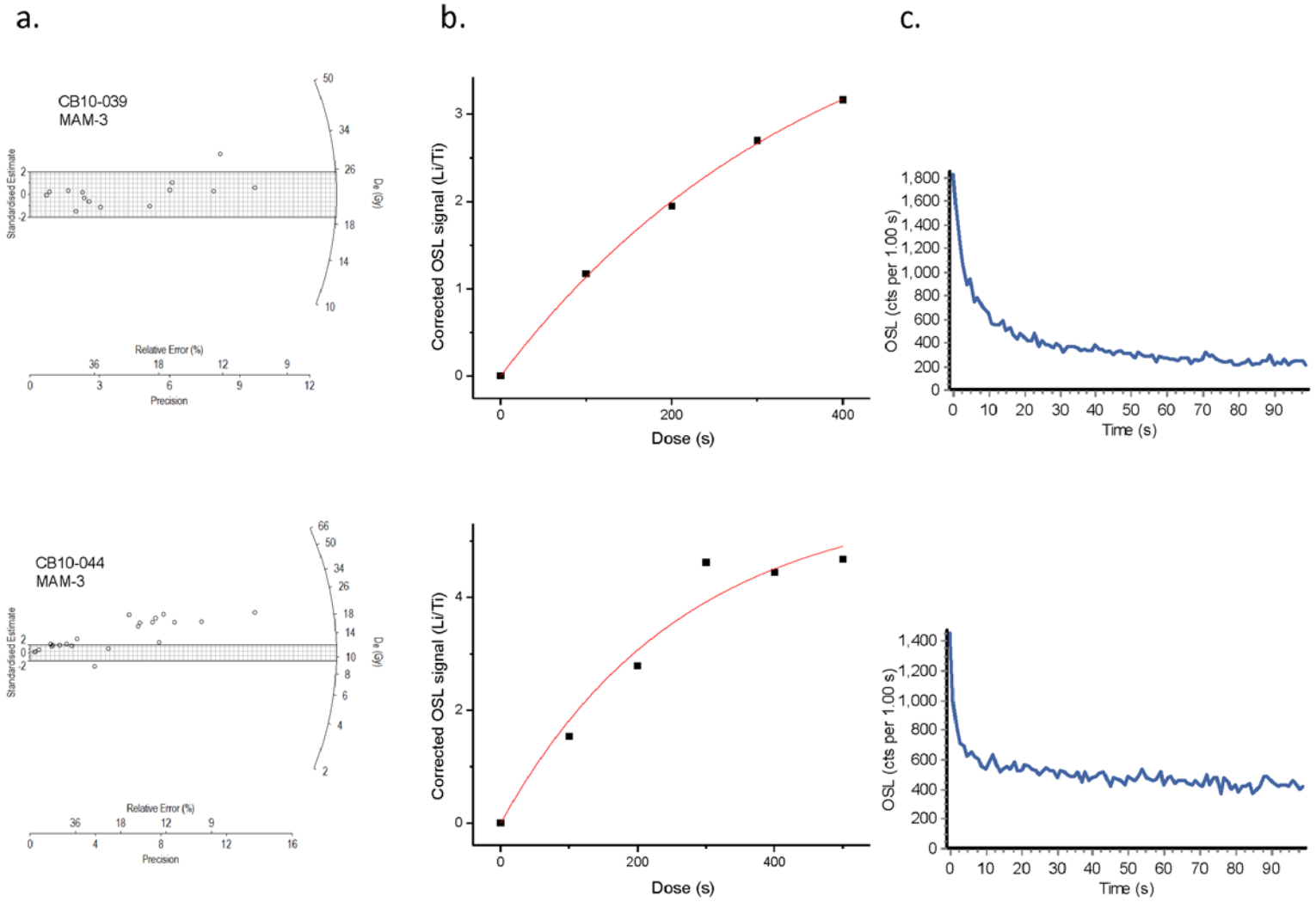
a.
b.
c.
CB10-039
MAM-3
Standardised Estimate
De (Gy)
Relative Error (%)
Precision
Corrected OSL signal (Li/Ti)
Dose (s)
OSL (cts per 1.00 s)
Time (s)
CB10-044
MAM-3
Standardised Estimate
De (Gy)
Relative Error (%)
Precision
Corrected OSL signal (Li/Ti)
Dose (s)
OSL (cts per 1.00 s)
Time (s)

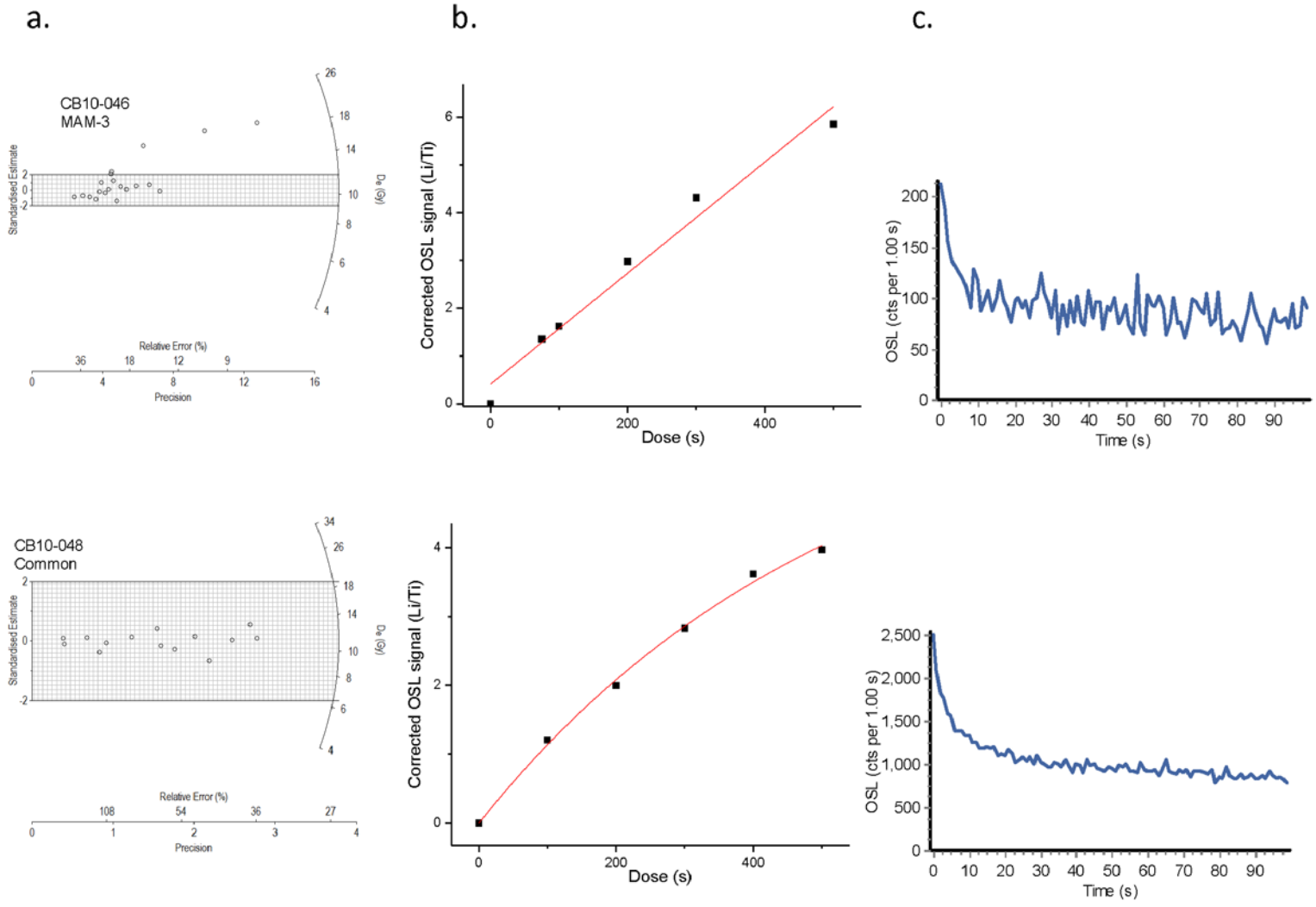
a.
b.
c.
CB10-046
MAM-3
Standardised Estimate
De (Gy)
Relative Error (%)
Precision
Corrected OSL signal (Li/Ti)
Dose (s)
OSL (cts per 1.00 s)
Time (s)
CB10-048
Common
Standardised Estimate
De (Gy)
Relative Error (%)
Precision
Corrected OSL signal (Li/Ti)
Dose (s)
OSL (cts per 1.00 s)
Time (s)

a.

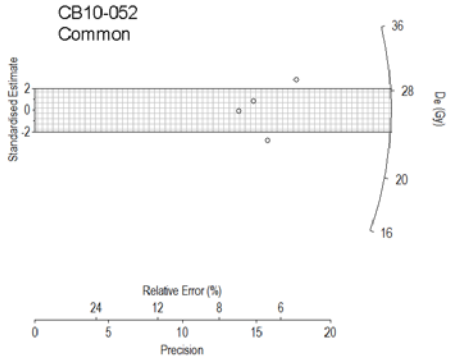
CB10-052
Common
Standardised Estimate
De (Gy)
Relative Error (%)
Precision
CB10-057
MAM-3
Standardised Estimate
De (Gy)
Relative Error (%)
Precision

b.

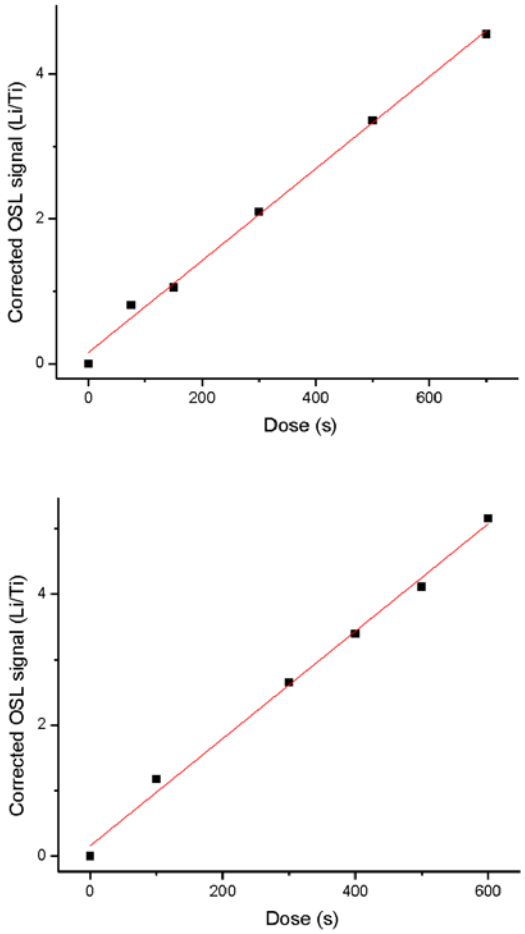
Corrected OSL signal (Li/Ti)
Dose (s)
Corrected OSL signal (Li/Ti)
Dose (s)

c.

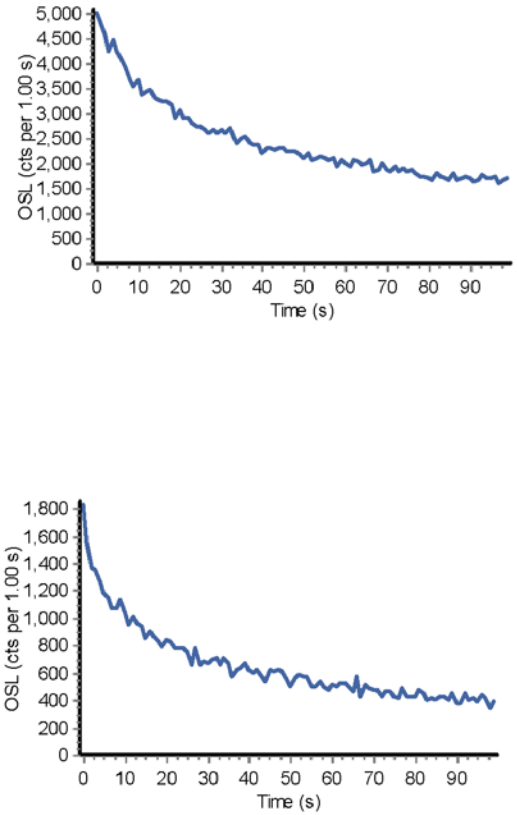
OSL (cts per 1.00 s)
Time (s)
OSL (cts per 1.00 s)
Time (s)

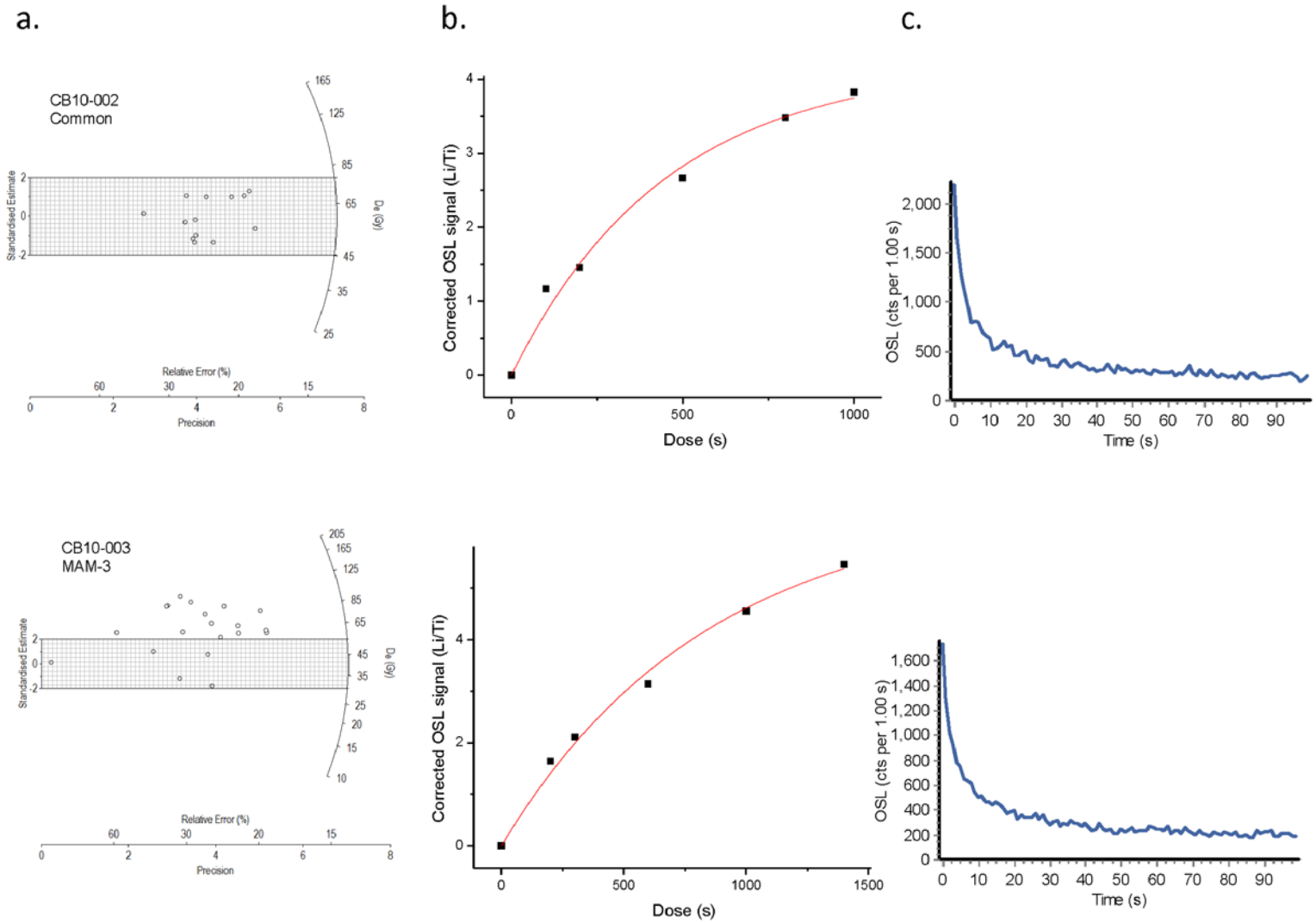
a.
b.
c.
CB10-002
Common
Standardised Estimate
De (Gy)
Relative Error (%)
Precision
Corrected OSL signal (Li/Ti)
Dose (s)
OSL (cts per 1.00 s)
Time (s)
CB10-003
MAM-3
Standardised Estimate
De (Gy)
Relative Error (%)
Precision
Corrected OSL signal (Li/Ti)
Dose (s)
OSL (cts per 1.00 s)
Time (s)

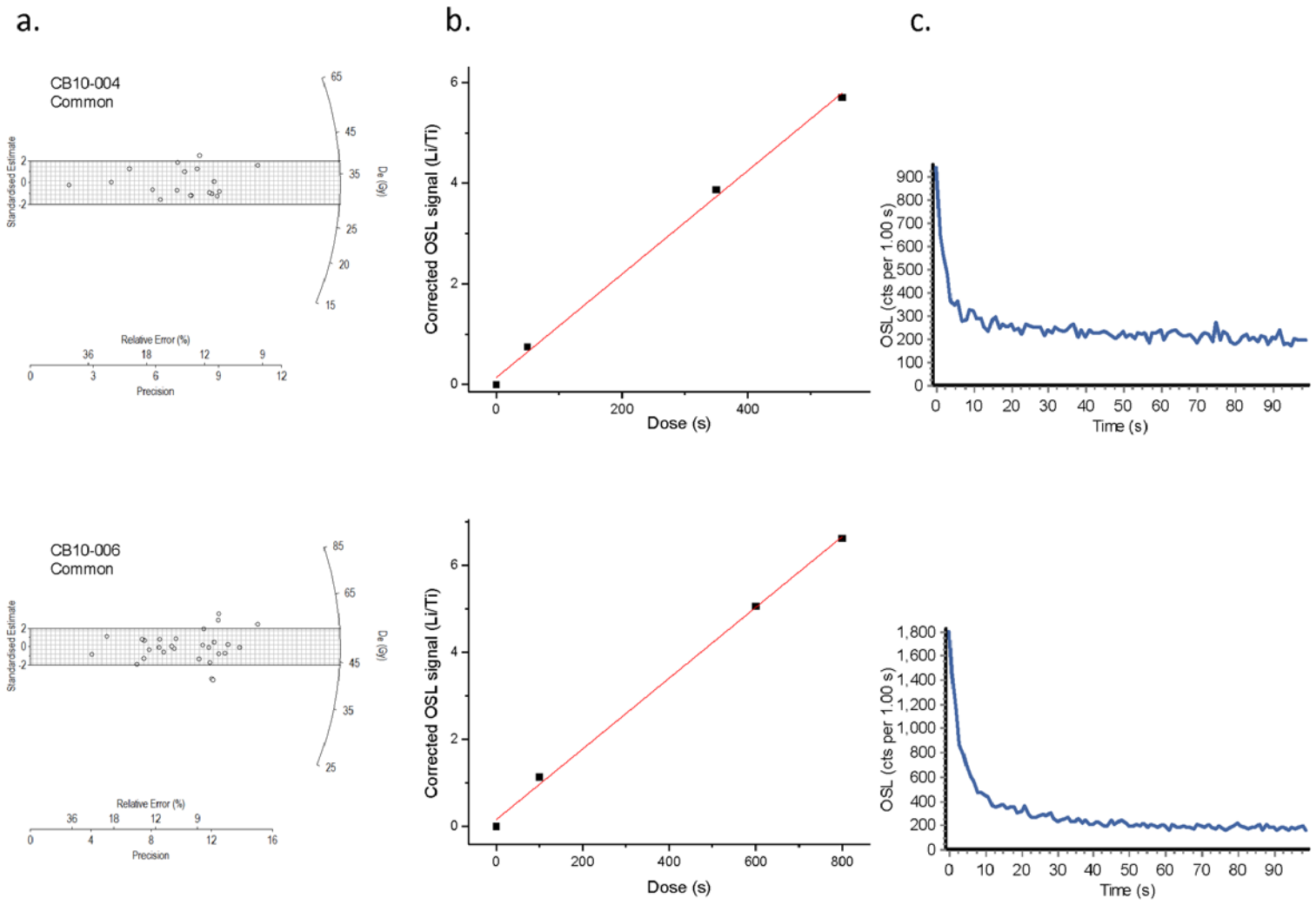
a.
b.
c.
CB10-004
Common
Standardised Estimate
De (Gy)
Relative Error (%)
Precision
Corrected OSL signal (Li/Ti)
Dose (s)
OSL (cts per 1.00 s)
Time (s)
CB10-006
Common
Standardised Estimate
De (Gy)
Relative Error (%)
Precision
Corrected OSL signal (Li/Ti)
Dose (s)
OSL (cts per 1.00 s)
Time (s)

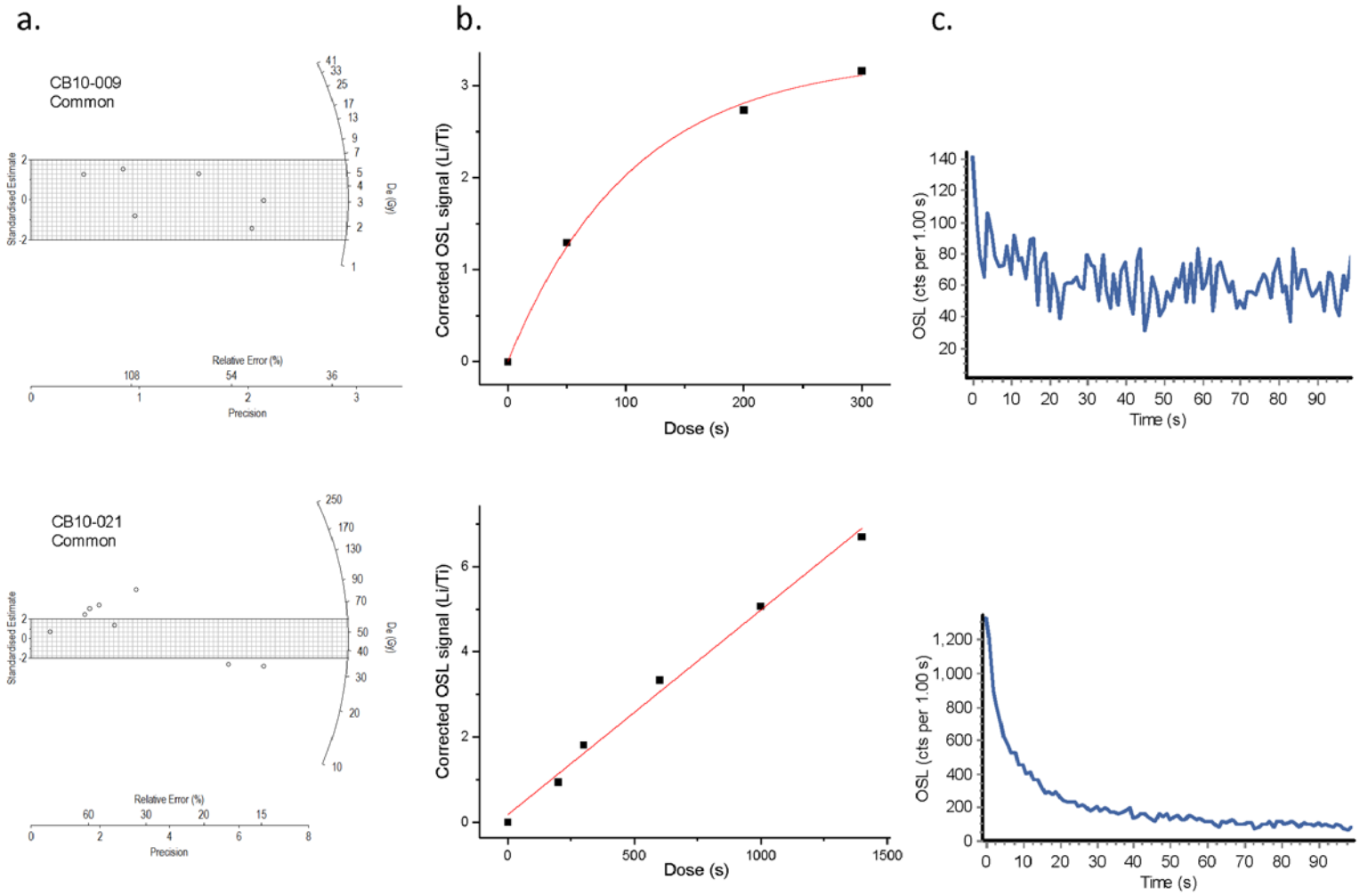
a.
b.
c.
CB10-009
Common
Standardised Estimate
De (Gy)
Relative Error (%)
Precision
Corrected OSL signal (Li/Ti)
Dose (s)
OSL (cts per 1.00 s)
Time (s)
CB10-021
Common
Standardised Estimate
De (Gy)
Relative Error (%)
Precision
Corrected OSL signal (Li/Ti)
Dose (s)
OSL (cts per 1.00 s)
Time (s)

a.

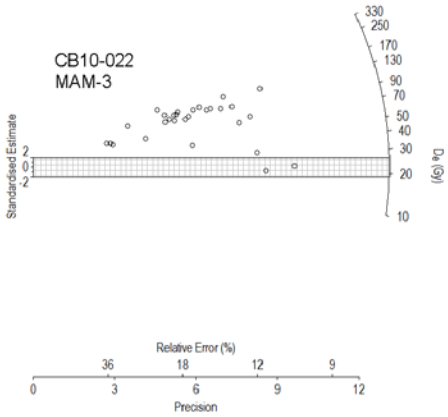
CB10-022
MAM-3
Standardised Estimate
De (Gy)
Relative Error (%)
Precision

b.

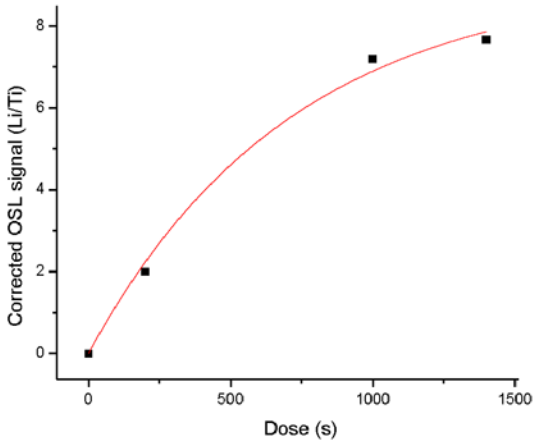
Corrected OSL signal (Li/Ti)
Dose (s)

c.

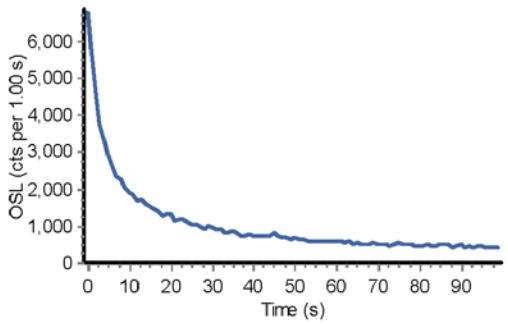
OSL (cts per 1.00 s)
Time (s)

APPENDIX V – MARGUERITE BAY RADIOCARBON AGES

Relative sea level (RSL) data orignially published in other sources include Wassell and Håkansson (1992), Emslie and McDaniel (2002), Bentley et al. (2005a), and Roberts et al. (2009). Radiocarbon ages were calibrated using Calib 6.0 (Reimer et al., 2009) using appropriate calibration curves for the type of material.

References

Bentley, M.J., Hodgson, D.A., Smith, J.A., Cox, N.J., 2005a. Relative sea level curves for the South Shetland Islands and Marguerite Bay, Antarctic Peninsula. Quaternary Science Reviews 24, 1203-1216.

Emslie, S.D., McDaniel, J.D., 2002. Adélie penguin diet and lcimat change during the middle to late Holocene in northern Marguerite Bay, Antarctic Peninsula. Polar Biology 25, 222-229.

Roberts, S.J., Hodgson, D.A., Bentley, M.J., Sanderson, D.C.W., Milne, G., Smith, J.A., Verleyen, E., Balbo, A., 2009. Holocene relative sea-level change and deglaciation on Alexander Island, Antarctic Peninsula, from elevated lake deltas. Geomorphology 112, 122-134.

Wassell, A., Håkansson, H., 1992. Diatom stratigraphy in a lake on Horseshoe Island, Antarctica. Diatom Research 7, 157-194.

Appendix V. RSL observations from Marguerite Bay published in other studies

Location	Dated material	Original source	Elevation (m)	Convential ^{14}C age (a)	Convential ^{14}C error (a)	Reservior error (a)	Corrected ^{14}C age (a)	Corrected ^{14}C error (a)	Calibrated mean age (cal yrs BP)	Calibrated error (cal yrs BP)	Age control
Ginger Is	Penguin bone	Emslie and McDaniel (2002)	5	1090	40	1130 ± 134†	modern	na	na	na	min
	Penguin bone	Emslie and McDaniel (2002)	5	1580	50	1130 ± 134†	450	140	340	340	min
	Penguin bone	Emslie and McDaniel (2002)	5	1770	40	1130 ± 134†	640	140	620	290	min
	Penguin bone	Emslie and McDaniel (2002)	5	3130	40	1130 ± 134†	2000	140	1980	350	min
Lagoon Is	Penguin bone	Emslie and McDaniel (2002)	9.16	1910	40	1130 ± 134†	780	140	740	215	min
	Penguin bone	Emslie and McDaniel (2002)	9.11	4440	50	1130 ± 134†	3310	140	3560	340	min
	Penguin bone	Emslie and McDaniel (2002)	9.06	439	50	1130 ± 134†	3260	140	3465	380	min
	Penguin bone	Emslie and McDaniel (2002)	9.16	4550	50	1130 ± 134†	3420	140	3725	355	min
	Penguin bone	Emslie and McDaniel (2002)	8.96	4240	50	1130 ± 134†	3110	140	3285	355	min
	Penguin bone	Emslie and McDaniel (2002)	17.27	2980	50	1130 ± 134†	1850	140	1770	355	min
	Penguin bone	Emslie and McDaniel (2002)	17.17	3510	70	1130 ± 134†	2380	150	2410	355	min
	Penguin bone	Emslie and McDaniel (2002)	17.07	5610	80	1130 ± 134†	4480	160	5120	465	min
	Penguin bone	Emslie and McDaniel (2002)	17.02	5920	50	1130 ± 134†	4790	140	5480	415	min
	Penguin bone	Emslie and McDaniel (2002)	17.02	6080	50	1130 ± 134†	4950	140	5660	330	min
	Penguin bone	Emslie and McDaniel (2002)	16.06	2490	50	1130 ± 134†	1360	140	1255	280	min
	Eggshell carbonate	Emslie and McDaniel (2002)	15.89	5550	40	1130 ± 134†	4420	140	5050	420	min
Horseshoe Is	Penguin feather	Bentley et al. (2005)	21.36	2310	40	1130 ± 134†	1180	140	1065	270	min
	Freshwater sediment	Wassell and Håkansson (1992)	3.5	1440	50	120 ± 45‡	1320	70	1200	110	min
	Marine sediment	Wassell and Håkansson (1992)	3.5	3160	60	1300 ± 100†	1860	120	1430	260	max
Pourquoi Pas Is	Fur seal hair	Bentley et al. (2005)	35.47	2970	40	Not given	1670	110	1540	240	min
	Freshwater sediment	Bentley et al. (2005)	19.4	6420	50	120 ± 45‡	6420	50	7300	125	min
Anchorage Is	Penguin bone	Bentley et al. (2005)	4.6	4474	50	1130 ± 134†	1670	140	1575	290	max
	Penguin bone	Bentley et al. (2005)	6.1	4480	40	1130 ± 134†	3340	140	3525	360	min
	Shell (*Nacella Concina*)	Bentley et al. (2005)	8.25	4310	40	Not given	3350	110	3175	280	min
	Penguin bone	Bentley et al. (2005)	8.25	3870	40	1130 ± 134†	3010	140	3110	330	min
Alexander Is	Delta sediment*	Roberts et al. (2009)	14.4	na	na	na	na	na	4550	400	min

Is = Island, na = not applicable, min = minimum, max = maximum

* OSL age

† Reservoir correction following Berkman and Forman (1996, 1998)

‡ Reservoir correction equivalent to lake surface sediment age

APPENDIX VI – RADIOCARBON AGES FOR ANTARCTIC RAISED BEACHES

Appendix VI. Published radiocarbon ages used in this study

Location		Material	Elevation (m)	^{14}C age (yr)	^{14}C age error (yr)	Calibrated age (cal yr BP)[1]	Calibrated age error (cal yr BP)	Source	Age constraint for beach formation	Used in age compilation
South Shetland Is										
Byers Peninsula, Livingston Island	South Beaches	w	2.0	1271	47	0	0	Hall and Perry, 2004	Minimum age	x
	South Beaches	w	2.0	1155	38	0	0	Hall, 2010	Minimum age	x
	President's Beaches	w	2.5	1038	54	0	0	Hall, 2010	Minimum age	x
	President's Beaches	w	3.0	1219	50	0	0	Hall, 2010	Minimum age	x
	Robbery Beaches	w	3.5	1126	58	0	0	Hall, 2010	Minimum age	x
	Robbery Beaches	w	3.5	932	48	0	0	Hall, 2010	Minimum age	x
	President's Beaches	w	4.0	958	39	0	0	Hall, 2010	Minimum age	
	South Beaches	w	4.0	1715	42	528	238	Hall and Perry, 2004	Dates beach	x
	South Beaches	w	4.0	1545	46	378	269	Hall and Perry, 2004	Dates beach	x
	South Beaches	w	4.0	1431	44	255	255	Hall and Perry, 2004	Minimum age	
	South Beaches	w	4.5	1132	57	0	0	Hall, 2010	Minimum age	x
	South Beaches	w	5.0	1625	42	448	298	Hall and Perry, 2004	Dates beach	x
	South Beaches	w	5.0	1627	68	448	302	Hall, 2010	Minimum age	
	South Beaches	w	5.0	1576	51	404	267	Hall, 2010	Minimum age	
	South Beaches	w	5.0	1545	41	378	263	Hall, 2010	Minimum age	
	South Beaches	w	5.0	1543	53	375	275	Hall, 2010	Minimum age	
	South Beaches	w	5.0	1461	42	304	304	Hall, 2010	Minimum age	
	President's Beaches	w	5.0	1445	50	287	287	Hall, 2010	Dates beach	x
	South Beaches	w	5.0	1431	39	255	255	Hall, 2010	Dates beach	x
	South Beaches	w	5.0	1370	47	213	213	Hall, 2010	Minimum age	
	South Beaches	w	5.0	1315	54	174	174	Hall, 2010	Minimum age	
	South Beaches	w	6.0	1692	42	509	232	Hall and Perry, 2004	Minimum age	x
	South Beaches	w	6.0	1572	42	401	262	Hall, 2010	Minimum age	x
	South Beaches	w	7.0	1622	42	445	296	Hall, 2010	Minimum age	x
	President's Beaches	w	8.0	1142	44	0	0	Hall, 2010	Minimum age	x
	South Beaches	w	8.0	2530	85	1293	327	Hall and Perry, 2004	Minimum age	x
	South Beaches	w	8.0	2530	85	1293	327	Curl, 1980	Minimum age	x
	South Beaches	w	9.0	849	41	0	0	Hall, 2010	Minimum age	
	South Beaches	w	9.0	1512	50	350	350	Hall, 2010	Minimum age	
	Robbery Beaches	w	9.0	1305	36	165	165	Hall, 2010	Minimum age	
	South Beaches	b	9.0	3115	47	1949	298	Hall and Perry, 2004	Dates beach	x
	South Beaches	w	10.1	3121	35	1956	283	Hansom, 1979	Dates beach	x
	South Beaches	w	10.3	2823	40	1604	287	Hansom, 1979	Dates beach	x
Maxwell Bay, King George Island	C. Aguirre	sh	3.0	1474	38	317	317	Hall, 2010	Dates beach	x
	C. Escondida	w	3.5	1219	44	0	0	Hall, 2010	Minimum age	x
	C. Escondida	w	4.0	1268	41	0	0	Hall, 2010	Minimum age	x
	C. Escondida	w	4.0	1309	46	169	169	Hall, 2010	Minimum age	x
	C. Escondida	w	4.0	1268	41	145	145	Hall, 2010	Minimum age	x
	C. Escondida	w	6.0	1265	51	0	0	Hall, 2010	Minimum age	x
	C. Aguirre	sh	3.0	1474	38	317	317	Hall, 2010	Dates beach	x
	C. Aguirre	sw	6.0	1656	40	477	221	Hall, 2010	Minimum age	x
	C. Aguirre	sw	6.0	1411	38	252	252	Hall, 2010	Minimum age	x
	C. Escondida	w	6.0	1265	51	146	146	Hall, 2010	Minimum age	x
	C. Aguirre	sw	7.0	1364	42	207	207	Hall, 2010	Minimum age	x
	Fildes Peninsula	mo	5.5	1650	50	471	228	Barsch and Mäusbacher, 1986	Maximum age	x
	Fildes Peninsula	pb	18.0	6650	90	6274	342	Barsch and Mäusbacher, 1986	Dates beach	x
	Fildes Peninsula	pb	18.0	6560	55	6173	284	Barsch and Mäusbacher, 1986	Dates beach	x
	Ardley Is	w	5.5	1383	39	224	224	Hall, 2010	Minimum age	x
	Ardley Is	pb	6.5	1512	44	350	350	Hall, 2010	Dates beach	x
	Ardley Is	w	7.5	895	79	0	0	Hall, 2010	Minimum age	x
	Ardley Is	pb	10.0	2959	40	1759	301	Hall, 2010	Dates beach	x
	Ardley Is	g	18.0	1336	37	185	185	Hall, 2010	Minimum age	x
	North Spit	w	3.0	1031	53	0	0	Hall, 2010	Minimum age	
	North Spit	sw	3.0	1420	36	262	262	Hall, 2010	Dates beach	x
	North Spit	sw	4.0	1542	36	376	262	Hall, 2010	Dates beach	x
	Marian Cove	sw	4.0	1430	470	415	415	Sudgen and John, 1973	Dates beach	x
	Marian Cove	sw	5.5	1300	81	0	0	Sudgen and John, 1973	Dates beach	
	Marian Cove	sw	5.5	1300	81	173	173	Sudgen and John, 1973	Dates beach	x
	Marian Cove	w	6.0	1360	165	234	234	Curl, 1980	Dates beach	x
	Marian Cove	w	6.0	1440	55	282	282	Curl, 1980	Dates beach	x
	Barton Peninsula	w	4.0	1450	47	292	292	Hall, 2010	Minimum age	x
	Winship Point	w	4.0	1410	43	252	252	Hall, 2010	Minimum age	x
	South Spit	sh	5.0	1582	56	409	271	Hall, 2010	Dates beach	x
	South Spit	sh	5.0	1581	42	409	264	Hall, 2010	Dates beach	x
	South Spit	w	6.0	Modern		0	0	Hall, 2010	Minimum age	
	South Spit	sh	6.0	1596	40	422	275	Hall, 2010	Dates beach	x
	South Spit	sh	6.0	1520	38	358	358	Hall, 2010	Dates beach	x
	South Spit	sw	6.5	1605	48	430	283	Hall, 2010	Dates beach	x
	Barton Peninsula	w	6.5	1390	140	246	246	Sudgen and John, 1973	Minimum age	x
	Potter Cove	pb	15.6	5840	40	5392	360	Del Valle et al., 2002	Dates beach	x
	Potter Cove	pb	16.5	5750	40	5282	341	Del Valle et al., 2002	Dates beach	x
	Potter Peninsula	pb	17.0	1592	47	418	273	Hall, 2010	Minimum age	x
	Potter Cove	sh	3.5	9670	230	9595	644	Sudgen and John, 1973	Maximum age	x
	Potter Cove	sw	4.0	7683	86	7398	285	Sudgen and John, 1973	Maximum age	x
	Potter Cove	w	6.0	1578	54	405	269	Hall, 2010	Minimum age	
	Potter Peninsula	sw	6.0	1696	40	512	232	Hall, 2010	Dates beach	x
Greenwich Is	Ash Point	sw	12.0	3085	39	1927	322	Hall, 2010	Dates beach	x
	Ash Point	sw	12.0	3116	40	1966	321	Hall, 2010	Dates beach	x
Antarctic Peninsula										
Marguerite Bay	Pourquoi Pas Is	pb	4.6	4474	50	3605	296	Bentley et al., 2005	Maximum age	x
	Ginger Is	pb	5.0	1580	50	407	266	Emslie and McDaniel, 2002	Minimum age	x
	Ginger Is	pb	5.0	1770	40	573	248	Emslie and McDaniel, 2002	Minimum age	x

	Ginger Is	pb	5.0	3130	40	1967	288	Emslie and McDaniel, 2002	Minimum age	x
	Pourquoi Pas Is	pb	6.1	4480	40	3612	291	Bentley et al., 2005	Maximum age	x
	Pourquoi Pas Is	sh	8.3	4310	40	3408	341	Bentley et al., 2005	Minimum age	x
	Pourquoi Pas Is	pb	8.3	3870	40	2878	321	Bentley et al., 2005	Minimum age	x
	Lagoon Is	pb	9.0	4240	50	3319	353	Emslie and McDaniel, 2002	Minimum age	x
	Lagoon Is	pb	9.1	4440	50	3564	311	Emslie and McDaniel, 2002	Minimum age	x
	Lagoon Is	pb	9.2	1910	40	689	197	Emslie and McDaniel, 2002	Minimum age	x
	Lagoon Is	pb	9.2	4550	50	3699	319	Emslie and McDaniel, 2002	Minimum age	x
	Lagoon Is	pe	15.9	5550	40	5034	337	Emslie and McDaniel, 2002	Minimum age	x
	Lagoon Is	pb	16.1	2490	50	1248	282	Emslie and McDaniel, 2002	Minimum age	x
	Lagoon Is	pb	17.0	5920	50	5480	346	Emslie and McDaniel, 2002	Minimum age	x
	Lagoon Is	pb	17.0	6080	50	5661	328	Emslie and McDaniel, 2002	Minimum age	x
	Lagoon Is	pb	17.1	5610	80	5104	364	Emslie and McDaniel, 2002	Minimum age	x
	Lagoon Is	pb	17.2	3510	70	2444	353	Emslie and McDaniel, 2002	Minimum age	x
	Lagoon Is	pb	17.3	2980	50	1784	305	Emslie and McDaniel, 2002	Minimum age	x
	Horseshoe Is	pf	21.4	2310	40	1072	278	Bentley et al., 2005	Minimum age	x
	Horseshoe Is	h	35.5	2970	40	1772	294	Bentley et al., 2005	Minimum age	x
Ross Sea										
	Adelie Cove	pb	2.0	1817	37	608	191	Baroni and Hall, 2004	Dates beach	x
	Adelie Cove	pb	5.0	2625	50	1394	270	Baroni and Hall, 2004	Dates beach	x
	Adelie Cove	pb	6.0	3130	46	1967	293	Baroni and Hall, 2004	Dates beach	x
	Adelie Cove	pb	6.0	3354	37	2232	314	Baroni and Hall, 2004	Dates beach	x
	Adelie Cove	pb	6.5	3383	38	2271	302	Baroni and Hall, 2004	Dates beach	x
	Adelie Cove	pb	6.8	3138	34	1976	286	Baroni and Hall, 2004	Dates beach	x
	Cape Roberts	ss	5.0	2487	51	1245	281	Hall and Denton, 2000a,b	Dates beach	x
	Cape Roberts	ss	5.0	2295	55	1057	284	Hall and Denton, 2000a,b	Dates beach	x
	Cape Roberts	ss	5.5	2820	56	1601	297	Hall and Denton, 2000a,b	Dates beach	x
	Cape Roberts	ss	5.5	2704	65	1476	263	Hall and Denton, 2000a,b	Dates beach	x
	Cape Roberts	ss	5.5	2190	65	951	267	Hall and Denton, 2000a,b	Dates beach	x
	Cape Roberts	sw	5.5	1665	45	484	226	Hall et al., 2004	Dates beach	x
	Cape Roberts	ss	6.0	1830	50	619	195	Hall et al., 2004	Dates beach	x
	Cape Roberts	ss	8.0	2864	48	1650	303	Hall and Denton, 2000a,b	Dates beach	x
	Cape Roberts	ss	8.0	2732	48	1503	248	Hall and Denton, 2000a,b	Dates beach	x
	Cape Roberts	ss	8.0	2725	60	1497	258	Hall et al., 2004	Dates beach	x
	Cape Roberts	ss	8.5	4569	57	3723	330	Hall and Denton, 2000a,b	Dates beach	x
	Cape Roberts	ss	10.0	2966	58	1767	319	Hall and Denton, 2000a,b	Dates beach	x
	Cape Roberts	ss	17.0	3977	73	3004	296	Hall and Denton, 2000a,b	Dates beach	x
	Cape Ross	g	21.0	4780	160	4006	536	Baroni and Orombelli, 1994	Minimum age	x
	Cape Ross	g	24.5	4555	90	3708	365	Baroni and Orombelli, 1994	Minimum age	x
	Cape Ross	g	24.5	4135	125	3186	425	Hall et al., 2004	Minimum age	x
	Cape Ross	g	27.5	4570	90	3726	366	Baroni and Orombelli, 1994	Minimum age	x
	Cape Ross	g	28.1	4255	155	3335	492	Baroni and Orombelli, 1994	Minimum age	x
	Cape Ross	g	28.7	4735	165	3947	516	Baroni and Orombelli, 1994	Minimum age	x
	Cape Ross	g	29.2	4310	155	3406	514	Baroni and Orombelli, 1994	Minimum age	x
	Cape Ross	g	31.2	4465	90	3597	367	Baroni and Orombelli, 1994	Minimum age	x
	Cape Ross	g	31.5	4220	160	3290	501	Baroni and Orombelli, 1994	Minimum age	x
	Cape Ross	g	31.7	4315	90	3414	384	Baroni and Orombelli, 1994	Minimum age	x
	Cape Ross	g	31.7	4310	60	3408	352	Lambert et al., 2002	Minimum age	x
	Cape Ross	pb	32.0	5600	400	5053	1089	Hall et al., 2004	Minimum age	x
	Depot Is	ss	8.0	3572	41	2513	336	Hall et al., 2004	Minimum age	x
	Depot Is	ss	12.0	2735	34	1506	242	Hall et al., 2004	Minimum age	x
	Depot Is	ss	14.0	3118	55	1952	307	Hall et al., 2004	Minimum age	x
	Depot Is	ss	15.0	3290	43	2156	326	Hall et al., 2004	Minimum age	x
	Depot Is	g	16.5	3825	150	2822	484	Baroni and Orombelli, 1994	Minimum age	x
	Depot Is	g	16.5	3320	50	2192	331	Lambert et al., 2002	Minimum age	x
	Depot Is	g	21.0	3990	100	3020	335	Baroni and Orombelli, 1994	Minimum age	x
	Depot Is	g	28.0	7140	45	6823	301	Hall et al., 2004	Minimum age	x
	Depot Is	g	28.0	4720	30	3920	337	Hall et al., 2004	Minimum age	x
	Depot Is	g	28.0	3920	35	2936	260	Hall et al., 2004	Minimum age	x
	Dunlop Is	sh	3.5	4540	60	3687	323	Hall et al., 2004	Maximum	x
	Dunlop Is	ss	6.0	3011	64	1821	331	Hall and Denton, 2000a,b	Dates beach	x
	Dunlop Is	ss	7.0	3560	45	2501	339	Hall and Denton, 2000a,b	Dates beach	x
	Dunlop Is	ss	7.0	2985	60	1789	317	Hall et al., 2004	Dates beach	x
	Dunlop Is	ss	7.0	2593	92	1362	325	Hall and Denton, 2000a,b	Dates beach	x
	Dunlop Is	ss	7.5	3425	45	2331	315	Hall and Denton, 2000a,b	Dates beach	x
	Dunlop Is	ss	10.5	3786	50	2773	373	Hall and Denton, 2000a,b	Minimum age	x
	Dunlop Is	ss	10.5	3410	45	2309	313	Hall and Denton, 2000a,b	Minimum age	x
	Dunlop Is	ss	10.5	3380	50	2267	310	Hall et al., 2004	Minimum age	x
	Dunlop Is	ss	11.5	2692	48	1462	250	Hall and Denton, 2000a,b	Minimum age	x
	Dunlop Is	sh	13.0	5649	59	5147	326	Hall and Denton, 2000a,b	Dates beach	x
	Dunlop Is	ss	15.0	2964	47	1765	303	Hall and Denton, 2000a,b	Minimum age	x
	Dunlop Is	g	16.5	4260	80	3344	391	Hall et al., 2004	Minimum age	x
	Dunlop Is	g	18.8	3985	175	3016	539	Lambert et al., 2002	Minimum age	x
	Dunlop Is	g	18.8	3690	70	2639	333	Hall et al., 2004	Minimum age	x
	Dunlop Is	g	19.5	6330	80	5930	311	Lambert et al., 2002	Minimum age	x
	Dunlop Is	g	19.5	5750	70	5278	377	Lambert et al., 2002	Minimum age	x
	Dunlop Is	g	19.5	5630	70	5126	326	Lambert et al., 2002	Minimum age	x
	Dunlop Is	g	19.5	3530	60	2467	345	Lambert et al., 2002	Minimum age	x
	Dunlop Is	g	20.0	4350	60	3458	328	Hall et al., 2004	Minimum age	x
	Dunlop Is	ss	21.0	5675	55	5178	340	Hall et al., 2004	Dates beach	x
	Dunlop Is	ss	21.0	3330	50	2204	331	Hall et al., 2004	Minimum age	
	Dunlop Is	ss	21.0	3210	62	2062	353	Hall and Denton, 2000a,b	Minimum age	
	Dunlop Is	ss	21.0	2890	62	1679	320	Hall and Denton, 2000a,b	Minimum age	
	Evans Cove	sh	9.0	6815	90	6465	338	Baroni and Hall, 2004	Dates beach	x
	Evans Cove	sh	9.0	6935	100	6606	350	Baroni and Hall, 2004	Dates beach	x
	Evans Cove	sh	9.5	6765	355	6416	815	Baroni and Hall, 2004	Dates beach	x
	Evans Cove	sh	10.5	6620	190	6231	504	Baroni and Hall, 2004	Dates beach	x
	Evans Cove	sh	10.5	6645	95	6264	342	Baroni and Hall, 2004	Dates beach	x

	Evans Cove	sh	10.5	6915	230	6575	584	Baroni and Hall, 2004	Dates beach	x
	Evans Cove	sh	12.5	6890	100	6551	347	Baroni and Hall, 2004	Dates beach	x
	Evans Cove	sh	12.5	7480	260	7129	597	Baroni and Hall, 2004	Dates beach	x
	Evans Cove	sh	12.5	7505	230	7192	536	Baroni and Hall, 2004	Dates beach	x
	Evans Cove	sh	14.0	6260	70	5848	275	Baroni and Hall, 2004	Dates beach	x
	Evans Cove	sh	14.0	6500	70	6109	316	Baroni and Hall, 2004	Dates beach	x
	Evans Cove	sh	15.0	6570	70	6184	299	Baroni and Hall, 2004	Dates beach	x
	Gneiss Pt	sh	12.5	6580	65	6195	300	Hall et al., 2004	Dates beach	x
	Gneiss Pt	sh	18.5	5980	50	5546	268	Hall and Denton, 2000a,b	Dates beach	x
	Gneiss Pt	sh	18.5	5925	60	5485	350	Hall et al., 2004	Dates beach	x
	Gneiss Pt	sh	18.5	5787	68	5327	382	Hall and Denton, 2000a,b	Dates beach	x
	Gneiss Pt	sh	18.5	5590	55	5082	300	Hall et al., 2004	Minimum age	
	Gneiss Pt	sh	18.5	5330	45	4727	340	Hall and Denton, 2000a,b	Dates beach	x
	Gneiss Pt	ss	19.0	5712	69	5226	353	Hall and Denton, 2000a,b	Dates beach	x
	Gneiss Pt	sh	20.5	6575	50	6190	288	Hall et al., 2004	Dates beach	x
	Gneiss Pt	sh	20.5	6520	55	6130	276	Hall and Denton, 2000a,b	Dates beach	x
	Gneiss Pt	sh	20.5	6430	60	6041	319	Hall and Denton, 2000a,b	Dates beach	x
	Gneiss Pt	sh	20.5	6430	55	6041	314	Hall et al., 2004	Dates beach	x
	Gneiss Pt	sh	20.5	6090	60	5672	340	Hall et al., 2004	Dates beach	x
	Gneiss Pt	sh	20.5	5645	50	5143	317	Hall and Denton, 2000a,b	Dates beach	x
	Gneiss Pt	ss	20.5	5590	50	5082	294	Hall and Denton, 2000a,b	Minimum age	
	Inexpressible Is	ss	4.0	2520	71	1282	313	Baroni and Hall, 2004	Dates beach	x
	Inexpressible Is	ss	5.5	2798	44	1576	277	Baroni and Hall, 2004	Dates beach	x
	Inexpressible Is	ss	5.5	2938	40	1734	316	Baroni and Hall, 2004	Dates beach	x
	Inexpressible Is	pb	5.5	3106	41	1937	292	Baroni and Hall, 2004	Dates beach	x
	Inexpressible Is	pb	5.5	3155	53	1997	306	Baroni and Hall, 2004	Dates beach	x
	Inexpressible Is	ss	8.0	2354	51	1113	275	Baroni and Hall, 2004	Dates beach	x
	Inexpressible Is	sh	8.0	6085	80	5667	350	Baroni and Hall, 2004	Dates beach	x
	Inexpressible Is	pb	8.0	3551	41	2491	335	Baroni and Hall, 2004	Dates beach	x
	Inexpressible Is	sb	8.0	3593	29	2534	290	Baroni and Hall, 2004	Dates beach	x
	Inexpressible Is	sh	9.0	7065	54	6734	321	Baroni and Hall, 2004	Dates beach	x
	Inexpressible Is	ss	11.0	2269	37	1032	263	Baroni and Hall, 2004	Dates beach	x
	Inexpressible Is	pb	11.5	4709	60	3906	355	Baroni and Hall, 2004	Dates beach	x
	Inexpressible Is	pb	11.5	4796	68	4023	361	Baroni and Hall, 2004	Dates beach	x
	Inexpressible Is	ss	11.5	4817	43	4051	343	Baroni and Hall, 2004	Dates beach	x
	Inexpressible Is	ss	14.0	2174	50	933	257	Baroni and Hall, 2004	Dates beach	x
	Inexpressible Is	ss	14.0	2847	43	1631	294	Baroni and Hall, 2004	Dates beach	x
	Inexpressible Is	ss	15.0	2083	51	842	223	Baroni and Hall, 2004	Dates beach	x
	Inexpressible Is	ss	15.0	3190	48	2039	317	Baroni and Hall, 2004	Dates beach	x
	Inexpressible Is	ss	16.0	4314	59	3413	351	Baroni and Hall, 2004	Dates beach	x
	Inexpressible Is	ss	17.0	3459	46	2381	321	Baroni and Hall, 2004	Dates beach	x
	Inexpressible Is	ss	17.0	5276	57	4662	360	Baroni and Hall, 2004	Dates beach	x
	Inexpressible Is	ss	19.0	2089	43	847	221	Baroni and Hall, 2004	Dates beach	x
	Inexpressible Is	sh	21.0	6191	42	5775	265	Baroni and Hall, 2004	Dates beach	x
	Inexpressible Is	ss	24.0	3116	47	1950	297	Baroni and Hall, 2004	Dates beach	x
	Inexpressible Is	ss	24.0	3120	48	1955	298	Baroni and Hall, 2004	Dates beach	x
	Inexpressible Is	ss	24.0	5722	56	5241	344	Baroni and Hall, 2004	Dates beach	x
	Inexpressible Is	h	24.0	6740	59	6374	311	Baroni and Hall, 2004	Dates beach	x
	Inexpressible Is	pb	24.0	6924	73	6570	298	Baroni and Hall, 2004	Dates beach	x
	Inexpressible Is	ss	27.0	4874	83	4128	408	Baroni and Hall, 2004	Dates beach	x
	Inexpressible Is	h	28.0	5139	68	4491	379	Baroni and Hall, 2004	Dates beach	x
	Inexpressible Is	h	28.0	6883	52	6525	265	Baroni and Hall, 2004	Dates beach	x
	Inexpressible Is	h	30.0	7365	60	7078	309	Baroni and Hall, 2004	Dates beach	x
	Marble Point	sh	5.0	2181	59	941	261	Hall and Denton, 2000a,b	Dates beach	x
	Marble Point	ss	6.5	2680	55	1451	273	Hall and Denton, 2000a,b	Minimum age	x
	Marble Point	sh	7.0	3258	42	2119	313	Hall et al., 2004	Dates beach	x
	Marble Point	ss	8.0	3550	50	2490	342	Hall and Denton, 2000a,b	Minimum age	x
	Marble Point	g	10.0	3170	61	2015	321	Hall and Denton, 2000a,b	Minimum age	x
	Marble Point	sh	10.5	4545	55	3693	321	Hall and Denton, 2000a,b	Dates beach	x
	Marble Point	sh	10.5	4520	45	3661	313	Hall and Denton, 2000a,b	Dates beach	x
	Marble Point	sh	10.5	4495	50	3631	304	Hall and Denton, 2000a,b	Dates beach	x
	Marble Point	sh	10.5	4345	55	3451	321	Hall and Denton, 2000a,b	Dates beach	x
	Marble Point	ss	10.5	2430	45	1186	268	Hall and Denton, 2000a,b	Minimum age	
	Marble Point	sh	13.4	5650	150	5145	493	Nichols, 1961	Dates beach	x
	Marble Point	sh	18.0	6780	56	6434	294	Hall and Denton, 2000a,b	Dates beach	x
	Marble Point	sh	18.0	6550	97	6161	331	Hall and Denton, 2000a,b	Dates beach	x
	Marble Point	sh	18.0	5860	79	5410	394	Hall and Denton, 2000a,b	Dates beach	x
	Marble Point	ss	18.0	2990	45	1796	301	Hall and Denton, 2000a,b	Minimum age	
	Prior Is	g	17.0	1860	75	647	221	Baroni and Orombelli, 1994	Minimum age	x
	Prior Is	g	17.0	1845	75	634	221	Baroni and Orombelli, 1994	Minimum age	x
	Prior Is	g	18.3	2385	80	1141	310	Baroni and Orombelli, 1994	Minimum age	x
	Prior Is	g	18.3	2205	75	967	277	Baroni and Orombelli, 1994	Minimum age	x
	Prior Is	g	18.3	2105	75	865	245	Baroni and Orombelli, 1994	Minimum age	x
	Prior Is	g	18.3	1910	75	692	225	Baroni and Orombelli, 1994	Minimum age	x
	South Stream	sh	12.5	5864	96	5361	386	Hall and Denton, 2000a,b	Dates beach	
	Spike Cape	sh	15.0	4195	120	3259	426	Hall et al., 2004	Dates beach	x
East Antarctica										
	Bunger Hills	sh	1.3	6210	100	5797	324	Adamson and Colhoun, 1992	Maximum age	x
	Bunger Hills	sh	2.0	6880	160	6531	447	Adamson and Colhoun, 1992	Maximum age	x
	Bunger Hills	sh	2.6	6010	100	5580	348	Adamson and Colhoun, 1992	Maximum age	x
	Bunger Hills	sh	2.8	8950	490	8734	1113	Adamson and Colhoun, 1992	Maximum age	x
	Bunger Hills	sh	3.0	4960	120	4243	437	Adamson and Colhoun, 1992	Maximum age	
	Bunger Hills	sh	3.3	6900	120	6549	362	Adamson and Colhoun, 1992	Dates beach	x
	Bunger Hills	sh	4.0	5630	90	5126	339	Adamson and Colhoun, 1992	Dates beach	x
	Bunger Hills	sh	5.2	6250	140	5842	379	Adamson and Colhoun, 1992	Dates beach	x
	Soya Coast	sh	2.0	2510	110	1273	351	Omoto, 1977	Dates beach	x

	Soya Coast	sh	2.0	1450	110	290	289	Omoto, 1977	Dates beach	x
	Soya Coast	sh	2.2	4360	70	3470	346	Maemoku et al., 1997	Dates beach	x
	Soya Coast	sh	3.2	4060	60	3098	331	Maemoku et al., 1997	Dates beach	x
	Soya Coast	sh	3.5	3840	110	2840	444	Omoto, 1977	Dates beach	x
	Soya Coast	sh	4.2	4090	80	3133	361	Maemoku et al., 1997	Dates beach	x
	Soya Coast	sh	4.5	4050	80	3087	341	Maemoku et al., 1997	Dates beach	x
	Soya Coast	sh	7.7	5000	50	4296	373	Maemoku et al., 1997	Dates beach	x
	Soya Coast	sh	8.5	5270	60	4655	367	Maemoku et al., 1997	Dates beach	x
	Soya Coast	sh	8.6	4900	60	4163	363	Maemoku et al., 1997	Dates beach	x
	Soya Coast	sh	8.9	4850	60	4096	384	Maemoku et al., 1997	Dates beach	x
	Soya Coast	sh	9.2	4350	70	3458	348	Maemoku et al., 1997	Dates beach	x
	Soya Coast	sh	9.2	4920	60	4189	368	Maemoku et al., 1997	Dates beach	x
	Soya Coast	sh	16.0	5850	100	5395	433	Omoto, 1977	Maximum age	x

w = whalebone, b = bone, pb = penguin bone, g = guano, sw = seaweed, sh = shell, mo = marine organics, pe = penguin egg shell, pf = penguin feather, h = seal hair, ss = seal skin, sb = seal bone

[1] Calibrated using a delta-R value of 791±121 following Hall et al. (2010)

APPENDIX VII – OSL AGES FOR ANTARCTIC RAISED BEACHES

Appendix VII. Published OSL ages used in age compilation

Location	Sample	Elevation (masl)	Aliquots[a]	D_e (Gy)	D_e error (Gy)	DR (Gy ka^{-1})	DR error (Gy ka^{-1})	Age (ky BP)[b]	Age error (ky BP)[c]	Source
Antarctic Peninsula										
Calmette Bay	CB10-026	3.3	3	3.6	0.85	3.4	0.56	1.00	0.60	Simkins et al., 2013a
	CB10-027	3.3	14	3.0	0.87	3.8	0.26	0.73	0.47	Simkins et al., 2013a
	CB10-030	3.4	7	24	2.6	9.0	1.4	2.56	1.02	Simkins et al., 2013a
	CB10-069	3.4	17	11	0.42	3.5	0.29	2.98	0.56	Simkins et al., 2013a
	CB10-033	6.5	14	7.0	0.58	3.5	0.38	1.94	0.55	Simkins et al., 2013a
	CB10-044	9.0	23	11	0.96	3.2	0.18	3.23	0.70	Simkins et al., 2013a
	CB10-046	11.3	20	10	0.55	4.2	0.39	2.37	0.51	Simkins et al., 2013a
	CB10-048	13.1	14	11	1.7	3.5	0.57	3.10	1.42	Simkins et al., 2013a
	CB10-057	21.7	15	15	0.42	3.5	0.33	4.09	0.82	Simkins et al., 2013a
	CB10-059	21.7	1	19	4.6	3.4	0.16	5.55	2.74	Simkins et al., 2013a
South Shetland Is										
Ardley Is	AI-01	11	25	1.3407	0.0713	1.63	0.037	1.66	0.60	Simms et al., 2011
	AI-02	11	16	2.0394	0.1322	1.56	0.034	1.73	0.26	Simms et al., 2011
	AI-03	11	17	1.0578	0.0833	1.45	0.033	2.24	0.43	Simms et al., 2011
	AI-04	6.6	29	0.5214	0.026	2.91	0.07	0.15	0.03	Simms et al., 2011
	PT-03	7.9	4	1.5642	0.2418	2.36	0.056	0.60	0.21	Simms et al., 2011
	PT-04	7.9	14	0.8009	0.0754	2.42	0.056	0.48	0.11	Simms et al., 2011
Potter Cove	PT-06	5.4	17	0.67	0.049	2.2	0.4	0.26	0.12	Simms et al., 2012
Suffield Point	SH-02	8.4	3	2.01	0.36	2.55	0.08	0.73	0.29	Simms et al., 2011

masl = meters above sea level, D_e = equivalent dose, DR = dose rate, ky BP = thousand years before present

[a] Aliquots presented pass all standard SAR procedure tests

[b] Ages are rounded to the nearest ten years. Samples corrected to obtain ages before preset as of 1950

[c] Errors are reported as 2-sigma

APPENDIX VIII – LATITUDES AND LONGITUDES FOR DATED ANTARCTIC BEACH SITES

Geographic context	*Site*	*Latitude* [1]	*Longitude*
Marguerite Bay, western AP	Horseshoe Island	67° 51' S	67° 12' W
	Ginger Island	67° 45' S	68° 42' W
	Lagoon Island	67° 35' 40.0" S	68° 14' 010.0" W
	Pourquoi Pas Island	67° 41' S	67° 30' W
	Anchorage Island	67° 36' 12.0" S	68° 12' 36.0" W
	Calmette Bay	68° 03' S	67° 10' W
	Rothera Station	65° 26' S	65° 30' W
Anvers Island, western AP	Litchfield Island	64° 46' S	64° 06' W
	Torgersen Island	64° 46' S	64° 05' W
	Biscoe Point	64° 49' S	63° 49' W
		62° 37' 58.8" S	61° 03' 57.6" W
South Shetland Islands	South Beaches, Byers Peninsula, Livingston Island	62° 39' 29.8" S	61° 03' 24.5" W
	President's Beaches, Byers Peninsula, Livingston Island	62° 37' 30" S	61° 07' 00" W
	Robbery Beaches, Byers Peninsula, Livingston Island	62° 36' 57.6" S	61° 04' 58.8" W
	Start Point, Livingston Island	62° 35' 20.0" S	61° 12' 57.9" W
	Potter Cove, S. King George Island	62° 14' 01.7" S	58° 41' 04.2" W
	Potter Peninsula, S. King George Island	62° 14' 44.1" S	58° 39' 27.7" W
	Ardley Island, Maxwell Bay, King George Island	62° 12' 47.1" S	58° 55' 59.4" W
	C. Aguirre Island, Maxwell Bay, King George Island	63° 19' S	57° 56' W
	Barton Peinsula, Maxwell Bay, King George Island	62° 13' 35.8" S	58° 44' 28.6" W
	Winship Point, Potter Cove, King George Island	62° 14' 32.3" S	58° 43' 42.7" W
	Fildes Peinsula, SW King George Island	62° 10' 55.7" S	58° 56' 53.3" W
	Suffield Point, Fildes Peninsula, King George Island	62° 11' 38.5" S	58° 55' 09.1" W
	Greenwich Island	62° 30' 00.0" S	59° 46' 58.8" W
East Antarctica	Bunger Hills, Knox Coast	66° 10' 00.1" S	100° 52' 59.9" E
	Lützow-Holm Bay, Soya Coast	69° 10' S	37° 30' E
Victoria Land, Western Ross Sea	Inexpressible Island	74° 54' S	163° 39' E
	Adelie Cove	74° 46' S	164° 00' E
	Franklin Island	76° 05' S	168° 19' E
	Prior Island	75° 41' S	162° 52' E
	Depot Island	76° 42' S	162° 58' E
	Cape Ross	76° 44'S	163° 01' E
	Cape Roberts	77° 02' S	163° 12' E
	Dunlop Island	77° 14' S	163° 30' E
	Spike Cape	77° 18' S	163° 34' E
	Gneiss Point	77° 24' S	163° 44' E
	Marble Point	77° 26' S	163° 50' E
	Explorers Cove	77° 34' S	163° 35' E
	South Stream	77° 27' S	163° 42' E
	Evans Cove	74° 53' S	163° 48' E

AP = Antarctic Peninsula

[1] Latitudes and longitudes were taken from *The SCAR Composite Gazetteer* managed by the Australian Antarctic Data Centre (https://data.aad.gov.au/aadc/gaz/scar/search.cfm) where latitude and longitudes were not published along with the dated beaches.

APPENDIX IX – REPRESENTATIVE AGES FOR INDIVIDUAL BEACHES USED IN AGE COMPILATION

Appendix IX. Ages for individual beaches using in age compilation

Location	Elevation (m)	Age (yrs BP)	Error (yrs BP)[1]	Comments[2]
South Shetland Islands				
Byers Peninsula, King George Island	2	0	0	2 min
	2.5	0	0	1 min
	3	0	0	1 min
	3.5	0	0	2 min
	4	453	329	2 date
	4.5	0	0	1 min
	5	330	373	3 date
	6	455	301	2 min
	7	445	296	1 min
	8	862	810	3 min
	9	1949	298	1 date
	10	1780	461	2 date
Maxwell Bay, Livingston Island				
Fildes Peninsula + C. Escondida + C. Aguirre + Suffield Point	3	317	317	1 dates
	3.5	0	0	1 min
	4	105	338	3 min
	5.5	471	228	1 min
	6	219	349	4 min
	7	207	207	1 min
	8.4	731	364	1 OSL
	18	6224	445	2 dates
North Spit + Marian Cove	3	0	0	1 min
	4	396	415	2 dates
	5.5	173	173	1 min
	6	258	282	2 dates
South Spit + Winship Point + Barton Peninsula	4	272	292	2 min
	5	409	271	2 dates
	6	390	349	2 dates
	6.5	430	283	1 dates
Ardley Island	17	418	273	1 min
	11	1875	805	3 OSL
	5.4	261	124	1 OSL
Potter Cove + Potter Peninsula	3.5	9595	644	1 max
	4	7398	285	1 max
	6	512	232	1 dates
	7.9	540	226	2 OSL
	15.6	5392	360	1 dates
	16.5	5282	341	1 dates
Greenwich Island	12	1947	455	2 dates
Antarctic Peninsula				
Marguerite Bay	3.3	1819	1640	4 OSL
	4.6	3605	296	1 min
	5	982	1057	3 min
	6.1	3612	291	1 min
	6.5	1939	549	1 OSL
	8.3	3143	896	2 min
	9	2818	1763	4 min
	9	3229	701	1 OSL
	11.3	2369	514	1 OSL
	13.1	3097	1418	1 OSL
	16	1248	282	1 min
	17	4095	2255	5 min
	21.4	1072	278	1 min
	35.5	1772	294	1 min
	21.7	4822	2510	2 OSL
Anvers Island	5	790	180	1 OSL
	5.5	1130	720	1 OSL
	7	1413	1190	3 OSL
Ross Sea				
Adelie Cove	2	608	191	1 dates

	5	1394	270	1 dates
	6	2100	436	2 dates
	6.5	2124	442	2 dates
Cape Roberts	5	1151	377	2 dates
	5.5	1128	820	4 dates
	6	619	195	1 dates
	8	1550	357	3 dates
	8.5	3723	330	1 dates
	10	1767	319	1 dates
	17	3004	296	1 dates
Cape Ross	21	4006	536	1 min
	24.5	3447	656	2 min
	27.5	3726	366	1 min
	28.1	3335	492	1 min
	28.7	3947	516	1 min
	29.2	3406	514	1 min
	31.5	3427	588	4 min
	32	5053	1089	1 min
Depot Island	8	2513	336	1 min
	12	1506	242	1 min
	14	1952	307	1 min
	15	2156	326	1 min
	16.5	2507	723	2 min
	21	3020	335	1 min
	28	3428	791	2 min
Dunlop Island	3.5	3687	323	1 max
	6	1821	331	1 dates
	7	1884	902	3 dates
	7.5	2331	315	1 dates
	10.5	2450	595	3 min
	11.5	1462	250	1 min
	13	5147	326	1 dates
	15	1765	303	1 min
	16.5	3344	391	1 min
	18.8	2828	625	2 min
	19.5	4700	2060	4 min
	20	3458	328	1 min
	21	5178	340	1 dates
Evans Cove	9	6536	415	2 dates
	9.5	6416	815	1 dates
	10.5	6357	716	3 dates
	12.5	7161	762	3 dates
	14	5979	426	2 dates
	15	6184	299	1 dates
Gneiss Point	12.5	6195	300	1 dates
	18.5	5271	714	4 dates
	19	5226	353	1 dates
	20.5	5870	826	6 dates
Inexpressible Island	4	1282	313	1 dates
	5.5	1811	502	4 dates
	8	2951	2590	4 dates
	9	6734	321	1 dates
	11	1032	263	1 dates
	1.5	3993	422	3 dates
	14	1282	624	2 dates
	15	1441	869	2 dates
	16	3413	351	1 dates
	17	3522	1481	2 dates
	19	847	221	1 dates
	21	5775	265	1 dates
	24	4418	2608	5 dates
	27	4128	408	1 dates
	28	5508	1339	2 dates
	30	7078	309	1 dates
Marble Point	5	941	261	1 dates

	6.5	1451	273	1 min
	7	2119	313	1 dates
	8	2490	342	1 min
	10	2015	321	1 min
	10.5	3609	442	4 dates
	13.4	5145	493	1 dates
	18	5788	856	4 dates
Prior Island	17	641	228	2 min
	18.3	916	492	4 min
South Stream	12.5	5361	386	1 dates
Spike Cape	15	3259	426	1 dates
East Antarctica				
Bunger Hills	1.3	5797	324	1 min
	2	6531	447	1 min
	2.6	7157	2309	2 min
	3.3	6549	362	1 dates
	4	5126	339	1 dates
	5.2	5842	379	1 dates
Soya Coast	2	1678	1908	3 dates
	3.5	2969	517	2 min
	4.5	3110	374	2 min
	7.7	4296	373	1 dates
	8.5	4409	611	2 dates
	9.2	3914	724	3 dates
	16	5395	433	1 min

[1] Errors were calculated using the difference from the average of the lowest and highest uncertainties of the averaged ages

[2] The number and indicative meaning of the beaches used to calculate representative age for beach where 'dates' indicates the ages date beach formation, 'min' indicates minimum ages for beach formation, 'max' indicates maximum ages for beaches, and 'OSL' indicates OSL ages that provide ags dating beach formation